ABSTRACT

FLUID FLOW THROUGH ROCK SALT UNDER VARIOUS STRESS STATES

Вy

Chia-Shing Lai

Concern for leakage of reactor fuel waste materials from underground salt cavities has prompted questions regarding the permeability of rock salt materials. To provide information on this question, the flow rate of kerosene through rock salt specimens was studied for a range of normal and octahedral shear stresses. Kerosene was used as the fluid because of similarity to radioactive waste materials and its nonrusting properties when in contact with steel. Expressions for the permeability of the rock salt were developed in terms of the stress conditions and void ratios of the rock salt material.

A high pressure triaxial cell was designed and constructed for permeability tests at various stress states. The cell permitted application of axial loads separate from lateral pressures. Independent hydraulic systems maintained axial and lateral pressures to about ± 5 psi of selected pressures. Fluid flow was permitted axially through the sample under a head differential of 125 psi.

Rock salt from an underground formation in Louisiana was cut into cylindrical samples 3 inches high by 3 inches in diameter.

Strain gages attached to the sides of the sample provided information

on tangential and axial strain. Overall axial deformation, obtained by means of a dial gage mounted outside the triaxial cell, provided a check on strain gage values. Kerosene flow through the sample was recorded at given time intervals.

The experimental data provided the basis for developing empirical expressions for the rock salt permeability in terms of the mean normal stresses and octahedral shear stresses. Strain measurements permitted incorporating changes in void ratio into the permeability expressions. The flow of kerosene through the rock salt appears to obey approximately the same laws as developed for flow of water through soils. Laboratory permeabilities for the rock salt varied from 0.0036 to 40.6752 milli-darcy for various stress states. Very low permeabilities indicate that leakage of radioactive waste materials from underground salt cavities will be very small to almost negligible.

FLUID FLOW THROUGH ROCK SALT UNDER VARIOUS STRESS STATES

Ву

Chia-Shing Lai

A THESIS

Submitted to
Michigan State University
in partial fulfillment of the requirements
for the degree of

DOCTOR OF PHILOSOPHY

Department of Civil Engineering

1971

PLEASE NOTE:

Some Pages have indistinct print. Filmed as received.

UNIVERSITY MICROFILMS

ACKNOW LEDGMENTS

The writer wishes to express his sincere appreciation to Dr. Shosei Serata, who helped initiate this project, and to Dr. O.B. Andersland for his assistance and encouragement throughout the latter part of the writer's doctoral studies, and for his many helpful suggestions during the preparation of this thesis. The writer also wishes to express his sincere appreciation to Dr. C.E. Cutts, Dr. R.F. McCauley, and Dr. M. Fox for serving as members of his guidance committee.

The writer acknowledges the U.S. Public Health Service and the Division of Engineering Research at Michigan State University for the financial aid that made this study possible.

TABLE OF CONTENTS

	Page
ACKNOW LEDGMENTS	ii
LIST OF FIGURES	v
LIST OF TABLES	vii
NOTATIONS	v iii
Chapter	
I. INTRODUCTION	1
II. LITERATURE STUDY	5
Underground Disposal of Waste and Groundwater	
Contamination	5
Permeability of Underground Porous Media	8
Effect of Stress and Strain Field Upon Porous Flow .	11
Leakage from an Underground Salt Cavity	14
III. EQUIPMENT AND TEST PROCEDURES	16
High Pressure Triaxial Cell	16
Specimen Preparation	19
Test Procedures and Porous Flow Measurements	23
IV. EXPERIMENTAL RESULTS	26
Stress and Strain Measurements	26
Flow Measurements	2 b
r tow measurements	23
V. STRESS AND STRAIN EFFECTS ON PERMEABILITY OF	
THE ROCK SALT	55
Stress Field	55
Strain Field	64
Compressibility	71
VI. FLOW FROM AN UNDERGROUND SALT CAVITY	82

Chapter		Page
VII.	SUMMARY AND CONCLUSIONS	88
	High Pressure Triaxial Cell	88
	upon Permeability	89 89
VIII.	FUTURE RESEARCH	91
BIBLIOGR	АРНУ	93
APPENDIX	DATA	97

LIST OF FIGURES

Figure		Page
3-1	High Pressure Triaxial Cell	17
3-2	Schematic Diagram Showing Layout of Triaxial Pressure Cells and Automatic Pressure Control System	20
3-3	Rock Salt Sample with Bronze Screens	22
3-4	Two Finished Samples and Cover of High Pressure Triaxial Cell	22
3-5	High Pressure Triaxial Cell with Sample	24
3-6	Test Set-up Showing Triaxial Cells, Pressure Gages, and Strain Gage Equipment	24
4-1	Strain-Time Relationship at Various Stress Field	30
4-2	Flow-Time Relationship at Various Stress Levels	45
5-1	Typical Curve Showing Time Versus Accumulated Flow .	56
5-2	The Effect of Mean Stress upon Permeability for Various Octahedral Shear Stress	58
5-3	The Effect of Octahedral Shearing Stress upon Permeability for Various Mean Stress	59
5-4	The Effect of Octahedral Shear Stress upon Permeability with Mean Stress Equal to Zero	60
5-5	Permeability under Various Combinations of Mean Stress and Octahedral Shear Stress	61
5-6	Three Dimensional Plot of Mean Stress, Octahedral Shear Stress, and Permeability	65
5-7	The Relationship between Taylor's Void Ratio Coefficient and Permeability	68
5 - 8	The Effect of Product of $\sigma_{\rm m}$ and (e ³ /1+e) on Permeability	69

Figure		Page
5-9	The Relationship between Unit Volume Change and Permeability of Rock Salt	70
5-10	The Effect of Mean Stress on Void Ratio	72
5-11	The Effect of Mean Stress on Taylor's Void Ratio Coefficient	73
5-12	The Effect of Mean Stress upon Compressibility for Various Octahedral Shearing Stress (I)	76
5-13	The Effect of Mean Stress upon Compressibility for Various Octahedral Shearing Stress (II)	77
5-14	The Effect of Mean Stress upon Compressibility for Various Octahedral Shearing Stress (III)	78
5-15	The Effect of Bulk Compressibility upon Permeability for Various Octahedral Shearing Stress	80
6-1	Hypothetical Storage Cavity in a Salt Formation	83
6-2	Two Dimensional Configuration of an Underground Formation	86

LIST OF TABLES

Tab le		Page
4-1	Stress Levels for the Test Program	28
5-1	Permeability as a Function of Mean Stress at Various Octahedral Shearing Stress	62
5-2	Octahedral Shearing Stress as a Function of Permeability at Various Mean Stresses	63
5-3	Compressibility as a Function of Mean Stress at Various Octahedral Shearing Stresses	75
5-4	Compressibility as a Function of Permeability at Various Octahedral Shearing Stresses	81
A-1	Strain-Rate, Deformation, and Flow-Test Data	97
A-2	Flow-Rate, Permeability, Strain and Deformation	127
A-3	Stress, Taylor's Coefficient, Void Ratio, Void, and Bulk Compressibility	128

NOTATIONS

A = cross-sectional area A = area of contact between solid particles $A_r = arrangement of solid$ a = ratio of area of contact between soil solids to gross area a = inner radius of cylindrical cavity α, β = constants b = outer radius of cylinder $\beta',C = compressibility'$ $c_h = bulk compressibility (1/psi)$ c_{σ} = grain compressibility (1/psi) D = average particle diameter d = particle size δ = uniform diameter of straight parallel capillaries δ_1 = axial deformation measured by dial gage $\Delta V = volume of flow$ e = void ratio $\epsilon_1, \epsilon_2, \epsilon_3$ = major, intermediate, and minor principal strains $\epsilon_L, \epsilon_L^{\dagger}$ = tangential strain measured by strain gage, lateral strain based on dial gage readings ϵ_1^{\bullet} = axial strain obtained by dial gage

 γ_0 = initial unit weight at atmospheric pressure

E = Young's modulus

 γ_b = bulk density

 $\gamma_{(1)} = fluid density$

i = hydraulic gradient

k = coefficient of permeability (cm/sec)

 $K = physical permeability = k \frac{\mu}{\gamma_{\omega}}$

 K_{O} = octahedral shear Strength at yield condition

 μ = viscosity of fluid

 ρ_0 = plastic radius

n = porosity

N = number of spheres

v = Poisson's ratio

P_f = average fluid pressure

P, = uniform internal pressure

P = uniform external pressure

 P_{u} = fluid pressure inside the cavity

 $P_{_{\rm I}}$ = initial lateral underground pressure

p = fluid pressure

 $Q = flow rate = \frac{\Delta V}{\Delta t}$

R = radius of sphere

r = Bergelin's tube radius

 $\sigma_{\rm m}$ = mean stress = $\frac{1}{3} (\sigma_1 + \sigma_2 + \sigma_3)$

 $\sigma_1, \sigma_2, \sigma_3$ = major, intermediate, and minor principal stress

 σ_{L} = lateral stress

 $\sigma = total stress$

 σ' = effective stress = $(\sigma - P_f)$

s' = saturation of the sample

S = specific internal area of model (Scheideggar, 1960)

```
s_o = Carman's specific surface exposed to fluid (Carman, 1937)

C_g = shape factor

\tau = octahedral shearing stress

T = tortuosity (Scheideggar, 1960)

t = time

v = discharge velocity

\Delta u = pore pressure change
```

 $V_{v} = void volume$

 $V_b = bulk volume$

Z = depth of formation

 $V_s = crystal \text{ or solid volume}$

CHAPTER I

INTRODUCTION

The wide use of radioactive materials in the present era, necessitates safe disposal of reactor fuel waste because of its potential harmful effects upon human life. A variety of measures to safeguard such radioactive waste have been investigated; for example, storage in artificial containers on the ground, dumping wastes into the deep sea, shooting them into the space or burying wastes in deep underground cavities (Kaufman, 1961). This study is concerned with the latter method, disposal in underground cavities.

Previous research has shown that underground burial of radioactive waste is the safest and the most efficient method for disposal (Serata, 1959). Cavities provide thick shielding, permit remote handling, and provide adequate cooling for high level radioactive waste. However, two problems related to underground disposal must be considered: one is structural stability of the underground cavity and the other is seepage of waste through the rock to ground water supplies or to the ground surface. More specifically, the problem of structural stability relates to deformation of the underground structure, while the problem of seepage deals with the rock permeability and is a function of existing stresses.

The problem of structural stability has been clarified to some extent. For example, the structural stability of salt cavities appears to be safe with regard to the high pressures associated with radioactive waste disposal (Reynolds, 1960). The problem of seepage, however, still remains unanswered, and the degree of permeability under complex stress conditions is not yet known.

In the decade following 1930, the state of stress in natural underground cavities was studied and experiments were carried out by many investigators (Dahir, 1964, Sakurai, 1966, Obert and Duvall, 1967). Sakurai (1966) and Dahir (1964) investigated the theoretical and experimental behavior of underground stress fields and provided a theory for the rheological model of salt behavior.

Since 1951, several experimental methods (Osoba, 1951; Fatt, 1952, 1953; Gray and Fatt, 1963; Douglas, 1953) have been developed for determination of the permeability of underground material with relation to stress states. These studies were concerned with hydrostatic compression. Gray and Fatt (1963) stated that permeability was a function of the ratio of radial to axial stress; i.e., triaxial stress conditions. Most of this research was conducted for the petroleum industry and for reservoir engineering.

Preliminary studies of reactor fuel waste disposal in salt cavities were undertaken by Serata (1959). From his theoretical analysis and experimental investigations, Serata showed that the storage of radioactive waste in salt cavities was feasible. In

1960, Reynolds also reported to the Atomic Energy Commission on permeability of rock salt and creep of underground salt cavities.

The purpose of this study is to determine the degree of seepage through a rock sample during a laboratory experiment, and to extrapolate the findings of this research to potential pollution. Because of test limitations imposed on the laboratory experiment, attention is focused on seepage through a typical Louisiana rock salt.

The objectives of this thesis are to provide experimental data on flow of liquids through rock salt under various stress states and to propose a method for predicting the permeability of underground formations. Specifically, the objectives are as follows:

- (1) To design and construct a device suitable for laboratory determination of permeability of rock salt under complex stress conditions.
- (2) To develop mathematical equations for prediction of permeability as a function of the complex stress conditions.
- (3) To evaluate the feasibility of radioactive waste disposal in an underground formation and/or storage of other substances such as fuel and water.

Rock salt has been chosen as the material for the underground formation in this study. From previous experience it has been demonstrated that rock salt shows isotropic and homogeneous qualities under static and dynamic loading and that its properties fall within a practical range for testing.

A complete analysis of radioactive waste disposal in underground salt formations requires a three dimensional stress loading scheme to determine seepage through a laboratory model for use in predicting the ultimate degree of pollution. This research has been undertaken to provide experimental data for three dimensional loading.

For permeability tests under various stress states, a high pressure triaxial cell was designed and constructed. The test machines were equipped with coordinated loading in lateral and axial directions and could be controlled by using two independent hydraulic systems. Uniform flow was applied to the specimen under a constant fluid pressure. The specific permeability was obtained for several stress states including transient and steady state flow conditions.

For this study, it was assumed that the rock salt is isotropic and homogeneous. Kerosene was used as the fluid representative of reactor waste. For convenience all tests were conducted at room temperatures. Since underground formations are warmer than room temperatures, corrections to the permeability can be made by allowing for changes in viscosity and density of the pore fluid.

CHAPTER II

LITERATURE STUDY

Underground Disposal of Waste and Groundwater Contamination

The treatment and disposal of radioactive waste is one of the increasingly serious problems related to growth of the nuclear power industry. It is impossible to destroy or eliminate radio-activity by any known chemical or physical means, and the maximum permissible concentrations (U.S. Department of Health, Education, and Welfare, 1960) for radionuclides in air and in water are several orders of magnitude lower than those specified for inactive contaminants. There are several alternatives in radio-active waste disposal. These include: storing in artificial containers in or on the ground; dumping the waste into the deep sea; shooting it into the space; or burying it in deep underground cavities. This study is concerned with the last of these disposal measures because it is the most promising solution.

Research has been in progress for a number of years on reducing radiation hazards to humans. An ultimate disposal operation is required that will insure that fission products are safely contained for centuries without requiring further monitoring. A unique property of these wastes is their intense radioactivity: they are capable of spontaneous and prolonged boiling from absorption of their own radiant energy. Unfortunately, the rate of heat

released is not constant and violent surging can occur, leading to rapid fluctuations in pressure build-up (Burns, 1960). In constructing waste disposal facilities in underground formations it is necessary to consider the maximum pressure produced by the waste itself, and also to design for high external earth pressures including that from groundwater acting on the structures.

During September 1955 the Committee on Waste Disposal of the Division of Earth Science, National Academy of Science (1957) (consisting of leading scientists in inter-related fields such as chemistry, physics, geology, geophysics, economics, and sanitary engineering) discussed disposal of radioactive waste in geologic formations. The committee then made a specific recommendation on storage of radioactive waste (solid or liquid) in salt formations as perhaps the most promising method of disposal. The major advantages of disposal in salt formations were (Serata, 1959): (1) Salt beds and domes are widely distributed and abundant throughout the country with an area of more than half a million square miles (Lang, 1957). The United States' salt reserves are estimated at greater than 6×10^{13} tons (Mineral Resources of the U.S., 1958); (2) Rock salt has a high thermal conductivity (2.5 BTU/hr-ft-OF at 200 F) (Birch and Clark, 1940) and a melting point sufficiently high for large quantities of heat to be dissipated during the storage of high level radioactive waste; (3) Rock salt has a compressive strength similar to that of concrete and lacks tensile strength. It flows plastically to relieve stress concentrations from mining and heating. However, under normal

mining conditions, stress concentration and temperatures are low and supports are not needed. Due to plastic behavior, salt acts as a self sealer for the storage cavity as well as an absorber of higher stress concentration around the cavity opening; (4) The total space created by mining rock salt during a period of 1934 to 1953 has been calculated as one billion cubic feet (National Academy of Science, 1957); (5) In the decade of the forties, hundreds of millions of gallons of liquid petrochemical products have been successfully stored in salt cavities by various oil companies (Reidel, 1952; Van Fossan, 1955). Disposal studies on high level liquid and solid wastes initiated at Oak Ridge National Laboratory indicate that it is feasible to construct underground storage cavities.

During 1954, over 1,000 gallons of acid waste, containing a liquid fission product with complexing agent and 1000 curies of Sr^{90} , was successfully poured into a pit lined with limestone (Parsons, 1963) at 233 Lake, Ontario, Canada for the Clark River Project. It has been estimated that Sr^{90} will be released to the environment in about 130 years but that the rate of release into a nearby stream will not produce concentrations of these radionuclides above the normal drinking water tolerance.

Hawkins demonstrated the value of Wyoming bentonite clay for preventing the seepage of rainwater into radioactive waste buried above the water table in a humid region. Other efforts to prevent this type of seepage had varied success at several sites (Hawkins and Horton, 1967).

High level waste fission product solution containing 100 curies was incorporated into glass blocks and the blocks were buried for 3 years in sand beneath the water table. The experiment showed that even in saturated soil with low exchange capacity, this method of disposal was safe and the escape of hazardous radionuclides was within acceptable limits. An underground formation was shown to provide permanent radiation shielding and ion-exchange media for the anticipated small release (Meritt and Parsons, 1964).

Fenimore (1964) reported on land burial of solid radioactive waste during a 10-year period. Since the initial land burial
of solid radioactive waste in 1953 at the Savannah River Plant,
577,000 curies of fission product and induced radioactivity were
buried. Routine surveillance of thirteen test and observation
wells indicated no migration of radioactive material. Geologic and
hydrologic studies, radioassays of soil samples and measurements
of ground water velocity using tritium as a tracer, indicated little
probability of introducing this buried radioactivity into public
zones.

The studies and experiments in the literature show that underground burial of radioactive wastes in rock salt formations is feasible if these conditions are satisfied: (1) the rock salt is structurally stable; and (2) seepage is at a permissible rate.

Permeability of Underground Porous Media

Since 1951 several experimental methods (Osoba, 1951; Fatt, 1952; Gray, 1963) have been developed for permeability measurement of rock materials under complex stresses. These experiments

were conducted for the petroleum and reservoir engineering industry and used sandstone as the porous medium. They were conducted under hydrostatic compression or uniaxial compression.

The most recent study (Gray and Fatt, 1963) was concerned with the stress effect on permeability of sandstone cores and was undertaken primarily to develop methods for studying permeability of sandstone under simulated overburden pressure. Findings demonstrate that the sandstone permeability decreases upon application of an overburden pressure and that this decrease is a function of the ratio of radial to axial stress. However, no extensive study on the relationship of radial to axial stress ratio upon permeability has been carried out.

Osoba, Richardson, and Kerver (1951) made laboratory
measurements on small core samples of reservoir rock to determine
relative permeability to oil and gas by five methods. These tests
included the Penn State Techniques, Single Core Dynamic Technique,
Gas Drive Technique, Stationary Liquid Technique, and Hasseler
Technique. Their study also included the influences of such factors
as boundary effects, hysteresis, and rate of flow upon these measurements. Results indicated that four of the five methods yielded
essentially the same relative permeability to gas; the Stationary
Liquid Technique was applicable to oil only.

Fatt and Davis (1952) worked on the reduction in permeability with increase in overburden pressure. Results showed that the specific permeability of sandstone decreased with increase in overburden pressure, and that most of the decrease took place in

the range of zero to 3,000 psi.

Wilson (1956) designed and constructed a useful apparatus for determination of relative permeability under simulated reservoir conditions. Water-oil relative permeability data and water saturation vs. relative permeability were obtained. Results showed that the application of overburden pressure caused a reduction in the effective permeability to both water and oil in about the same proportion as for reduction of single-phase permeability.

Fatt (1958) measured porosity and flow using packs of rubber spheres under compression and showed that ideal sphere packs did not model the flow porosity of consolidated sandstone.

McLatchie, et. al. (1958) reported the effective compressibility of reservoir rock and its influence on permeability. They concluded that the effective compressibility of the material could not be correlated with porosity and that other factors, such as the amount of clay material present, must be considered.

Mann and Fatt (1960) studied the effect of pore fluids on the elastic properties of sandstone and found that the presence of an aqueous solution in the pore spaces caused the elastic constant to change. For example: (1) Bulk compressibility increased by 10 to 30 percent; (2) Young's modulus decreased by 8 to 20 percent; and (3) Poisson's ratio increased by one hundred percent for Bandera sandstone and changed only a small amount for the two other sandstones.

Effect of Stress and Strain Field upon Porous Flow

Although extensive studies have been carried out on the effect of stress fields upon porous flow under hydrostatic compression, few studies have been made on the effect of triaxial compression upon porous flow. To date, the studies have been concerned with the gross effect of overburden pressure on permeability, porosity, electrical resistance, and sonic velocity.

The major conclusion drawn from these studies on porous flow are: (1) The permeability of sandstone decreases upon application of simulated overburden pressure, and (2) permeability reduction of sandstone cores subjected to simulated overburden pressure is a function of the ratio of radial to axial stress.

Secchi (1936) made experiments to study the dependence on permeability of a filter on external pressure and showed that such a dependence does exist, and is subject to hysteresis. A series of experiments published by Ruth (1946) and Tiller (1953) showed that the relationship of permeability k to fluid pressure p and the total pressure σ can be represented as follows:

$$k = K(\sigma - p)^{-m}$$
 (where m is constant)

This relationship was deduced from largely empirical investigations. The relationship is valid only if $(\sigma - p)$ is larger than some lower limiting value.

Athy (1930) found that the variation of clay porosity, with depth, can be represented by

$$n = n_0^{-\alpha z}$$

where n is the average porosity of surface clay, α is a constant, and z is depth below the surface.

Bergelin (1949), Porkhaev (1949), and Templeton (1953, 1954) studied the use of capillaric models to investigate the flow of several phases in a single capillary. These investigations were mainly experimental, since techniques had been devised for the observation of gas-liquid or liquid-liquid displacement in uniform capillaries with diameters as small as four microns.

The concepts of displacement in single capillaries represented as a bundle of capillaries have been studied by Gates and Lietz (1950), Fatt and Dykstra (1951), Burdine (1953), Hassan and Nielson (1953), and Irmay (1954). As is usual for capillaric model theories it was assumed that the sample could be represented by a bundle of capillary tubes in which the fluid path length was not the same as the bulk length. In addition, the fluid path length was considered to vary with saturation.

The following equations list the relationships of permeability to porosity and the other factors proposed by different investigators:

(1) Fatt and Dykstra (1951)
$$dk = \frac{nr^2(1+b)}{8a^2} ds'$$

where, k = permeability

n = porosity

r = tube radius

s' = saturation of the sample

a,b = constants

(2) Hagen-Poiseuille (Scheidegger, 1960)

$$k = \frac{n \delta^2}{32}$$
 or $k = \frac{n^3}{T^2 S^2}$

where, δ = uniform diameter of straight parallel capillaries

T = tortuosity

S = specific internal area of the model

n = porosity (as in (1) above)

(3) Kozeny Theory (Scheidegger, 1960)

$$k = \frac{cn^3}{TS^2}$$

where symbols are as identified in (2) above

(4) Modified Kozeny Theory (Kozeny-Carman Equation) (Carman, 1937, 1938, 1939)

$$k = \frac{n^3}{5s_0^2 (1 - n^2)}$$

with symbols as in (2) above, and s_{o} is Carman's "specific" surface exposed to the fluid

(5) Brinkman's Theory (Happel and Byrne, 1954)

$$k = \frac{R^2}{18} (3 + \frac{4}{1-n} - 3) \frac{8}{1-n} - 3)$$

where $\frac{4}{3} \pi NR^3 = 1-n = Total volume of spheres$

k = permeability

R = radius

N = number of spheres

n = porosity

(6) Taylor's Theory (Taylor, 1948)

$$k = D_s^2 \frac{\gamma_w}{\mu} \frac{e^3}{1+e} \quad C$$

where $D_e = diameter of particle$

 μ = fluid viscosity

e = void ratio

C = constant

 γ_{ω} = fluid density

From these relationships, it is noted that permeability is primarily affected by porosity of the media. Change of porosity for a material is, however, directly affected by external pressure.

Leakage from an Underground Salt Cavity

In 1960 the U.S. Atomic Energy Commission, in response to the urgent need for practical solution to reactor fuel disposal, supported research by Reynolds at the University of Texas on permeability of rock salt and creep of underground salt cavities.

From theoretical analysis and experimental studies the following conclusions resulted:

- 1. Storage of radioactive wastes in salt cavities is feasible.
- Though rock salt is relatively plastic and elastic when it is mined, localized fractures occur.
- 3. No flow can occur through the solid salt crystals.
- 4. Superficial cracks in a cavity can be sealed by the use of a diatomaceous earth suspension.
- 5. The non-reactive liquid permeability K can be estimated:

$$K = 7.1 \times 10^{-10} (\sigma_{\rm m} - P_{\rm f})^{-0.212}$$

where K = physical permeability in cm²

 $\sigma_{\rm m}$ = mean confining stress in psi

 P_f = average fluid pressure in psi

Proper selection of the piezometric head in a cavity

(internal pressure) can provide an additional safety factor for assuring that no leakage from a cavity will occur.

Data and analysis from the University of Texas work has suggested that wastes could be confined in salt cavities for over 500 years. It should be noted, however, that creep decreased with age and creep rate increased when temperature was increased.

CHAPTER III

EQUIPMENT AND TEST PROCEDURES

The equipment used in this research includes standard items except for the specially designed high pressure triaxial cell and the hook-up of hydraulic pumps and pressure shock absorbers. A detailed description is given for the high pressure triaxial cell. Details of the test procedures are given in two parts: specimen preparation and porous flow measurements.

High Pressure Triaxial Cell

A high pressure triaxial cell, designed to permit application of uniform confining pressures and axial loads, was fabricated. Two independent hydraulic load systems, were used to apply confining pressures and axial loads. The triaxial test simulated the complex stress conditions existing in an underground formation adjacent to the disposal cavity.

The triaxial cell used to measure rock properties at high pressure is shown in Fig. 3-1. It was designed so that pressure could be maintained on the internal fluid (kerosene) and external fluid (hydraulic oil) independently. This cell consisted of a base, an outer cylinder, cover plates, neoprene high pressure hoses, gages, and an axial pressure ram. Stainless steel tubes were used for the collector, distributor, and accessories. The

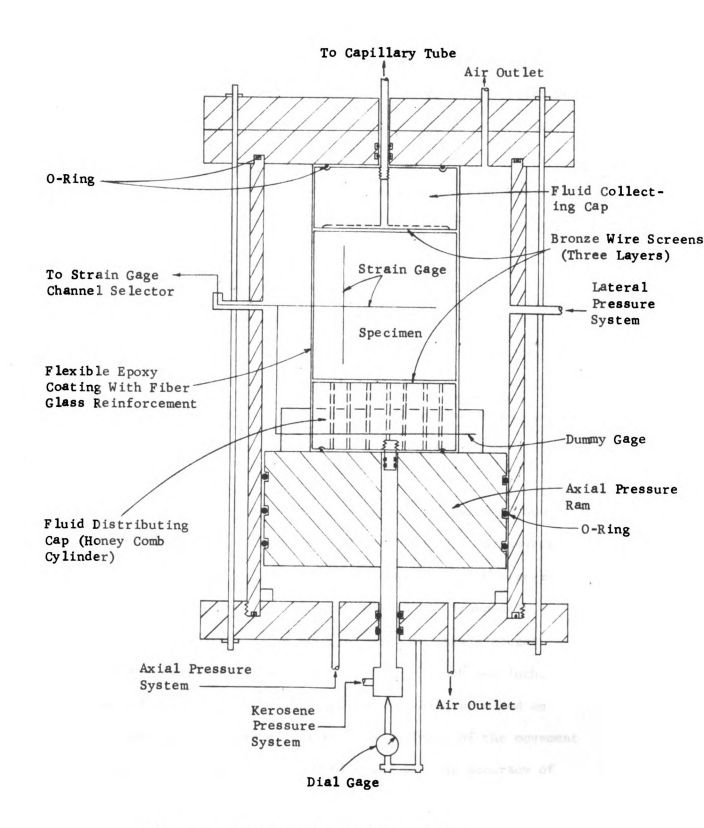


Fig. 3-1. High Pressure Triaxial Cell
(Scale 1:2)

base, cover, and cylinder were made of stainless steel. One of the stainless steel tubes was attached to the pressure ram, another tube was attached to the collector cylinder. The apparatus was designed to operate at confining pressures up to 10,000 psi. All other parts and appurtenances were capable of similar high pressure operation. Both top and base were drilled with small holes for attaching the air release valve with a ball bearing at the opening.

The major problem was prevention of leakage in order to maintain different pressures in the internal fluid (kerosene) and the external fluid (hydraulic oil). This requirement was accomplished by sealing with neoprene O-rings (see Fig. 3-1). Strain gages, placed in hard epoxy cement to prevent leakage, were attached to the sample with wires passing through openings in the cell.

The load capacities of the hydraulic pumps were 10,000 psi for both axial and lateral stress directions with pressures measured by a separate hydraulic pressure gauge in each system. Stresses could be controlled independently or simultaneously. Axial and lateral deformations were measured by strain gauges placed on the sample with an accuracy of \pm 10⁻⁶ inch per inch. A mechanical dial gauge, mounted outside the cell, provided an accurate reading on the axial deformation in terms of the movement of the ram piston relative to the cell body with an accuracy of \pm 10⁻⁴ inch.

The pressure applied to a test specimen was held reasonably constant by the automatic control system in both the lateral and axial stress directions. A shock absorber, used in each hydraulic system, reduced the shock impulse produced by the strating of automatic pump during the loading cycle. The sensitive pressure switch attached to the automatic pump maintained pressures at close to ± 5 psi in both pressure systems.

Specimen Preparation

Rock salt used in this research was obtained from Louisiana. The salt was mined at a depth of about 700 ft., was white in color, and consisted of crystalline grains of approximately 0.1 to 0.7 inches in diameter.

Cylindrical specimens, 3 inches in diameter and 3 inches in height (see Fig. 3-3), were prepared with a band saw, grinder, and lathe, and then smoothed with sand paper finishing. Small cavities on the sides of the specimen (which could permit a development of a puncture in the epoxy coating) were filled with Gypsum cement, then coated with a very thin layer of hard epoxy coating to prevent fluid leakage along the wall. Variation in specimen size was within $\pm 1/32$ inch for the height and diameter. Three bronze screens placed between the specimen and the steel caps separated the specimen from the fluid distributor and collector. The caps were drilled with 1/8" holes to provide openings for fluid movement. Strain gages were attached along the periphery at midheight of the specimen and vertically along the sides with thin epoxy cement.

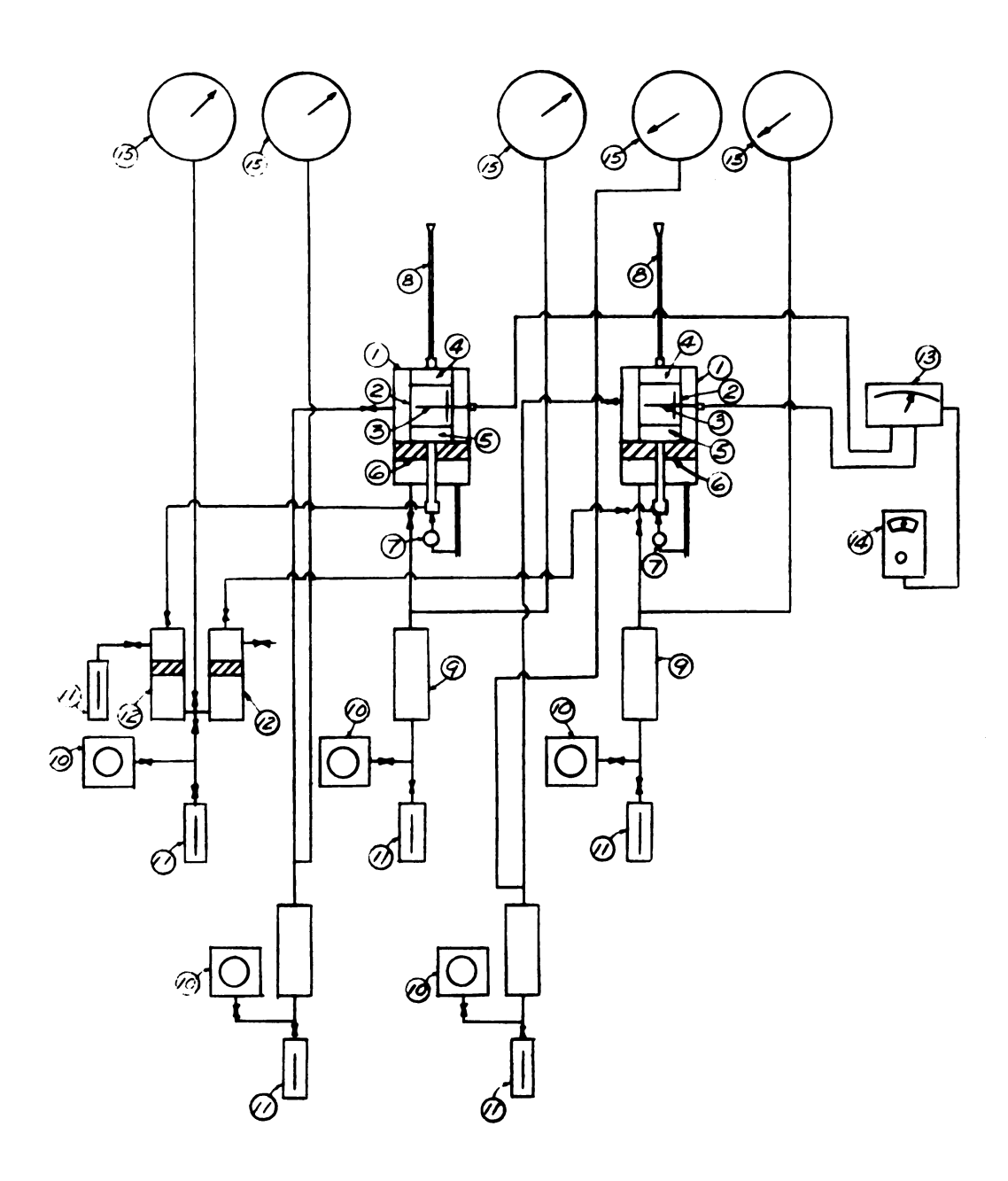


Fig. 3-2 SCHEMATIC DIAGRAM SHOWING LAYOUT
OF TRIAXIAL PRESSURE CELLS AND
AUTOMATIC PRESSURE CONTROL SYSTEM

Component Designations for Fig. 3-2

- 1. High Pressure Triaxial Cell (Fig. 4-1)
- 2. Specimen
- 3. Strain Gauges
- 4. Fluid Collector
- 5. Fluid Distributor
- 6. Axial Pressure Rams
- 7. Dial Gages
- 8. Capillary Tube or Burettes
- 9. Shock Absorbers
- 10. Automatic Pumps with Pressure Switches
- 11. Hand Pumps
- 12. Hydraulic Oil-Kerosene Transformers
- 13. Channel Selector
- 14. Strain Gage Recorder
- 15. Pressure Gages



Fig. 3-3. Rock Salt Sample with Bronze Screens







Gage and lead wires were embedded in the epoxy cement (see Fig. 3-4). The specimen and caps were coated with flexible epoxy cement (REN product) and with two layers of fiber glass cloth for reinforcement.

Test Procedures and Porous Flow Measurements

The laboratory tests provided information on the deformation and permeability of rock salt specimens at various stress levels. The specimens in which stress and strain distributions are examined were under non-plastic conditions.

The base, with triaxial cell and axial pressure ram, was set on the table of the testing machine. Next, hydraulic lines were connected for application of axial and lateral pressures. A dummy gage ring was placed on the top of the pressure ram to compensate for the fluid effect on the acting gage and a specimen was then placed in the cells. After connecting the strain gage wires, the cell was filled with hydraulic oil to the top (see Fig. 3-5). A small tube for collecting fluid was connected directly to the top cap as shown in Fig. 3-6. A cotton ball, soaked with kerosene, was placed at the top of the tube to prevent evaporation of the fluid. Assembly was finally completed by installation of the top cap and connection to the hydraulic system. Kerosene was used for all porous flow measurements because of its similarity to water and its nonrusting properties.

The air release valve was kept open and hydraulic pressure was gradually increased by means of a hand pump until the cell was completely filled with oil. The air release valve was then



Fig. 3-5. High Pressure Triaxial Cell with Sample (see Fig. 4-1)



Fig. 3-6. Test Set-up Showing Triaxial Cells, Pressure Gauges, and Strain Gauge Equipment

closed and axial pressure was gradually increased up to 10 psi to obtain perfect contact between the cover, specimen, and ram. Approximately 50 pound pressure increments were applied for both axial and lateral pressure until the calculated working stress was reached. Strain gage readings were recorded for each stress increment. After the pressures had reached the working value, the automatic pumps were turned on to maintain a constant pressure. Shock absorbers, inserted between the automatic pump and pressure cell, limited sudden increases of pressure to not more than \pm 10 psi.

Seepage pressures and confining pressures were held constant throughout the experiment except for the high τ -value working stress (τ = 1000 psi). The high-rate of flow which occurred under this τ -value required that the seepage pressure be reduced.

The strain reading and accumulated flow were recorded at selected time intervals until a constant flow rate was obtained.

Data are given in the appendix.

CHAPTER IV

EXPERIMENTAL RESULTS

Stress and Strain Measurements

The flow properties of porous media usually depend upon material characteristics such as bulk density or void ratio and particle size, shape, and arrangement. These characteristics vary from one material to another. They may also vary within the same material if it is subjected to factors such as strain hardening due to the stress applied upon the material or to chemical reaction, i.e., heat. However in this study only strain effects due to the stress change were included as an object of the research. In order to study flow properties, temperature and chemical reaction were considered constant for the laboratory conditions. Permeability of materials subjected to different strain conditions depended on the stress conditions and permeability measurements in this study were obtained under constant stress levels and recorded as a time function until a constant flow rate was observed.

The mean stress, $\sigma_{\rm m}$, applied to the material was calculated as $\sigma_{\rm m}=1/3$ ($\sigma_1+\sigma_2+\sigma_3$) psi, where σ_1 , σ_2 , σ_3 are principal stresses. The octahedral shearing stress, τ , was equal to $1/3 \int (\sigma_1-\sigma_2)^2 + (\sigma_2-\sigma_3)^2 + (\sigma_3-\sigma_1)^2$. Since no tectonic forces were considered, $\sigma_2=\sigma_3=\sigma_{\rm L}$ and $\sigma_{\rm m}$ becomes

1/3 $(2\sigma_L + \sigma_1)$ and $\tau = \sqrt{2}/3$ $(\sigma_1 - \sigma_L)$ for the triaxial test conditions. The axial and tangential strains were obtained by strain gage as ε_1 and ε_L . The temperature was assumed constant and equal to room temperature.

The test was designed to control stresses in the range of $\sigma_{\rm m}$ equal 1,000 psi to 5,000 psi which approximates the actual overburden pressure at depths of 1,000 ft. to 5,000 ft. below the ground surface. The range of octahedral shearing stresses were 100 psi to 1,000 psi. Rock salt has an ultimate octahedral shearing strength close to 1,000 psi.

The stress levels for each test condition are tabulated in Table 4-1. Since a five inch piston was used to apply pressure on a three inch cylindrical specimen, P_1 and P_L were computed to obtain σ_m and τ . P_1 and P_L are the vertical and lateral pressures, respectively. Constant stress conditions were maintained throughout each experiment by using the automatic hydraulic pump equipment. A minimum of 10,000 minutes was allowed for the flow rate to reach a steady state flow condition for each experiment.

Dial gage readings provided accurate data on axial deformations. SR-4 strain gages attached to the external specimen surface provided data on the ratio of axial to tangential strain. An apparent error in the strain gage readings should cancel when these data are used as a ratio. Lateral strain was calculated by multiplying this ratio of tangential to axial strain by the axial deformation. For example, consider test 1 where total axial strain ϵ_1 equals 615 x 10⁻⁶ in/in and total lateral strain ϵ_L = 145 x 10⁻⁶ in/in based on strain gage readings. Since the total axial

Table 4-1. Stress Levels for the Test Program

	$\sigma_{\mathfrak{m}}$	(psi)							
	•••			1000	1350	1700	3000	4000	5000
τ (psi)									
100			P ₁ :	1006	1356	1706	3006	4006	5006
			P _L :	929	1280	1629	2898	392 9	4929
				1017	1367	1717	3017	4017	5017
300				788	1138	1538	2788	3788	4788
				1028	1378	1728	3028	4028	5028
500				823	997	1347	2823	3647	4647
				1040	1390	1740	3040	4040	5040
700				505	855	1205	2505	3505	4505
				1057	1407	1757	3057	4057	5057
1000				293	643	993	2293	3293	429 3

deformation δ_1 , based on the dial gage, equals 109×10^{-4} in. $(\varepsilon_1' = \frac{109}{3} \times 10^{-4} \text{ in/in})$ the computed tangential strain $\varepsilon_L' = \varepsilon_1' \times \frac{\varepsilon_L}{\varepsilon_1} = 36 \times \frac{145}{615} \times 10^{-4} = 8.7 \times 10^{-4} \text{ in/in.}$ (See Table A-1 and A-2) All strain readings were recorded at selected time intervals until a constant flow of liquid was obtained. The results from strain measurements are plotted against time as shown in Fig. 4-1-1 to 4-1-30.

Flow Measurements

Flow measurements were obtained for selected stresses while strains were measured in the axial and tangential directions. This represents a simulation of the stress conditions on an element of salt material in an underground formation.

The flow of kerosene was measured by capillary tube, burette, or graduate cylinder according to the flow rate. The flow pressure was maintained constant by use of the automatic pump control system. The kerosene flow was vertical from the external supply into and through the salt specimen. The accumulated effluent was collected in the receiver and recorded at selected time intervals until a steady state flow rate was obtained. The pressure differential between entrance and exit locations, ΔP , should be equal to the gage pressure reading, P. Because the pressure at the outlet was equal to atmospheric pressure, it was assumed that ΔP was dissipated during flow through the specimen.

Accumulated flow ΣV is plotted against time in Fig. 4-2-1 to Fig. 4-2-10 for the selected stress conditions.

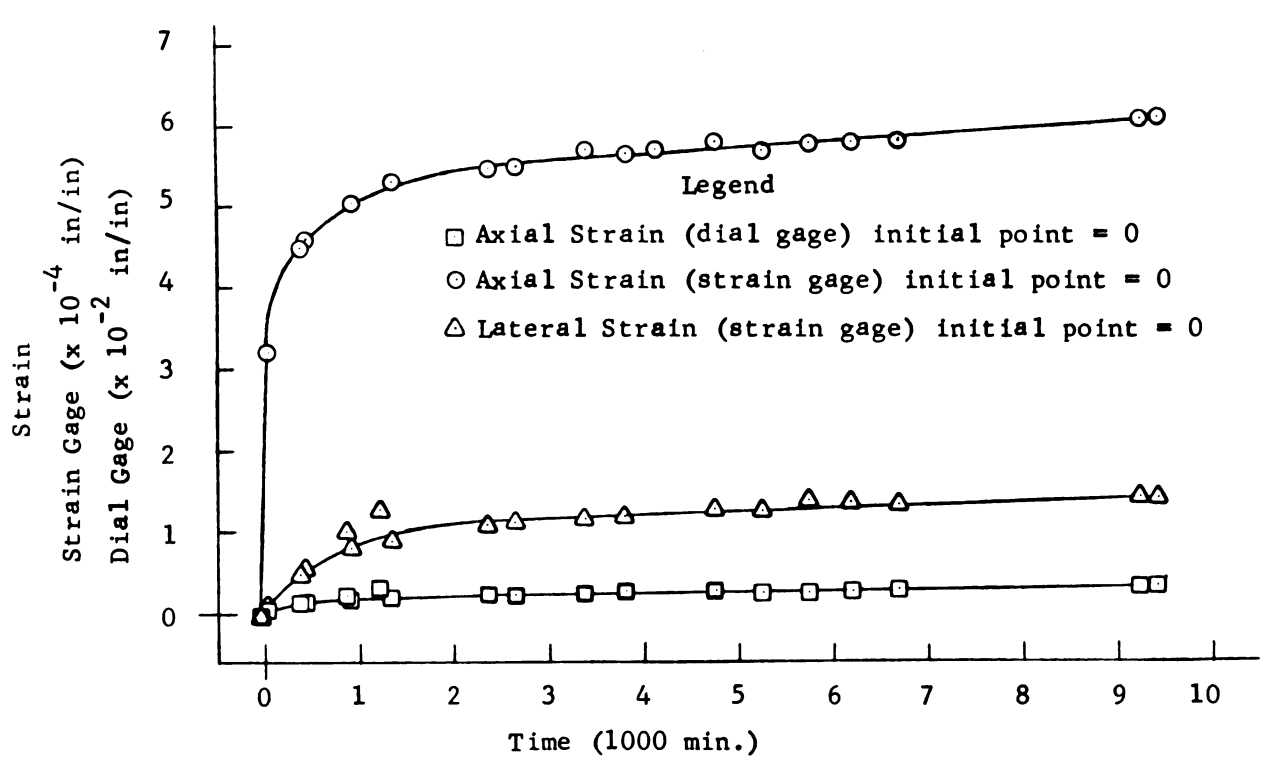


Fig. 4-1-1. Strain-Time Relationship at $\sigma_{\rm m}$ = 1000 psi τ = 100 psi

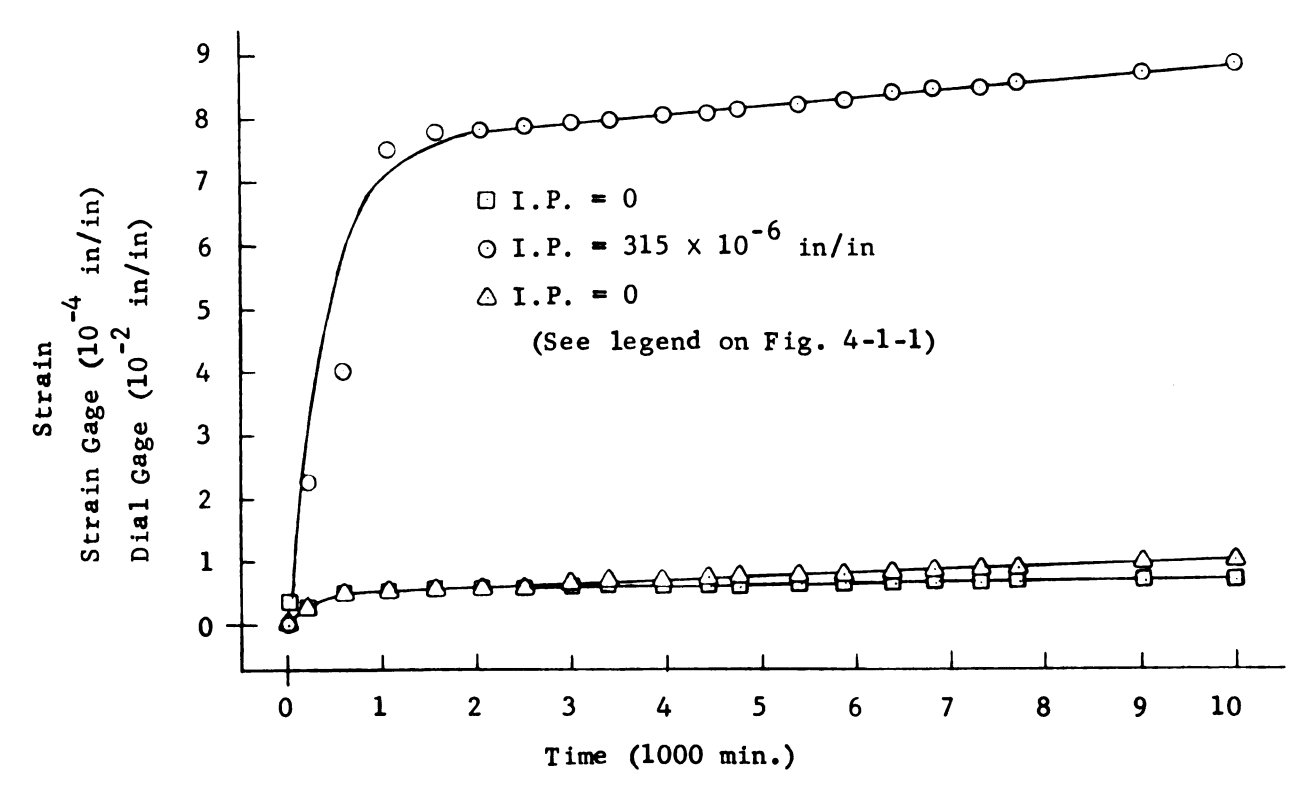


Fig. 4-1-2. Strain-Time Relationship at $\sigma_{\rm m}$ = 1350 psi τ = 100 psi

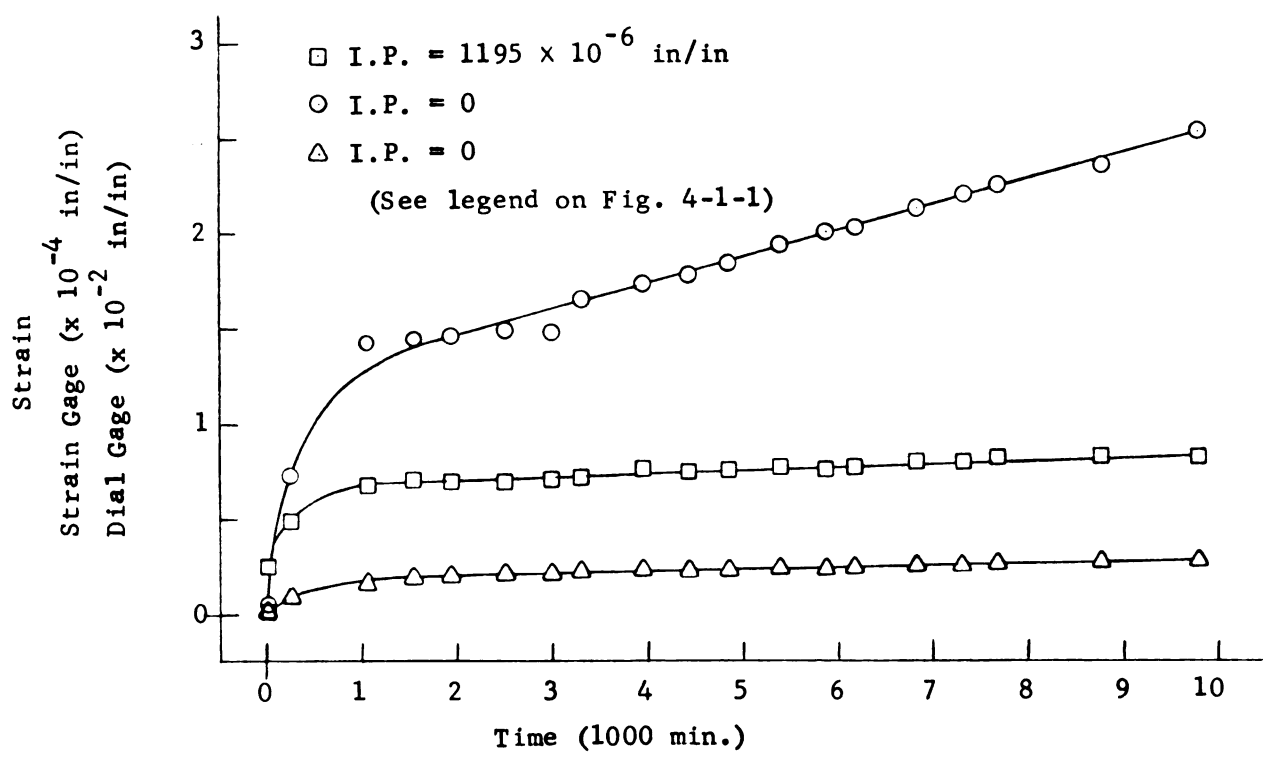


Fig. 4-1-3. Strain-Time Relationship at $\sigma_{\rm m}$ = 1700 psi τ = 100 psi

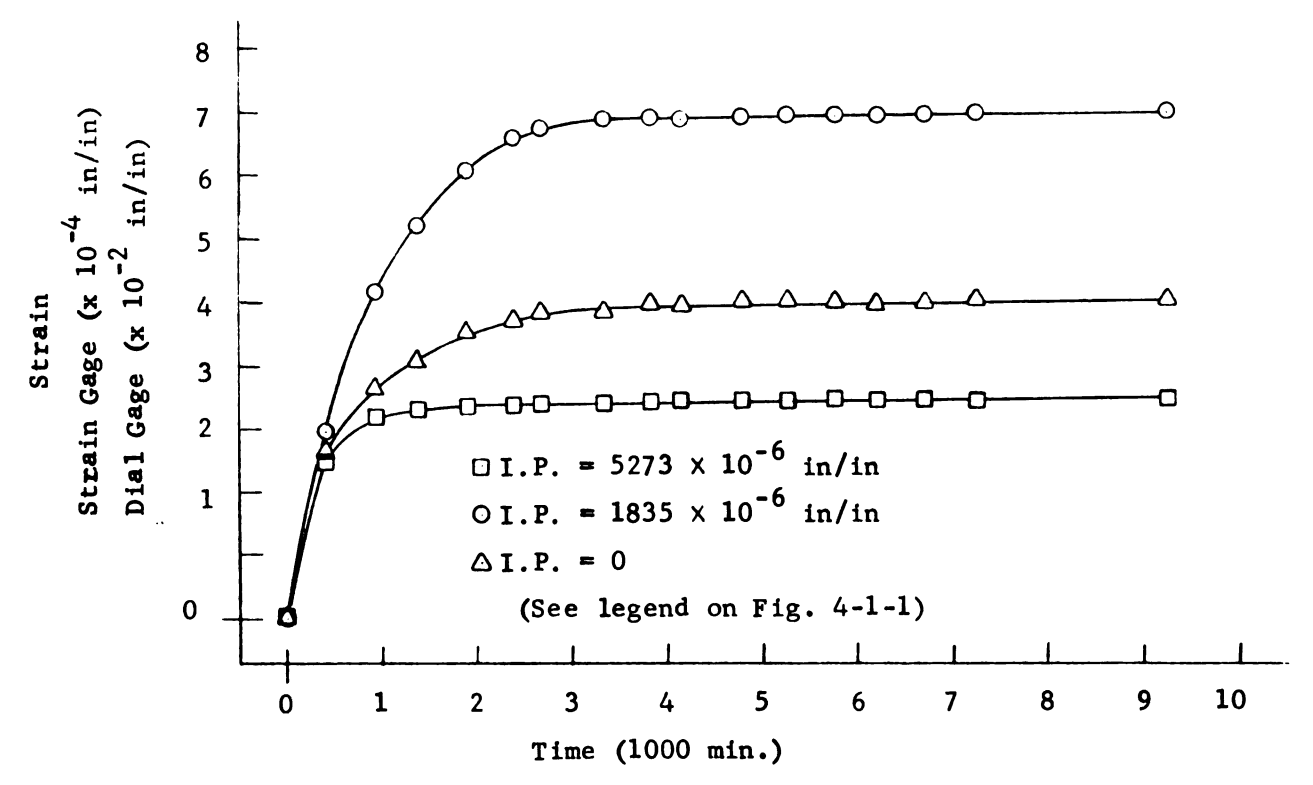


Fig. 4-1-4. Strain-Time Relationship at $\sigma_{\rm m}$ = 3000 psi τ = 100 psi

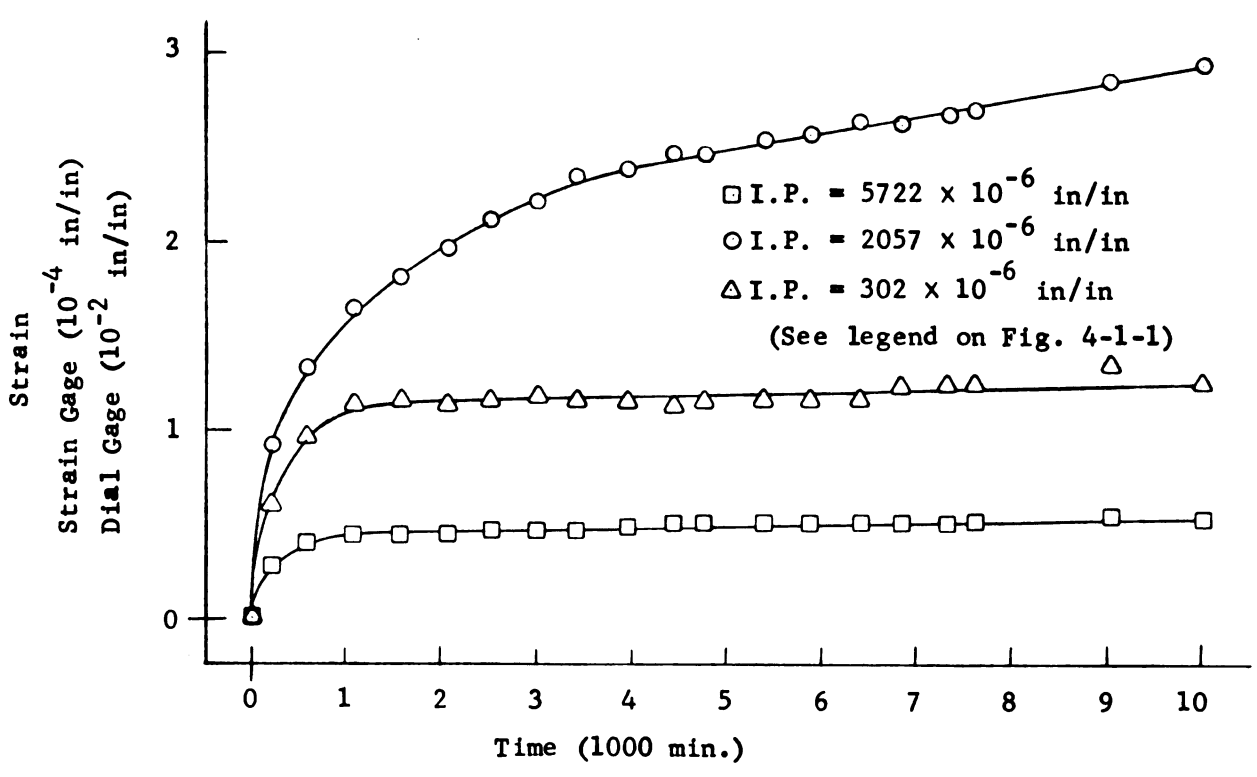


Fig. 4-1-5. Strain-Time Relationship at $\sigma_{\rm m}$ = 4000 psi τ = 100 psi

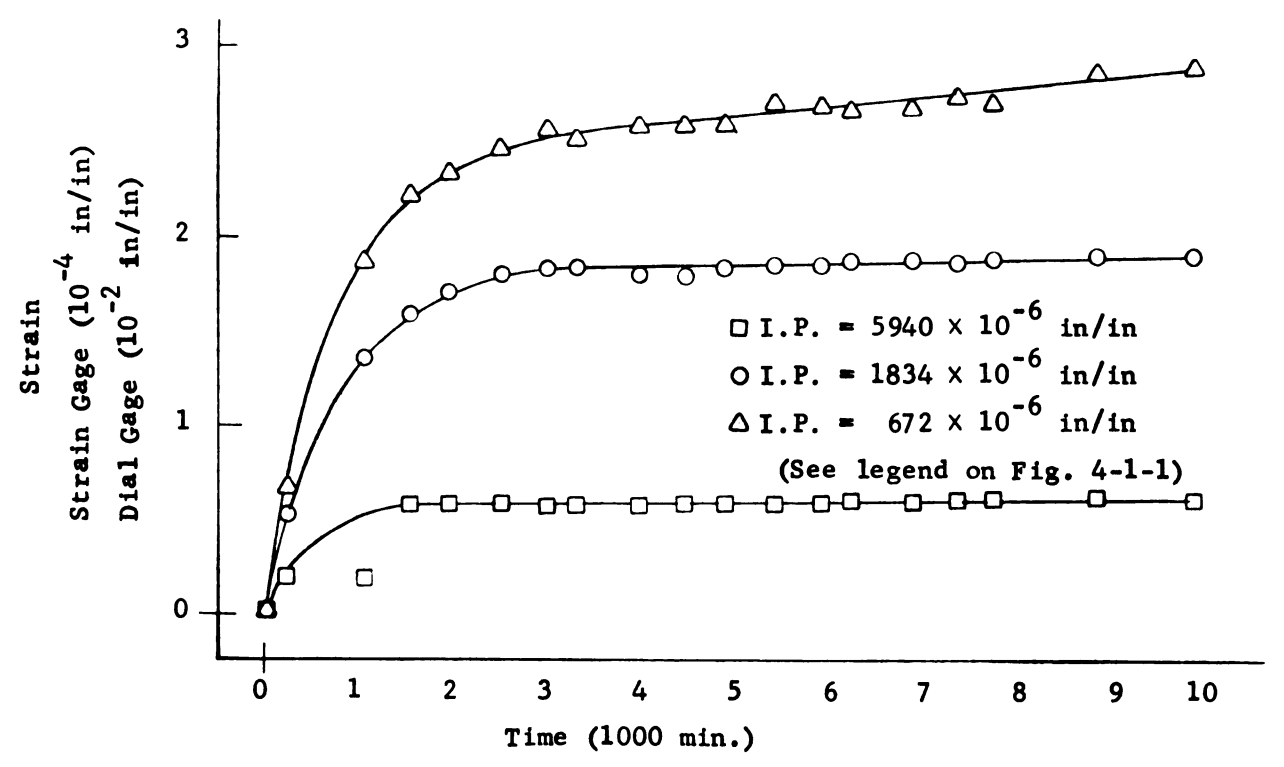


Fig. 4-1-6. Strain-Time Relationship at $\sigma_{\rm m} = 5000~{\rm psi}$ $\tau = 100~{\rm psi}$

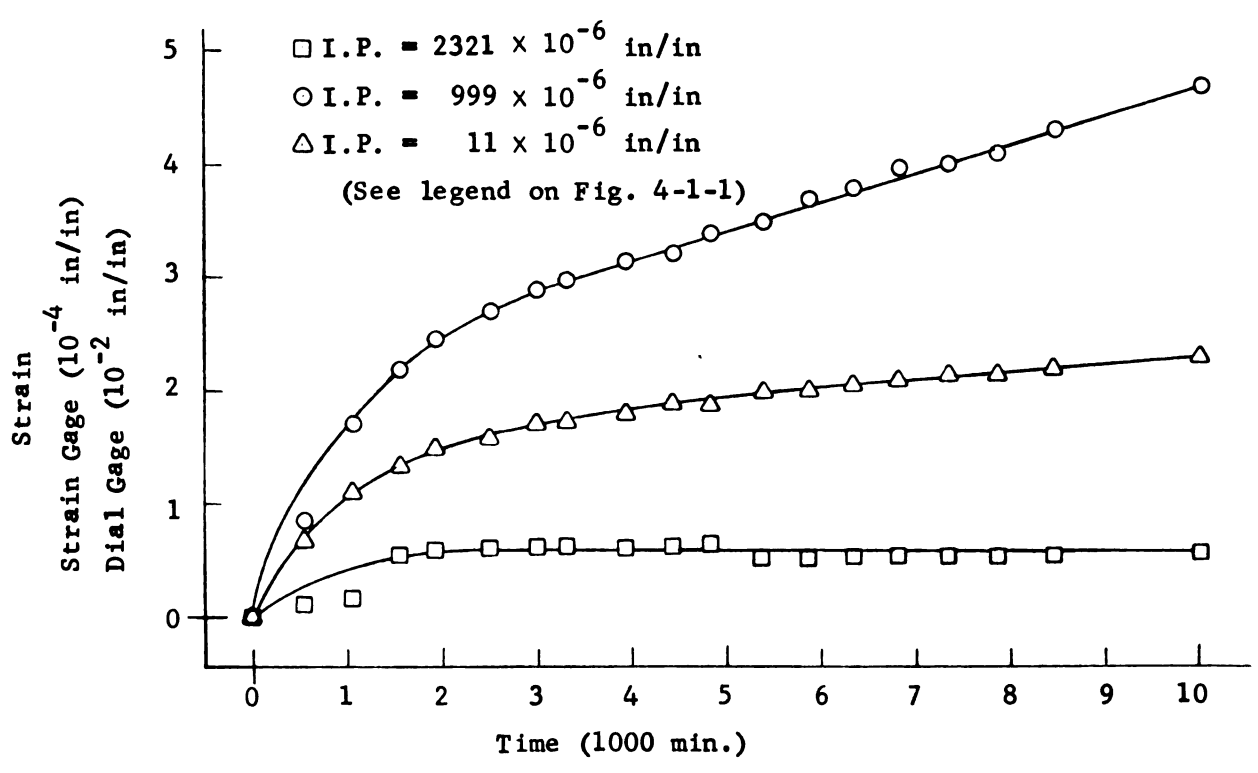


Fig. 4-1-7. Strain-Time Relationship at $\sigma_{\rm m}$ = 1000 psi τ = 300 psi

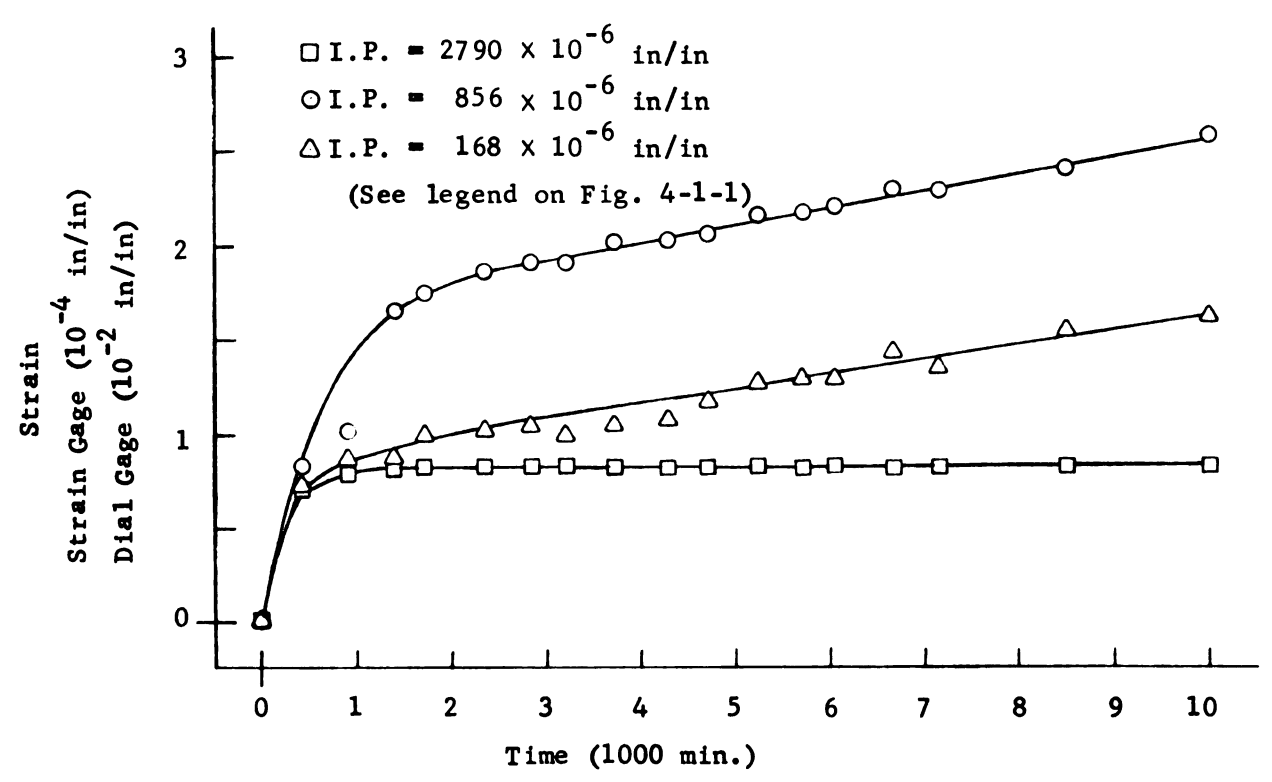


Fig. 4-1-8. Strain-Time Relationship at $\sigma_{\rm m}$ = 1350 psi τ = 300 psi

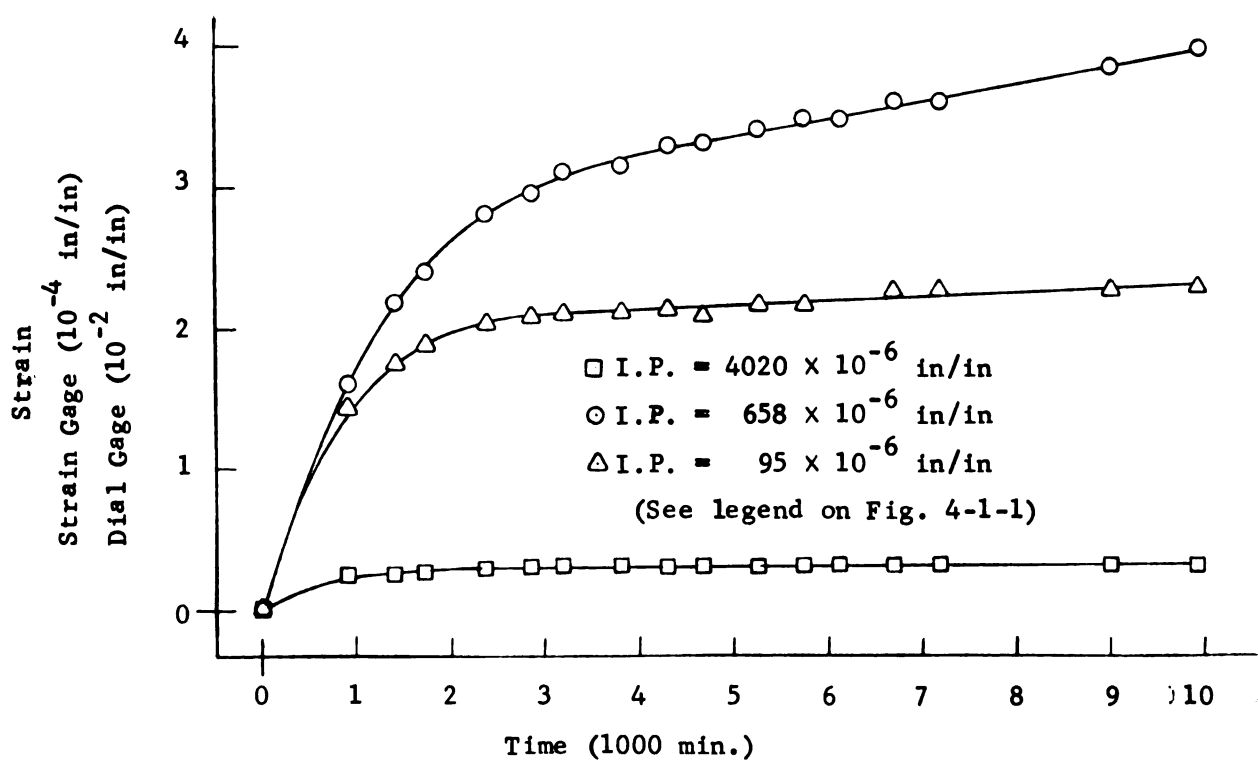


Fig. 4-1-9. Strain-Time Relationship at $\sigma_{\rm m} = 1700~{\rm psi}$ $\tau = 300~{\rm psi}$

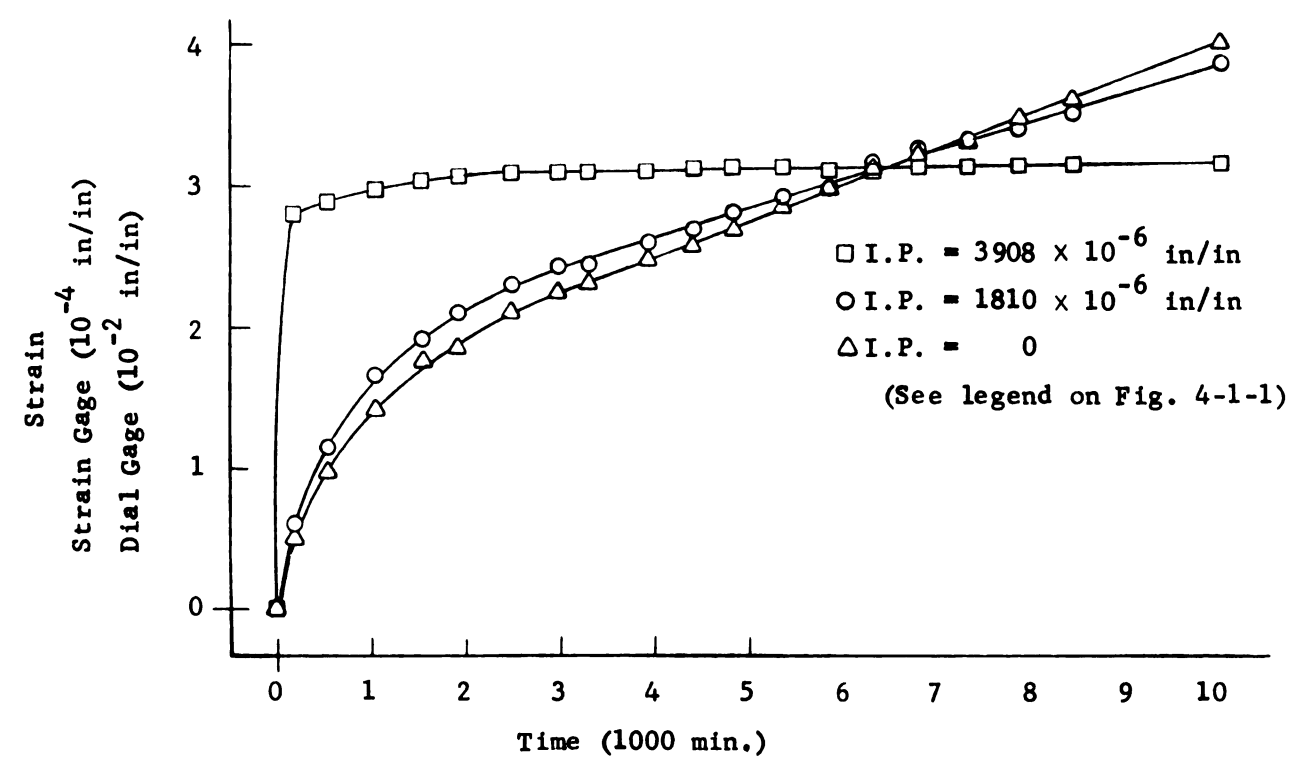


Fig. 4-1-10. Strain-Time Relationship at $\sigma_{\rm m}$ = 3000 psi τ = 300 psi

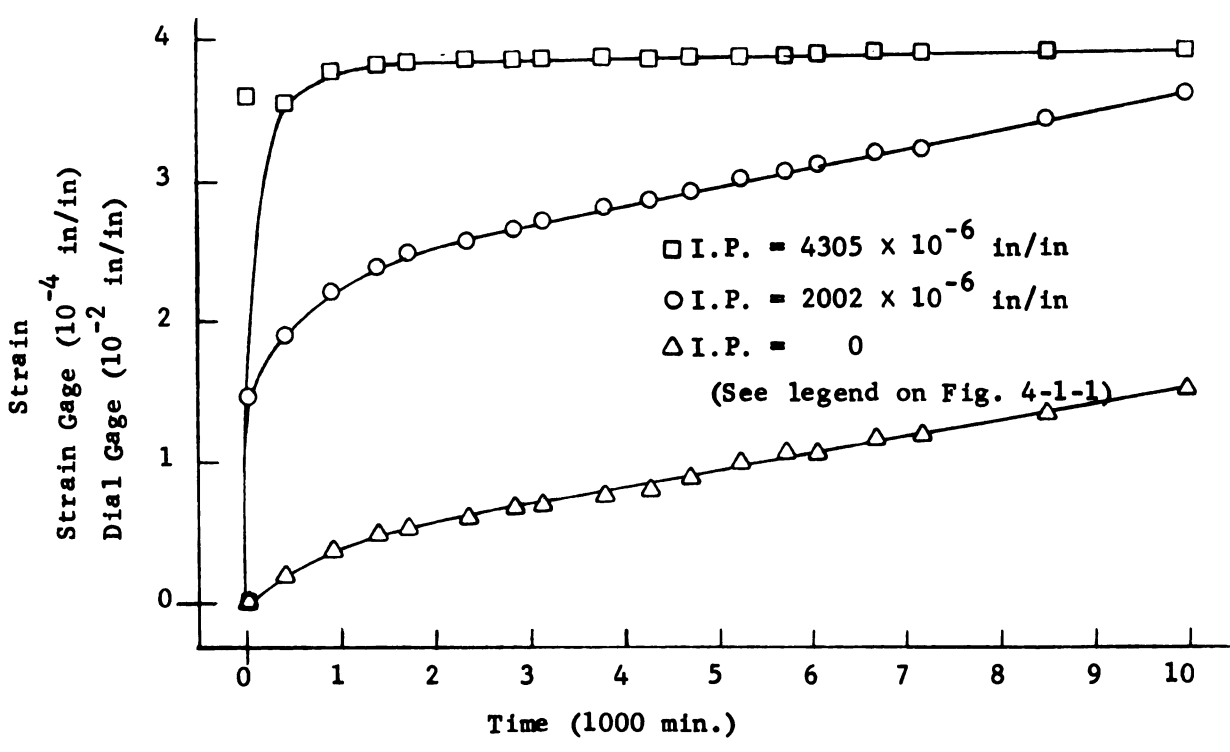


Fig. 4-1-11. Strain-Time Relationship at $\sigma_{\rm m}$ = 4000 psi τ = 300 psi

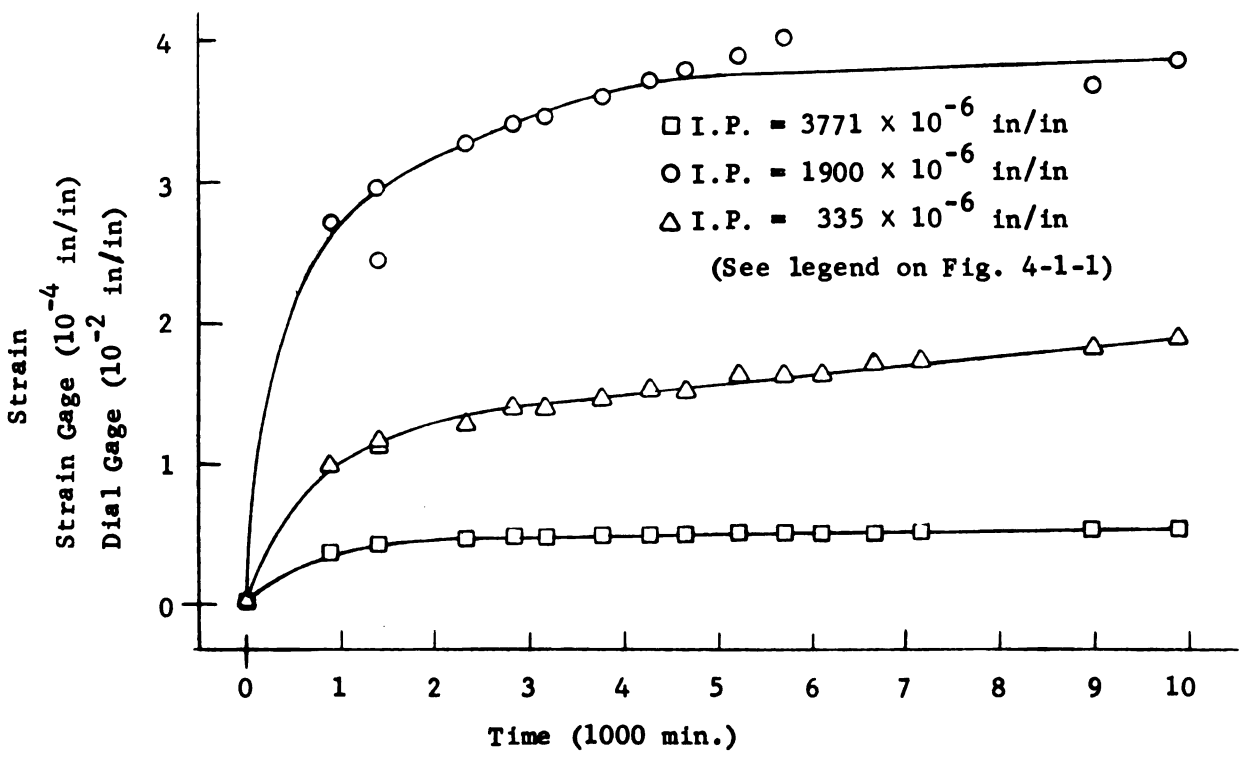


Fig. 4-1-12. Strain-Time Relationship at $\sigma_{\rm m}$ = 5000 psi τ = 300 psi

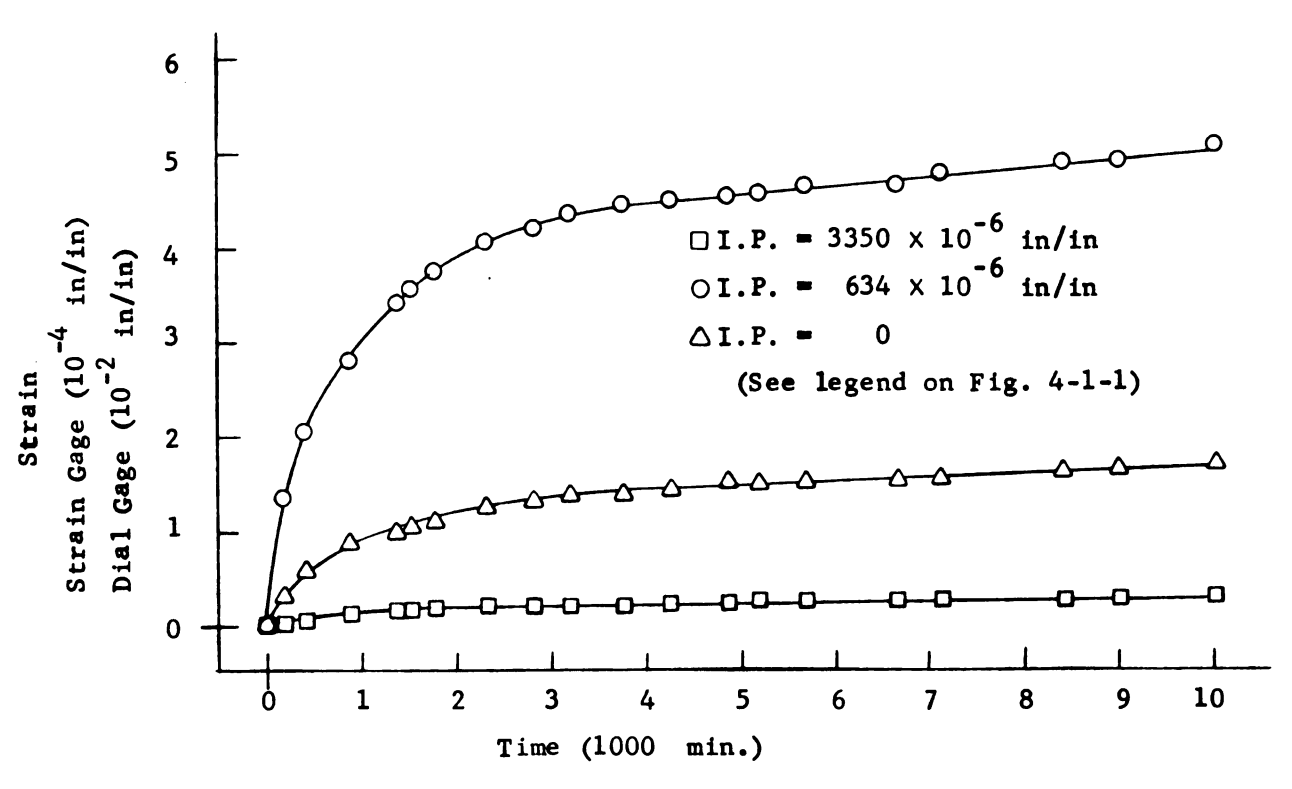


Fig. 4-1-13. Strain-Time Relationship at $\sigma_{\rm m}$ = 1000 psi τ = 500 psi

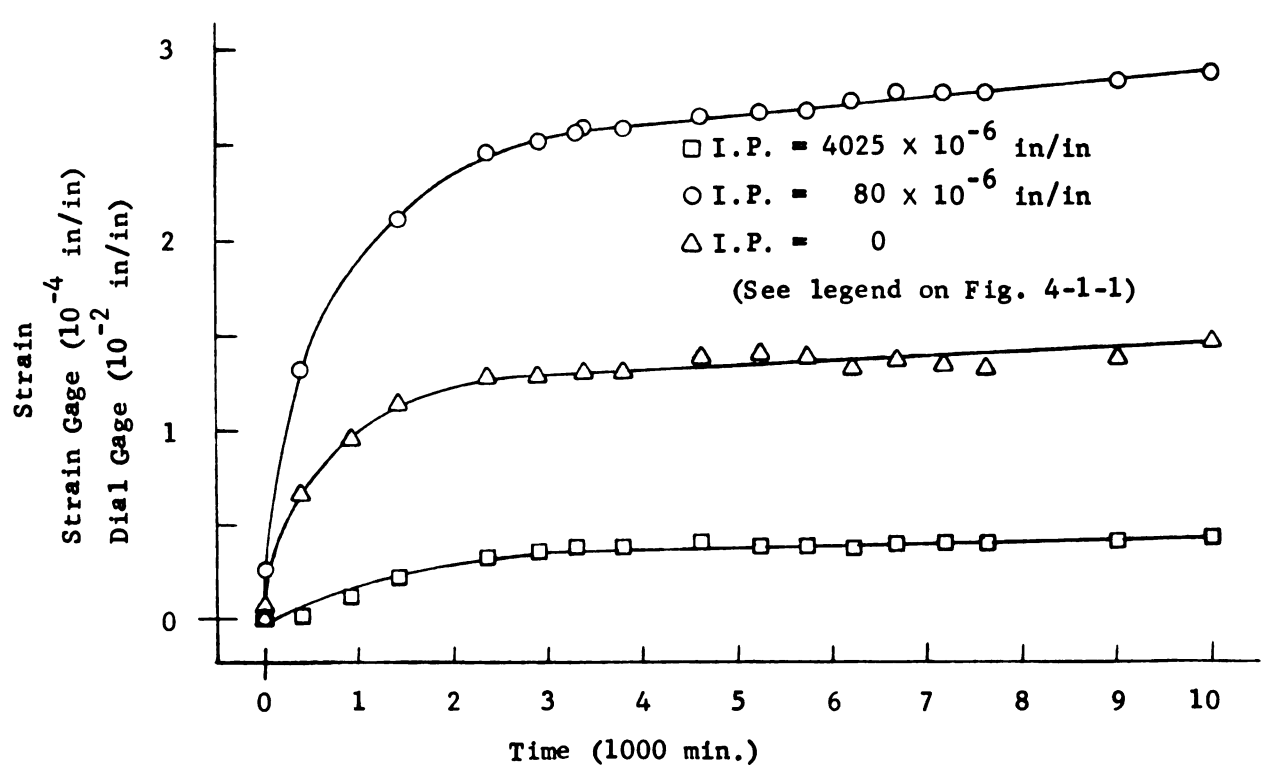


Fig. 4-1-14. Strain-Time Relationship at $\sigma_{\rm m}$ = 1350 psi τ = 500 psi

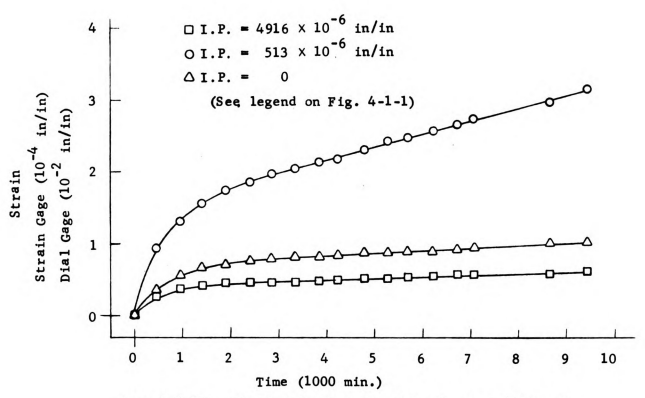


Fig. 4-1-15. Strain-Time Relationship at $\sigma_{\rm m}$ = 1700 psi $_{\rm T}$ = 500 psi

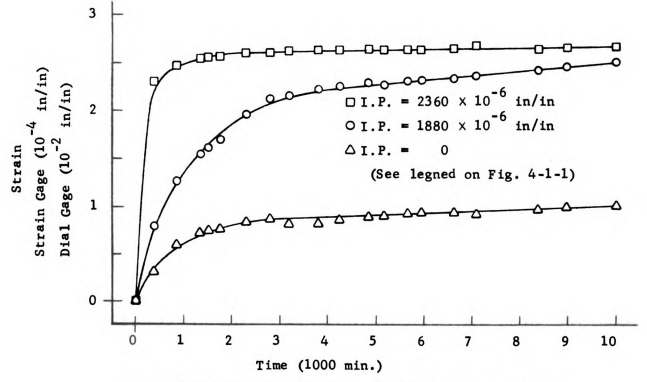


Fig. 4-1-16. Strain-Time Relationship at $\sigma_{\rm m}$ = 3000 psi $_{\rm T}$ = 500 psi

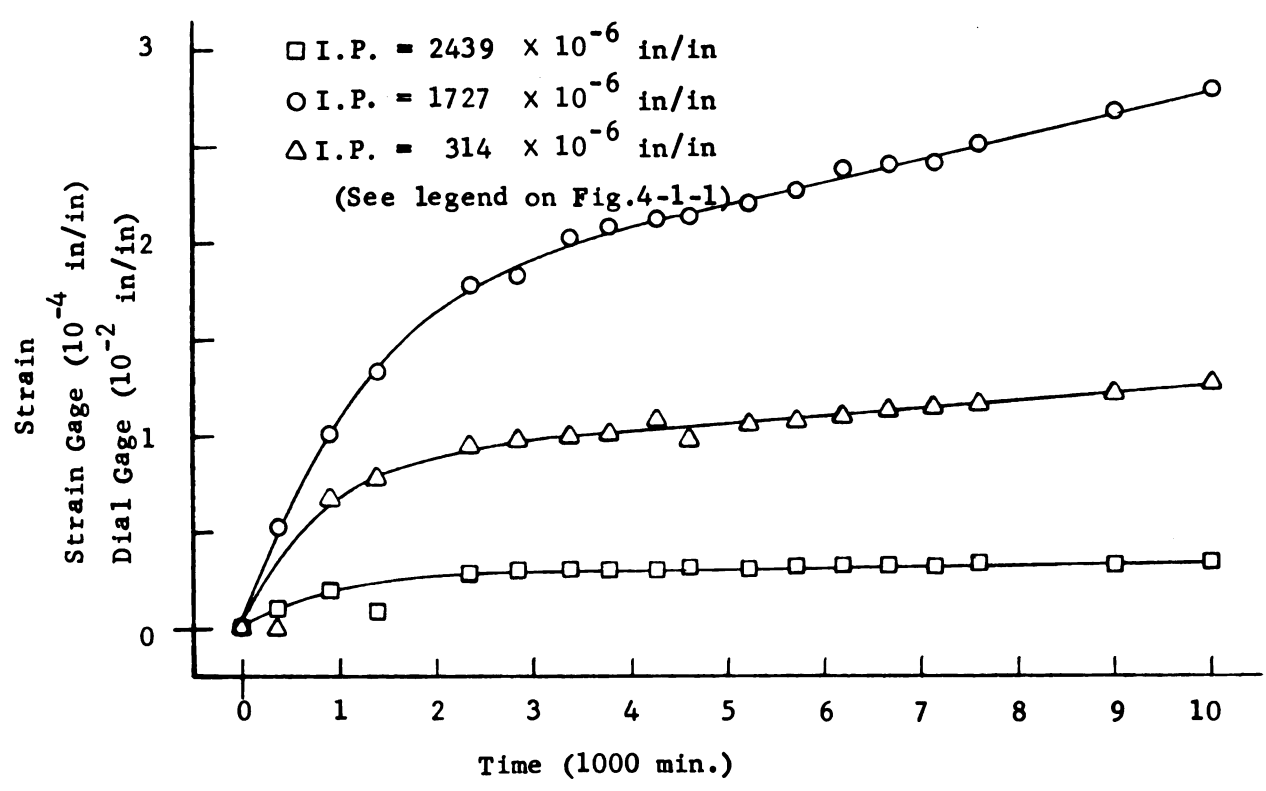


Fig. 4-1-17. Strain-Time Relationship at $\sigma_{\rm m}$ = 4000 psi τ = 500 psi

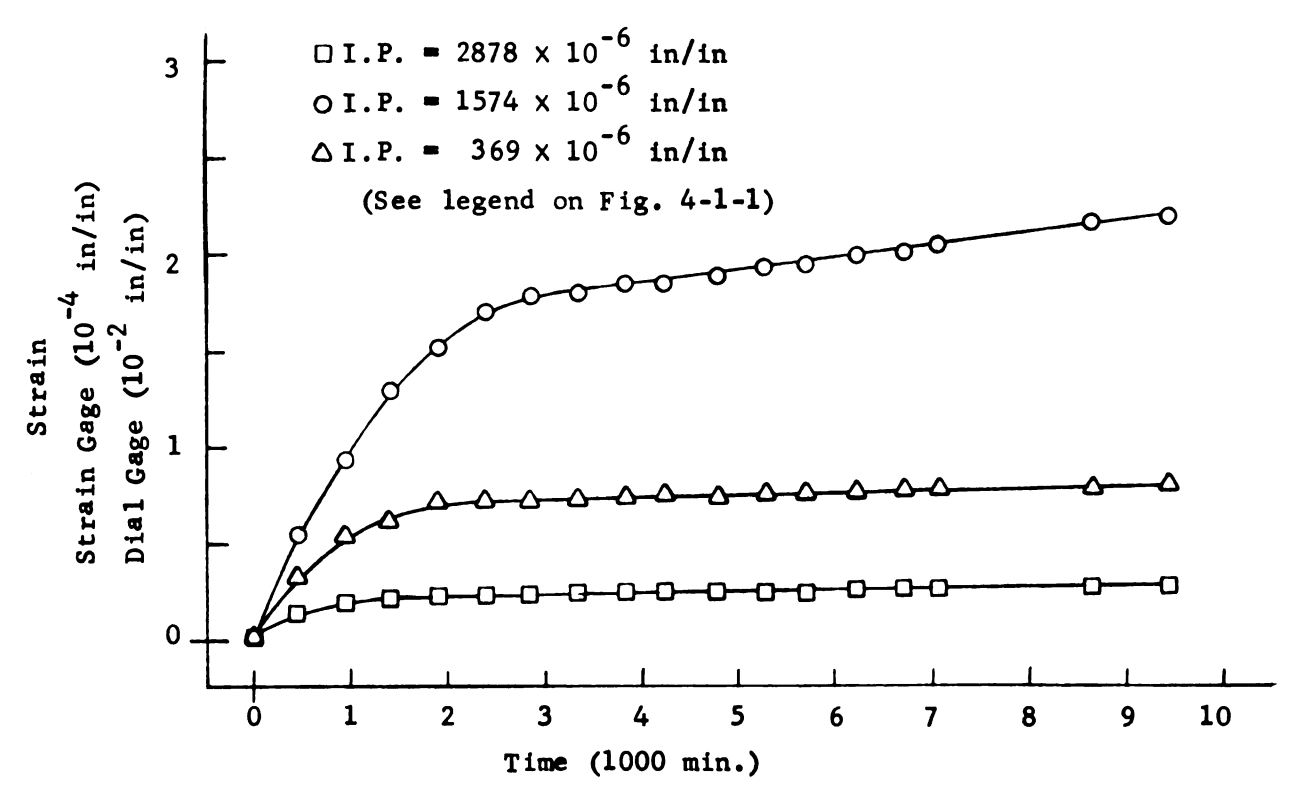


Fig. 4-1-18. Strain-Time Relationship at $\sigma_{\rm m}$ = 5000 psi τ = 500 psi

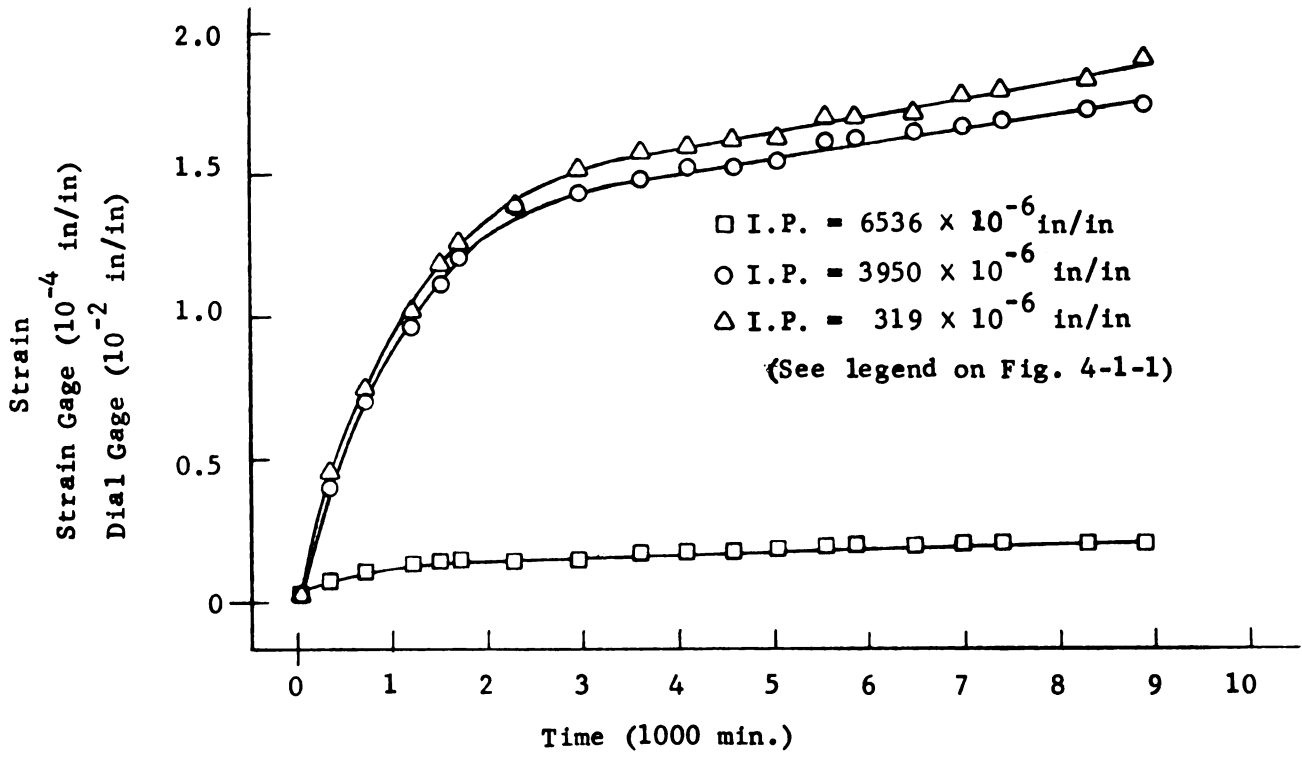


Fig. 4-1-19. Strain-Time Relationship at $\sigma_{\rm m}$ = 1000 psi τ = 700 psi

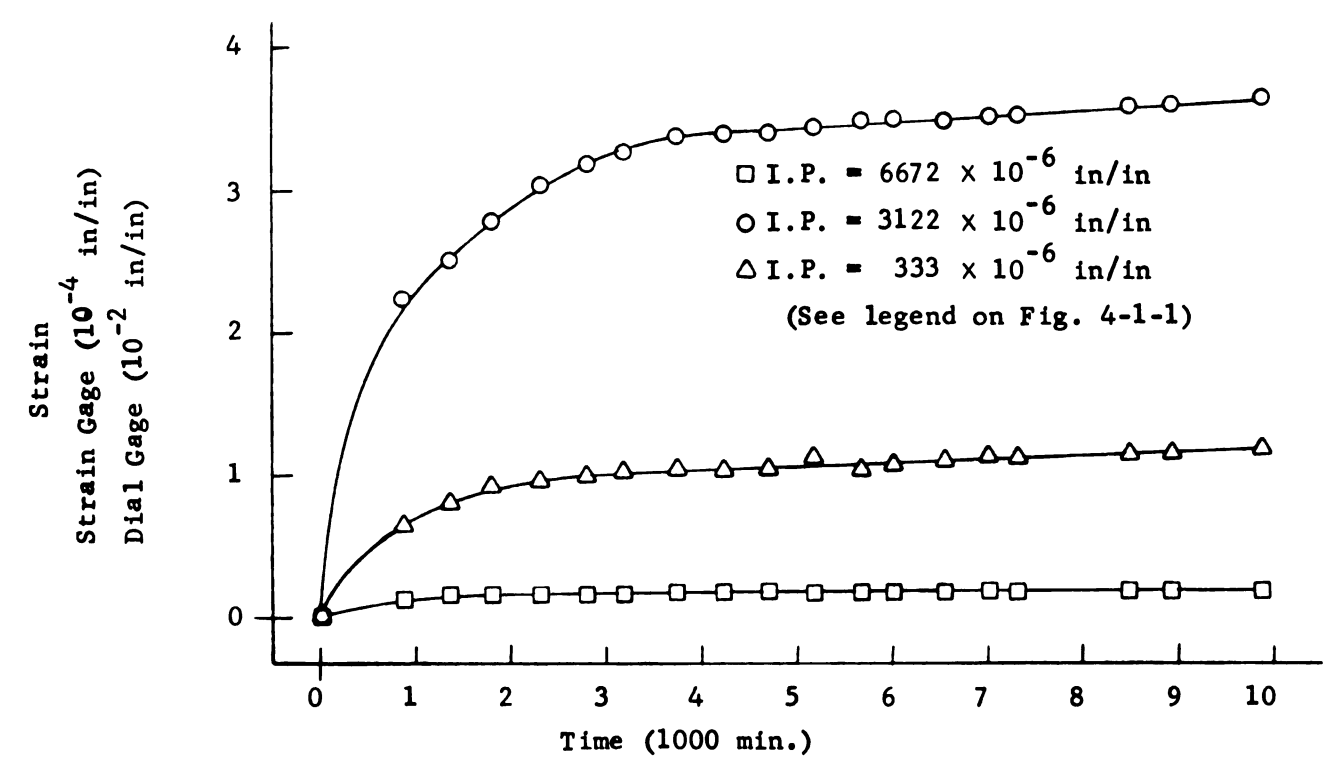


Fig. 4-1-20. Strain-Time Relationship at $\sigma_{\rm m}$ = 1350 psi τ = 700 psi

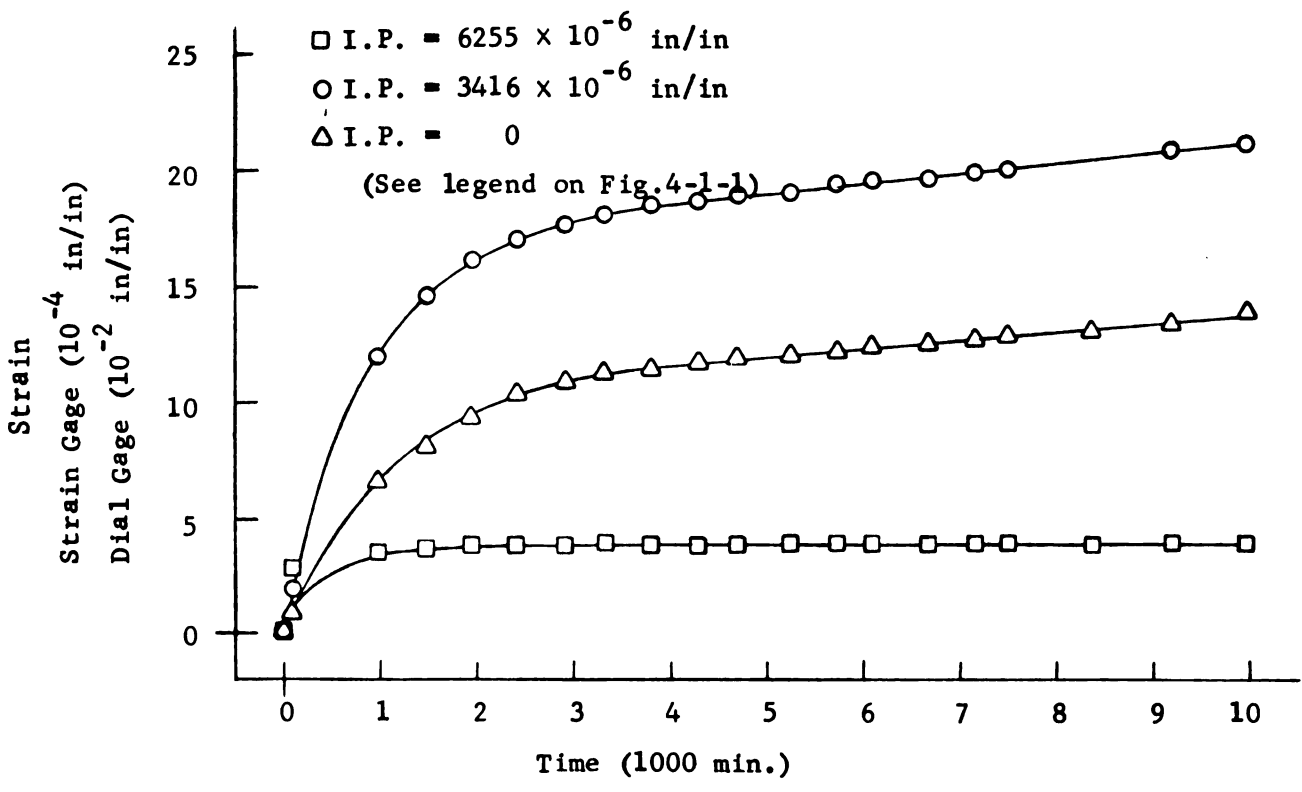


Fig. 4-1-21. Strain-Time Relationship at $\sigma_{\rm m}$ = 1700 psi τ = 700 psi

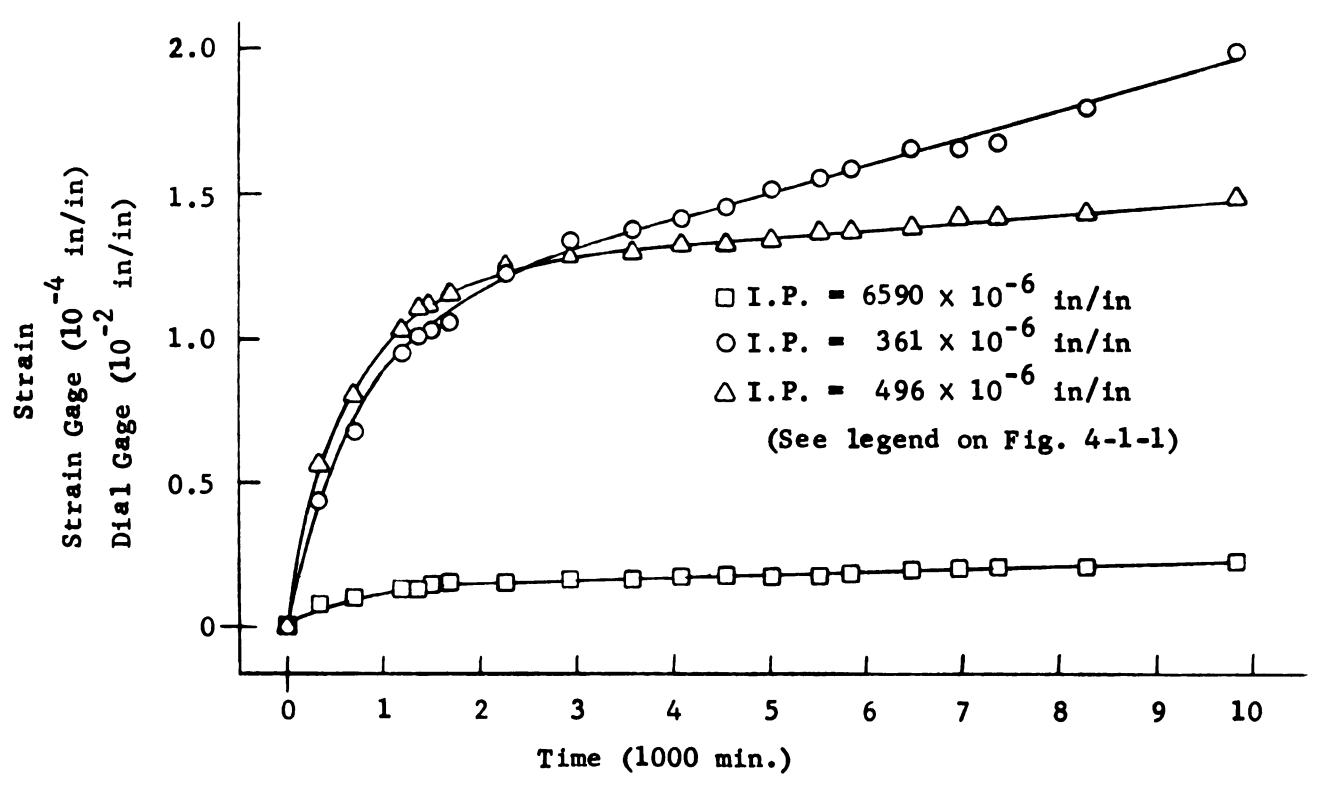


Fig. 4-1-22. Strain-Time Relationship at $\sigma_{\rm m}$ = 3000 psi τ = 700 psi

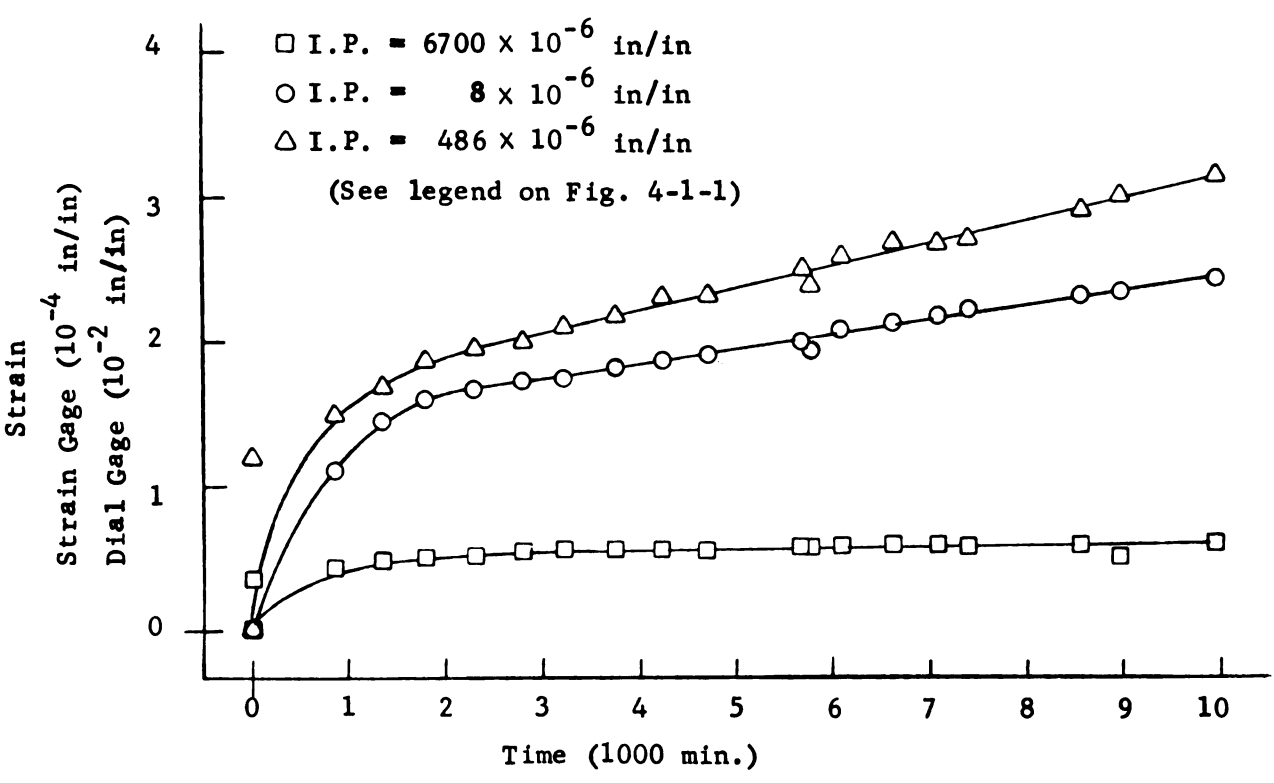


Fig. 4-1-23. Strain-Time Relationship at $\sigma_{\rm m}$ = 4000 psi τ = 700 psi

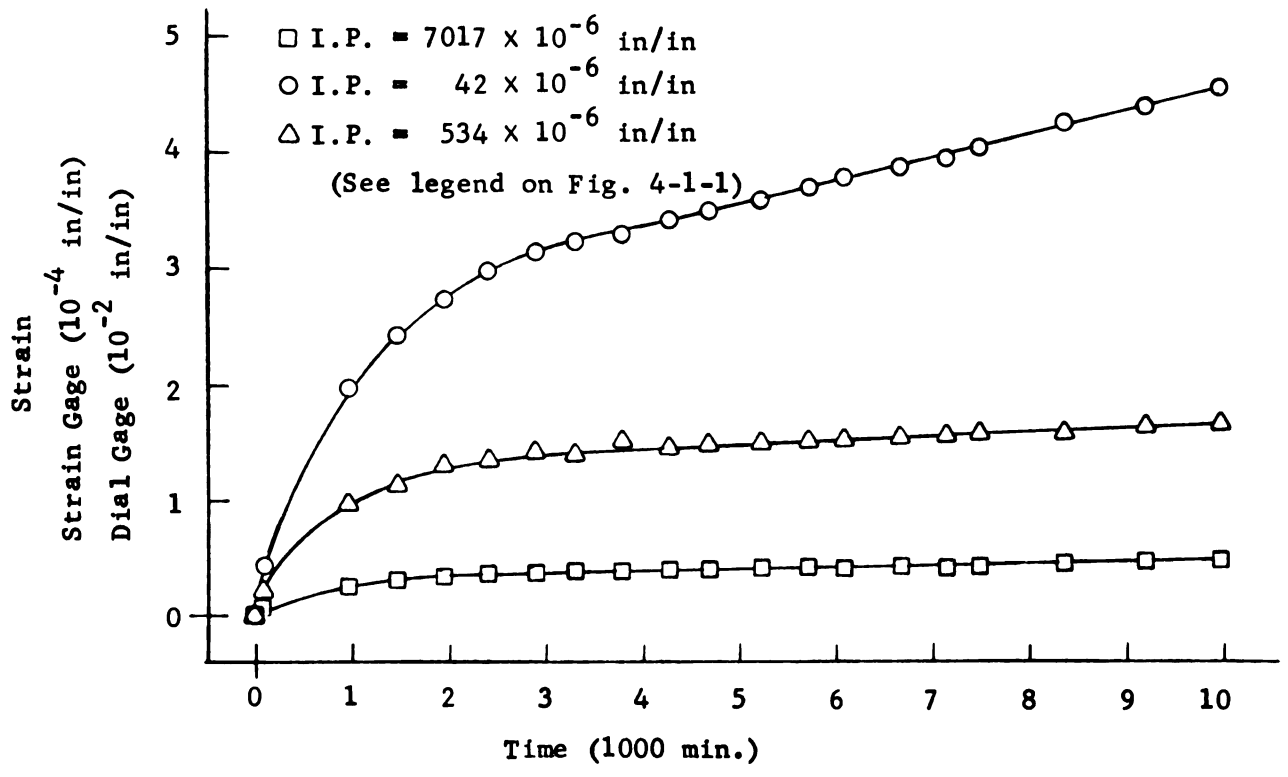


Fig. 4-1-24. Strain-Time Relationship at $\sigma_{\rm m} = 5000$ psi $\tau = 700$ psi

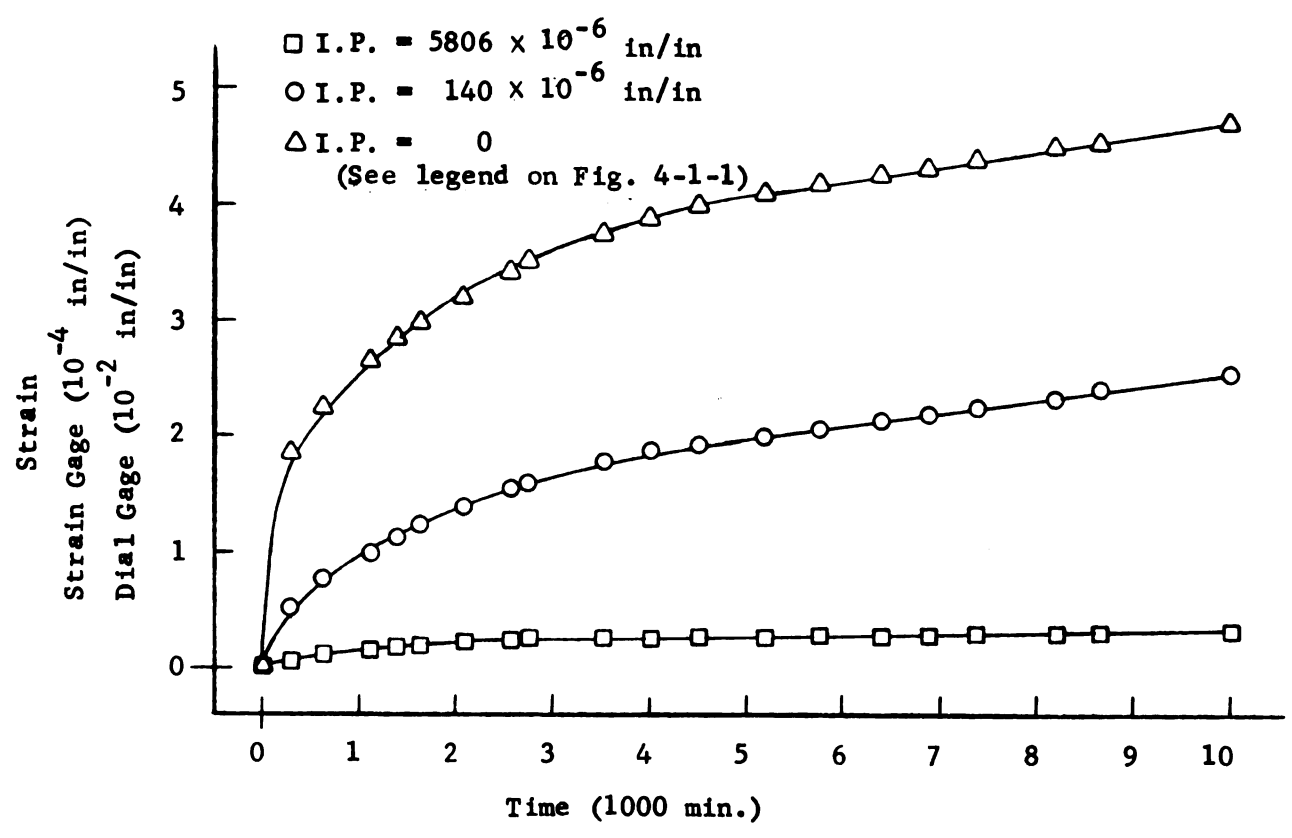


Fig. 4-1-25. Strain-Time Relationship at $\sigma_{\rm m}$ = 1000 psi τ = 1000 psi

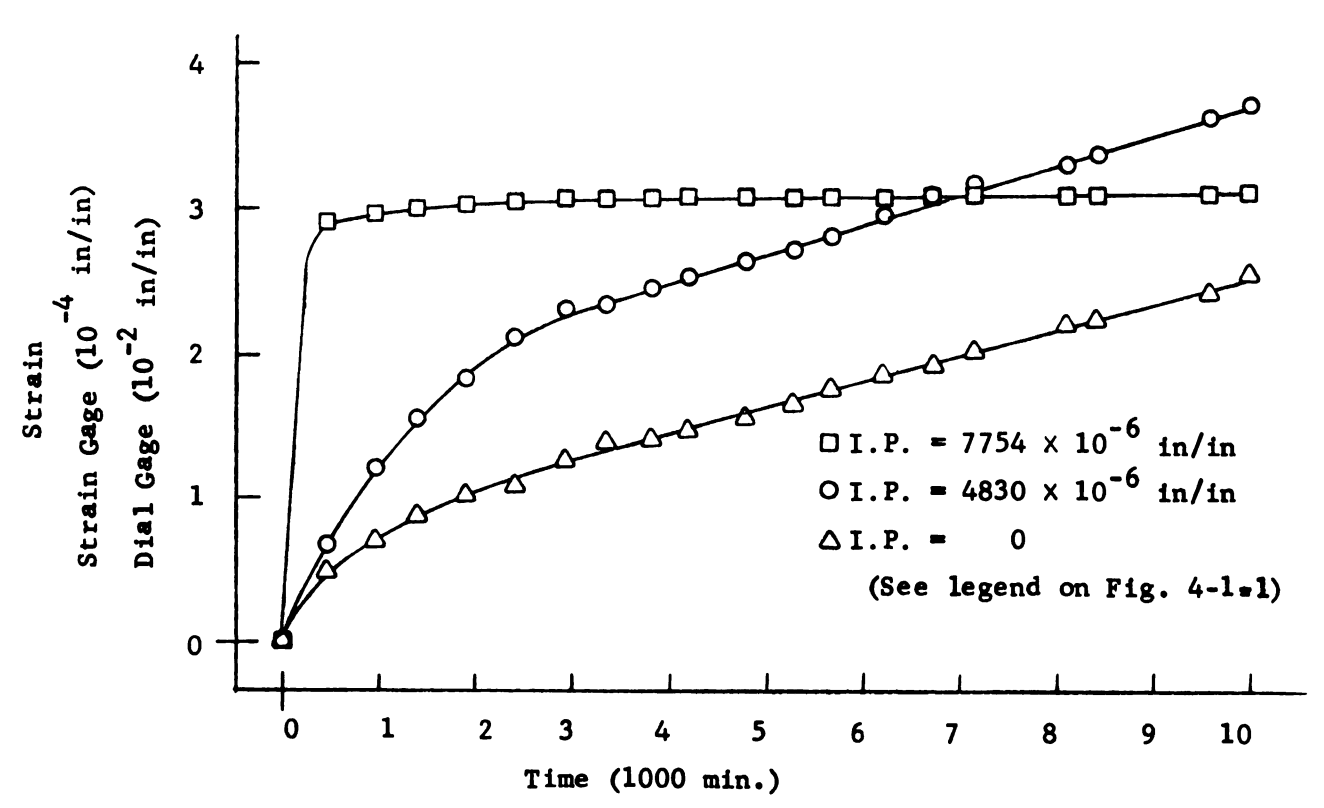


Fig. 4-1-26. Strain-Time Relationship at $\sigma_{\rm m}$ = 1350 psi τ = 1000 psi

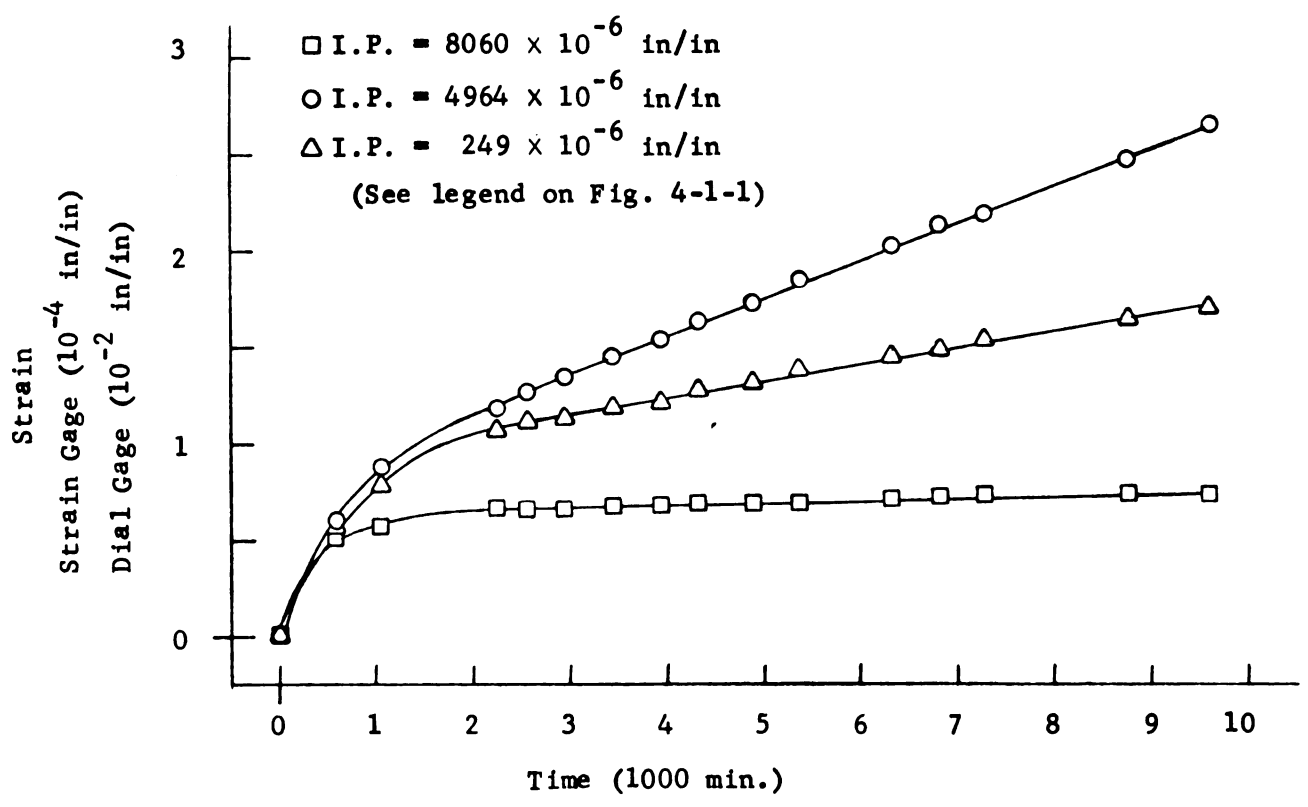


Fig. 4-1-27. Strain-Time Relationship at $\sigma_{\rm m}$ = 1700 psi τ = 1000 psi

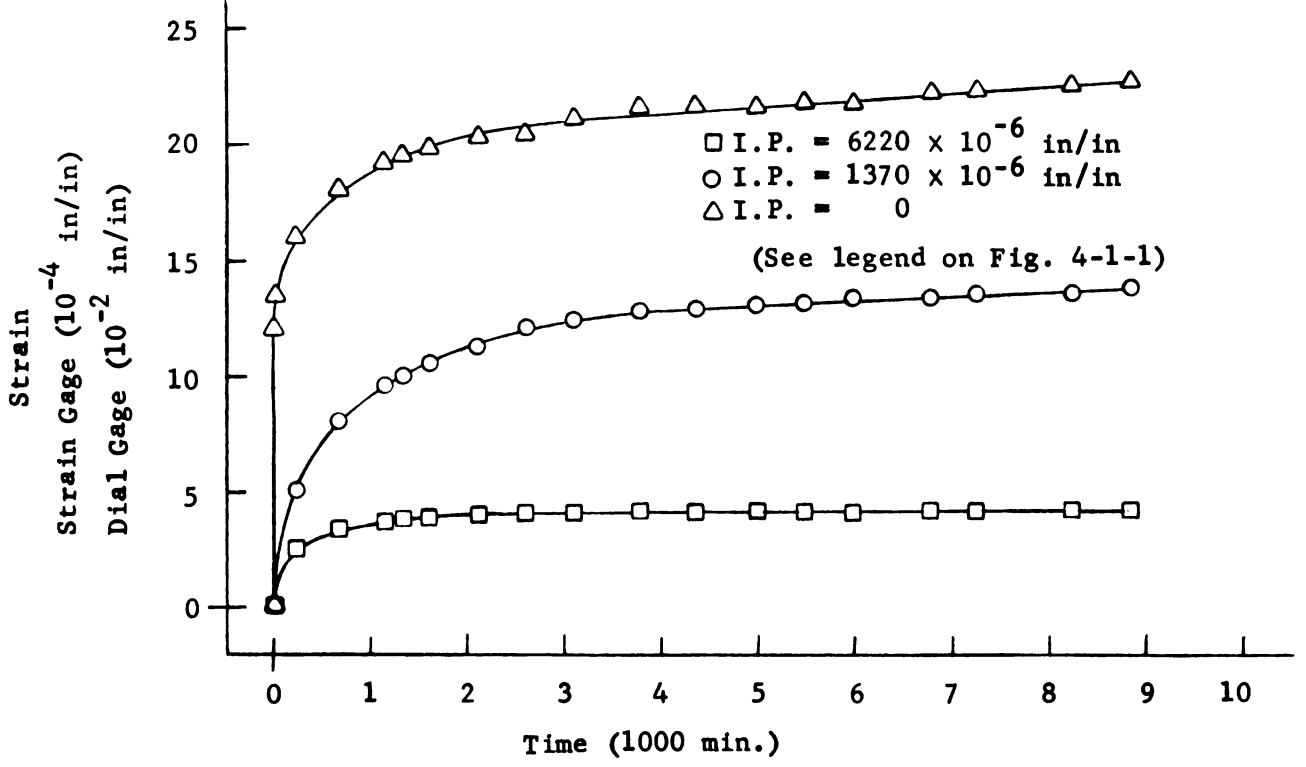


Fig. 4-1-28. Strain-Time Relationship at $\sigma_{\rm m}$ = 3000 psi τ = 1000 psi

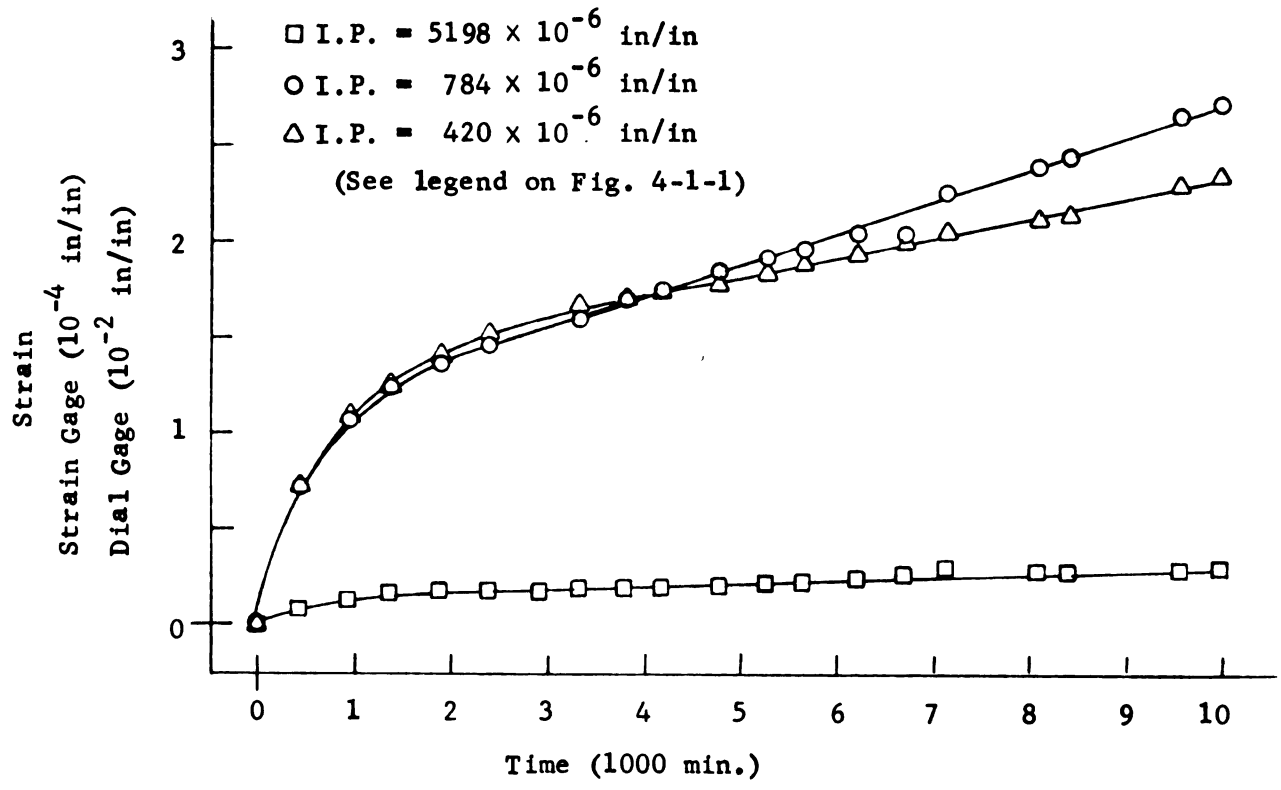


Fig. 4-1-29. Strain-Time Relationship at $\sigma_{\rm m}$ = 4000 psi τ = 1000 psi

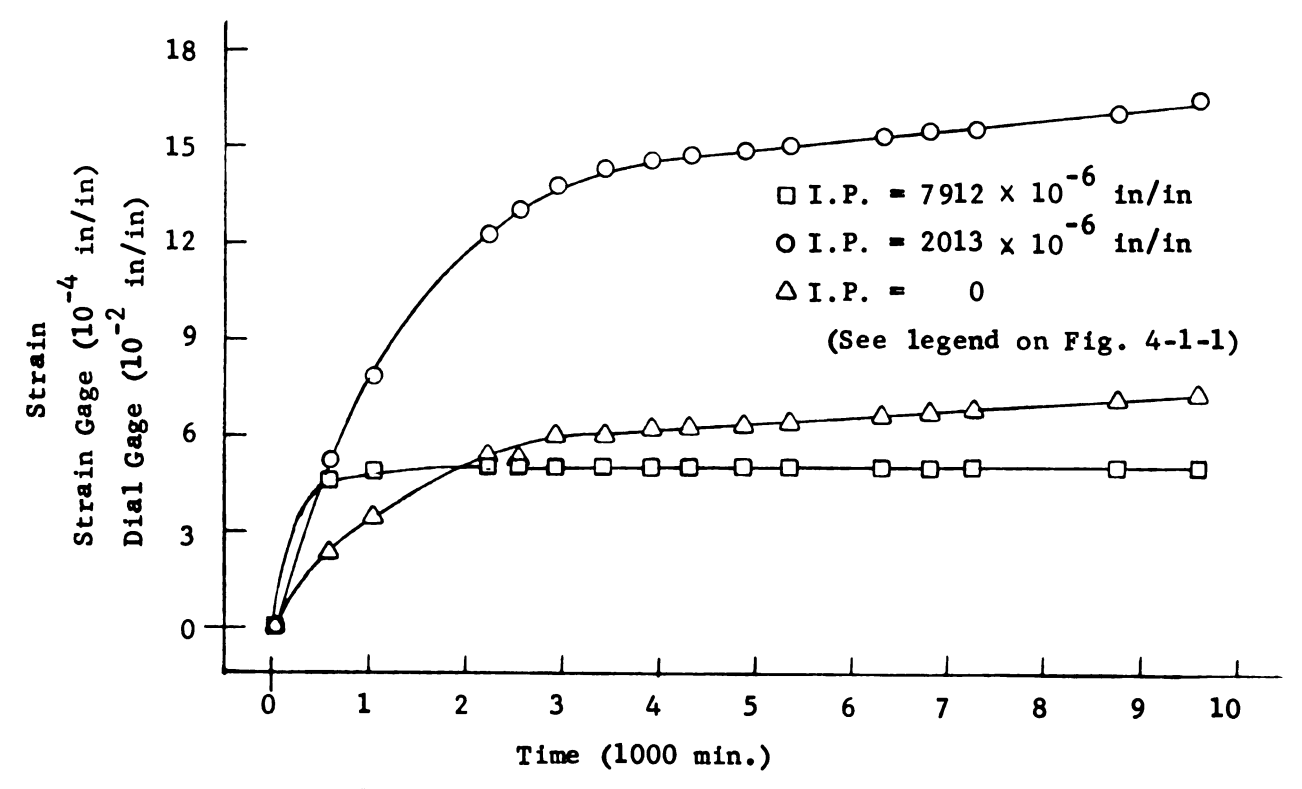


Fig. 4-1-30. Strain-Time Relationship at $\sigma_{\rm m}$ = 5000 psi τ = 1000 psi

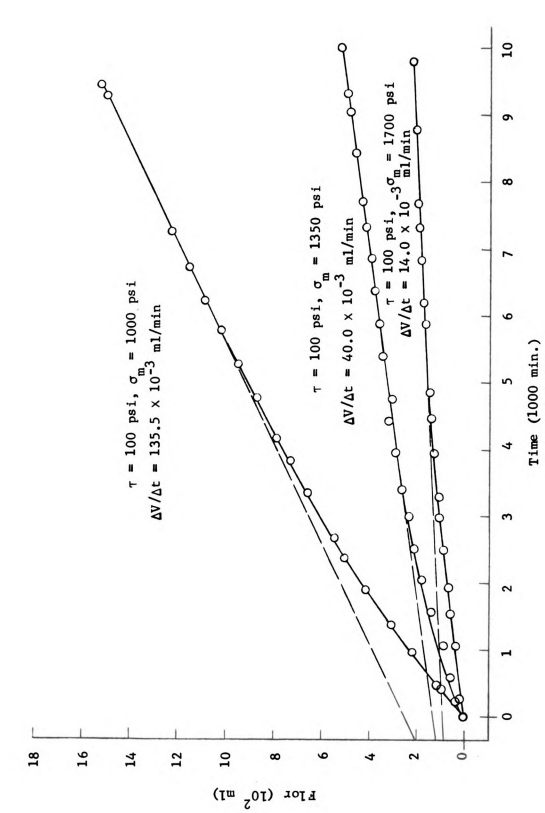


Fig. 4-2-1. Flow-Time Relationship at Various Stress Levels

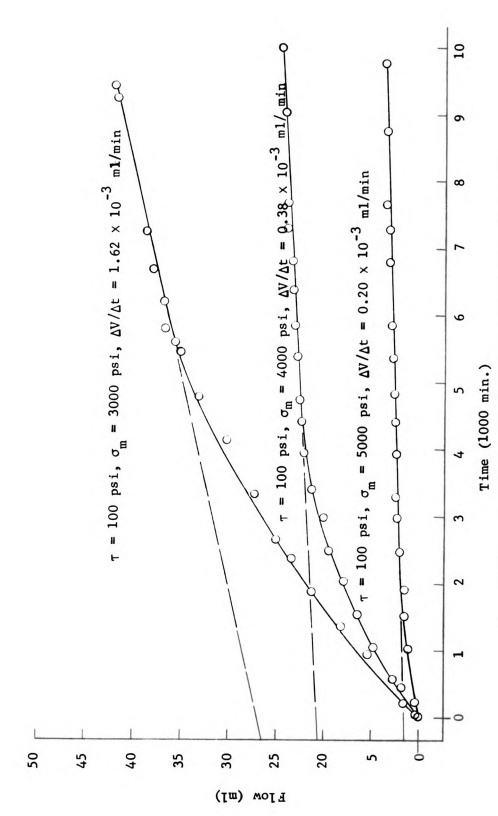
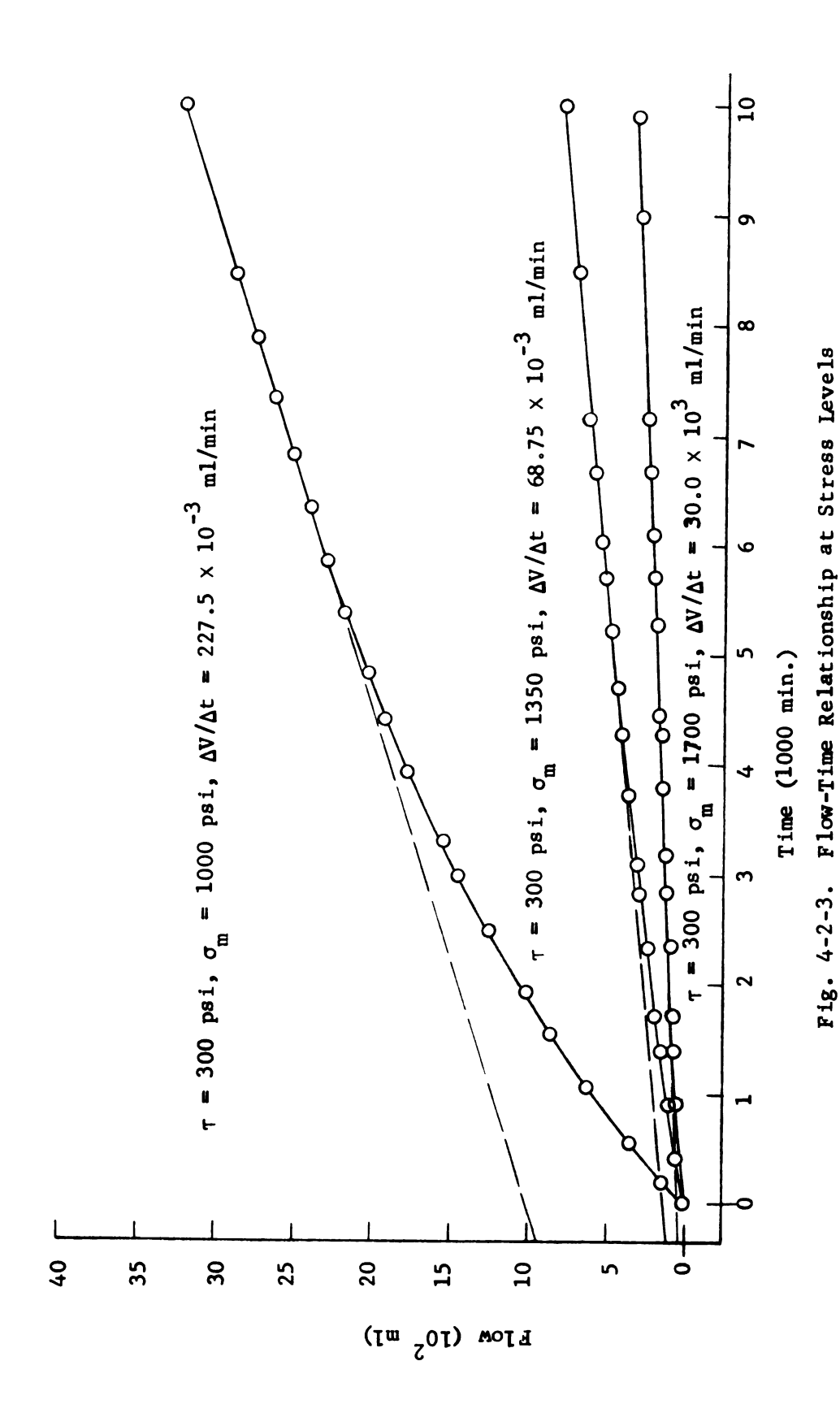
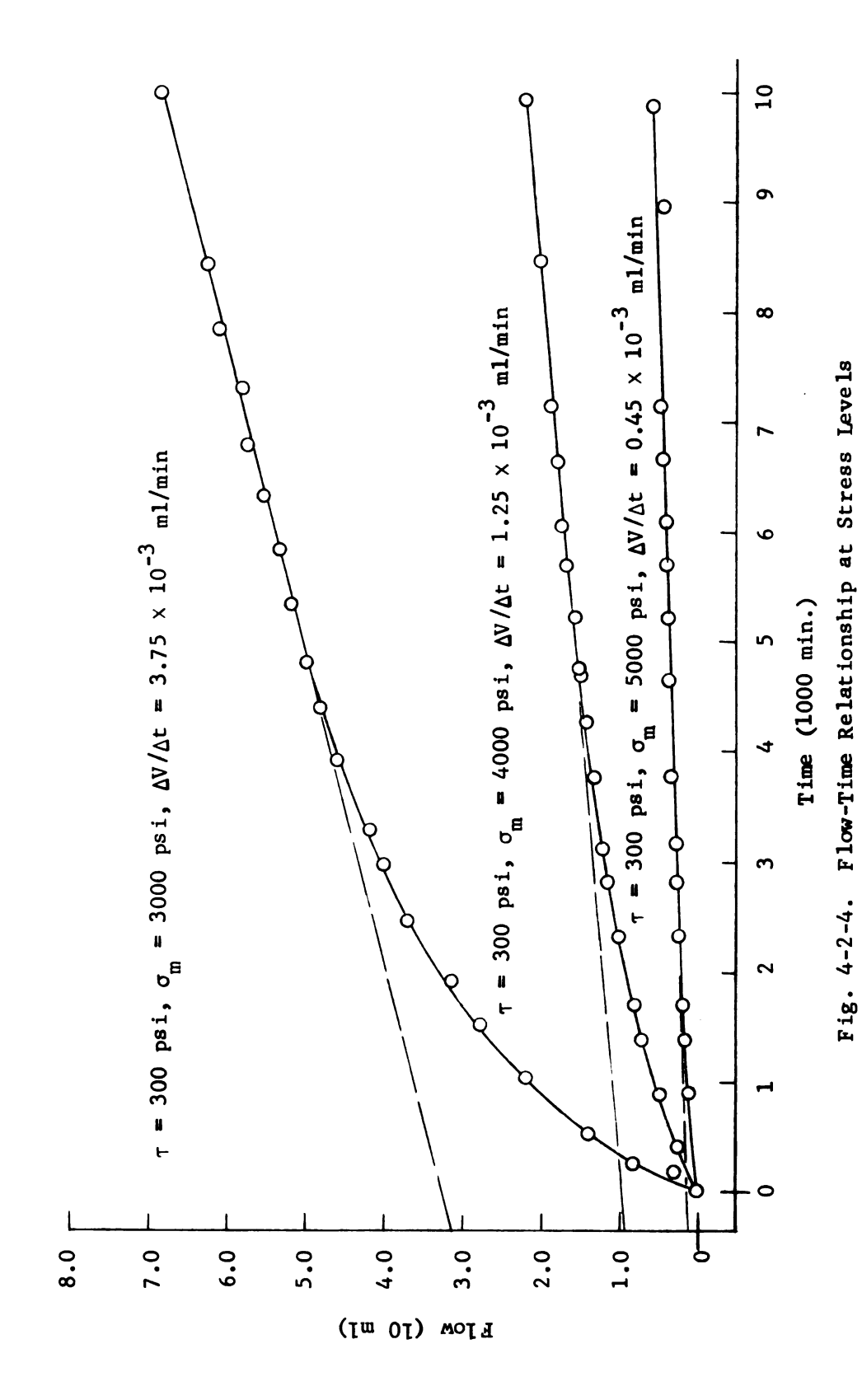


Fig. 4-2-2. Flow-Time Relationship at Various Stress Levels





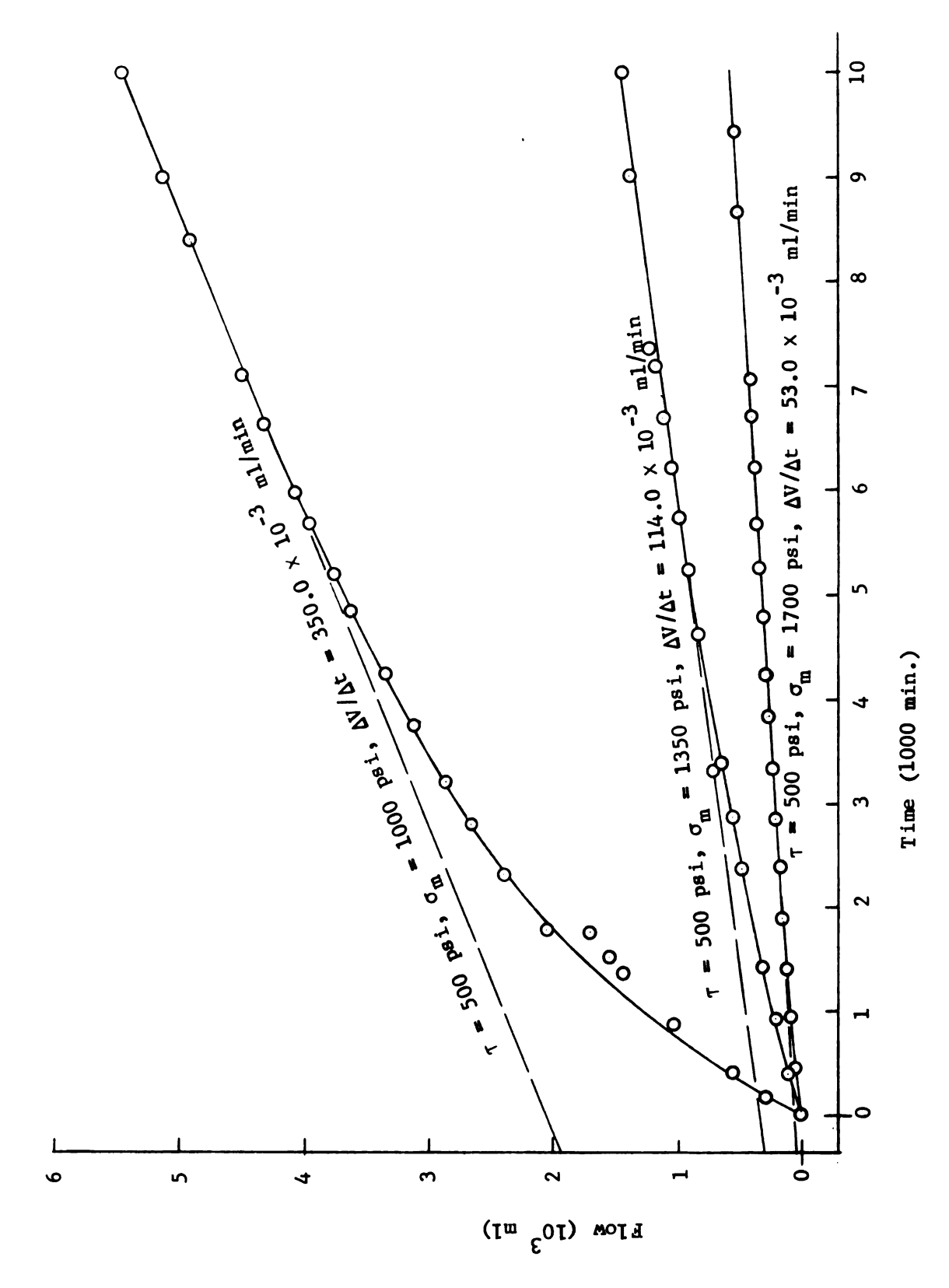


Fig. 4-2-5. Flow-Time Relationship at Stress Levels

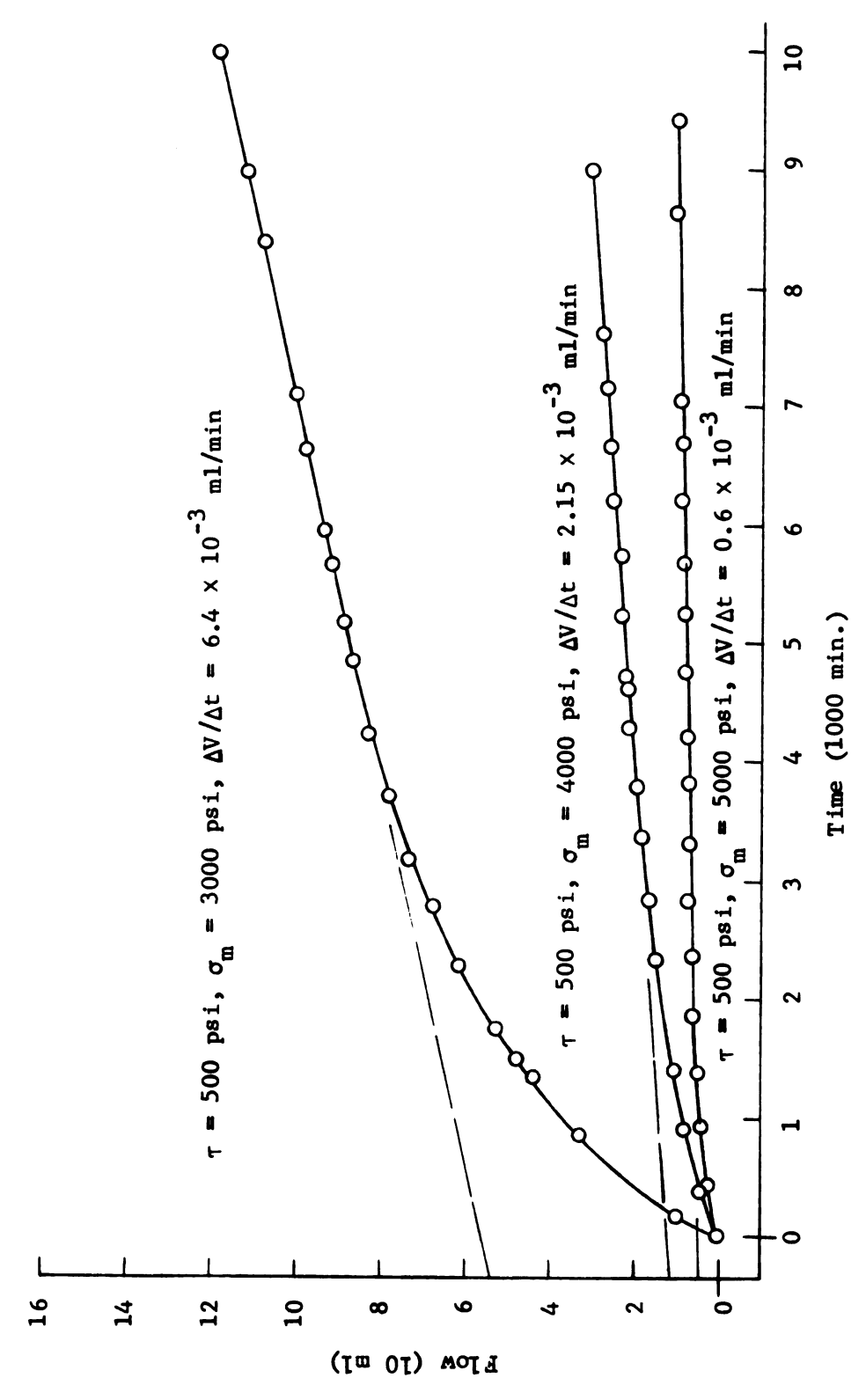
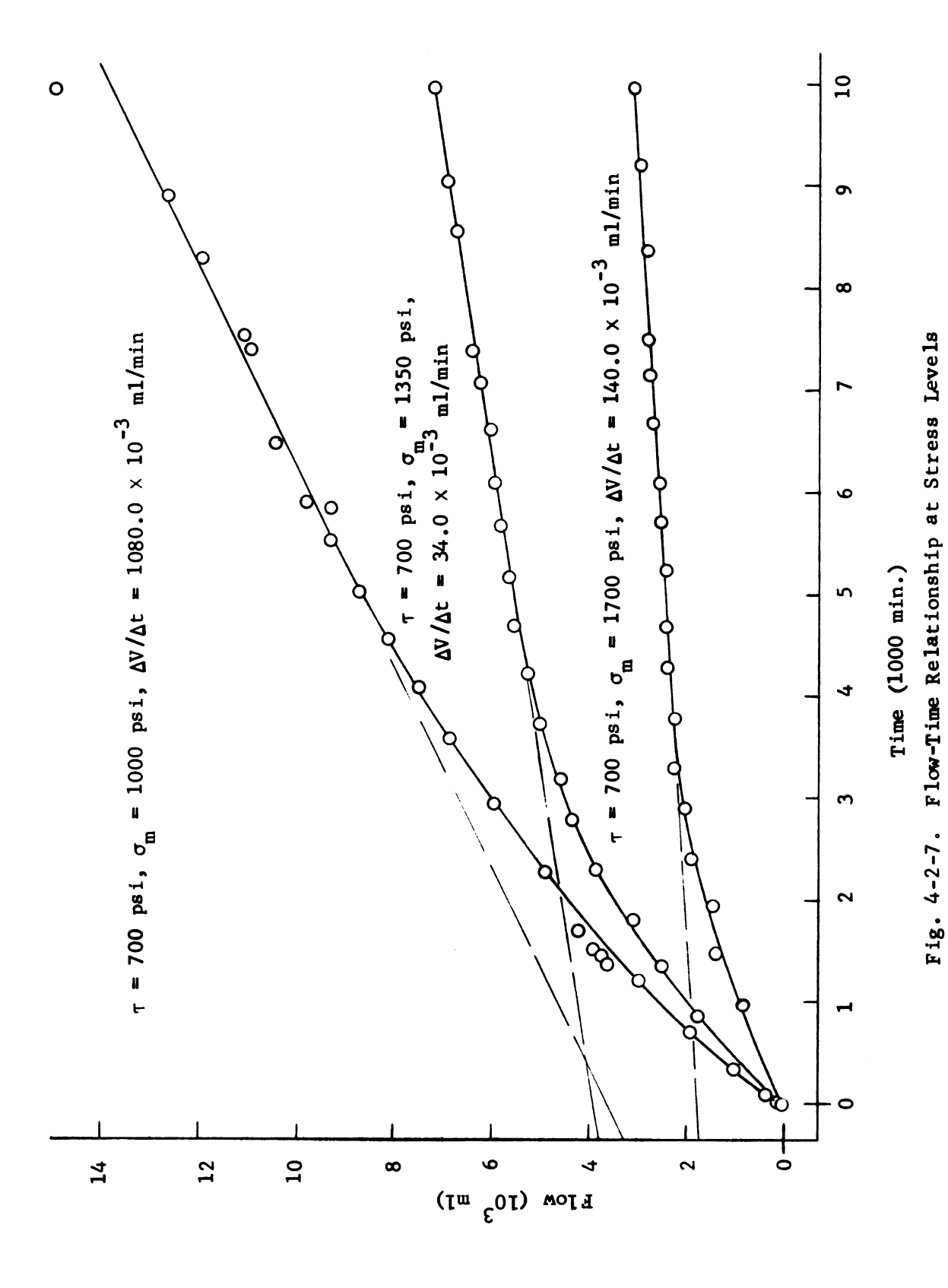
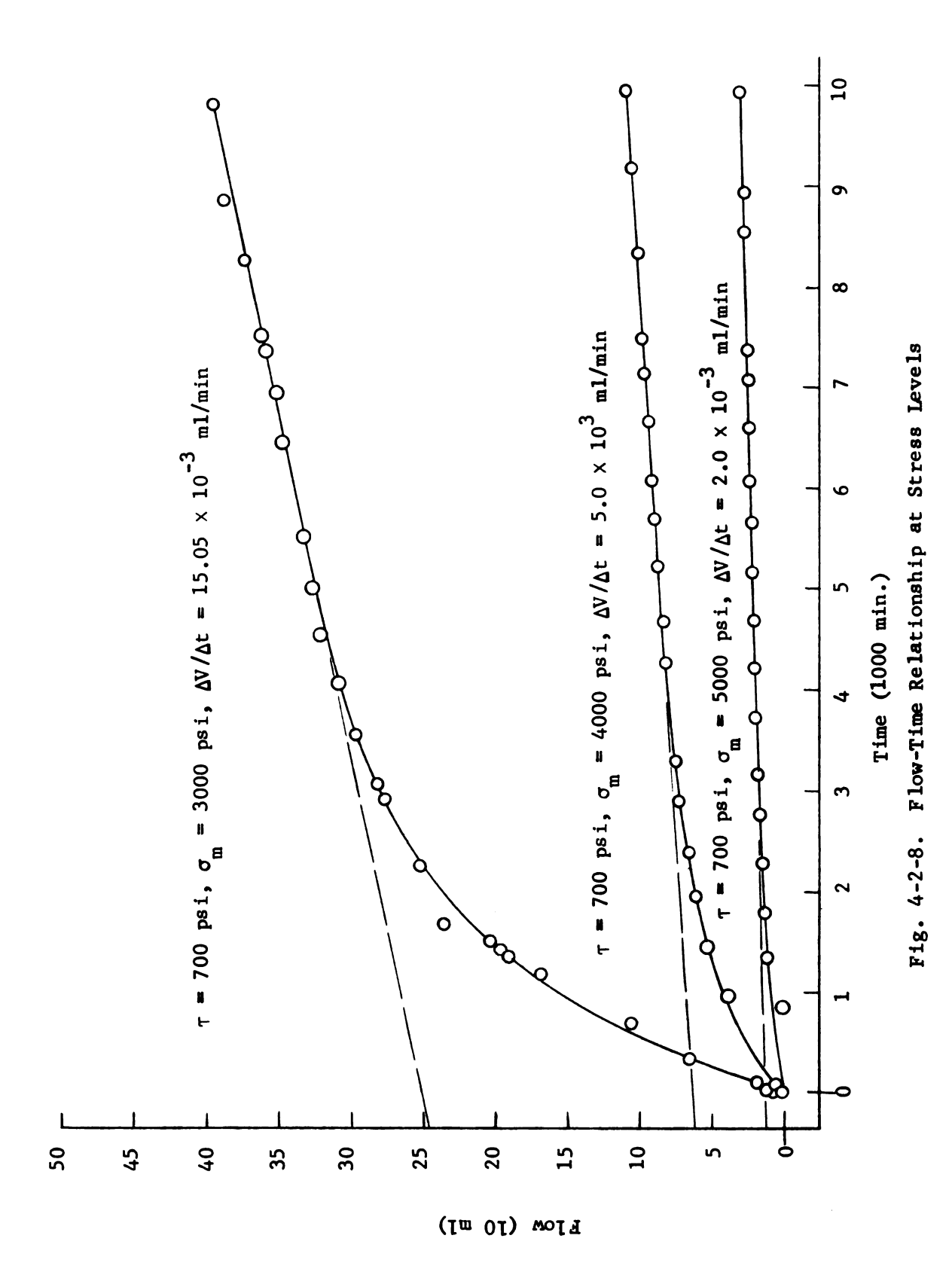
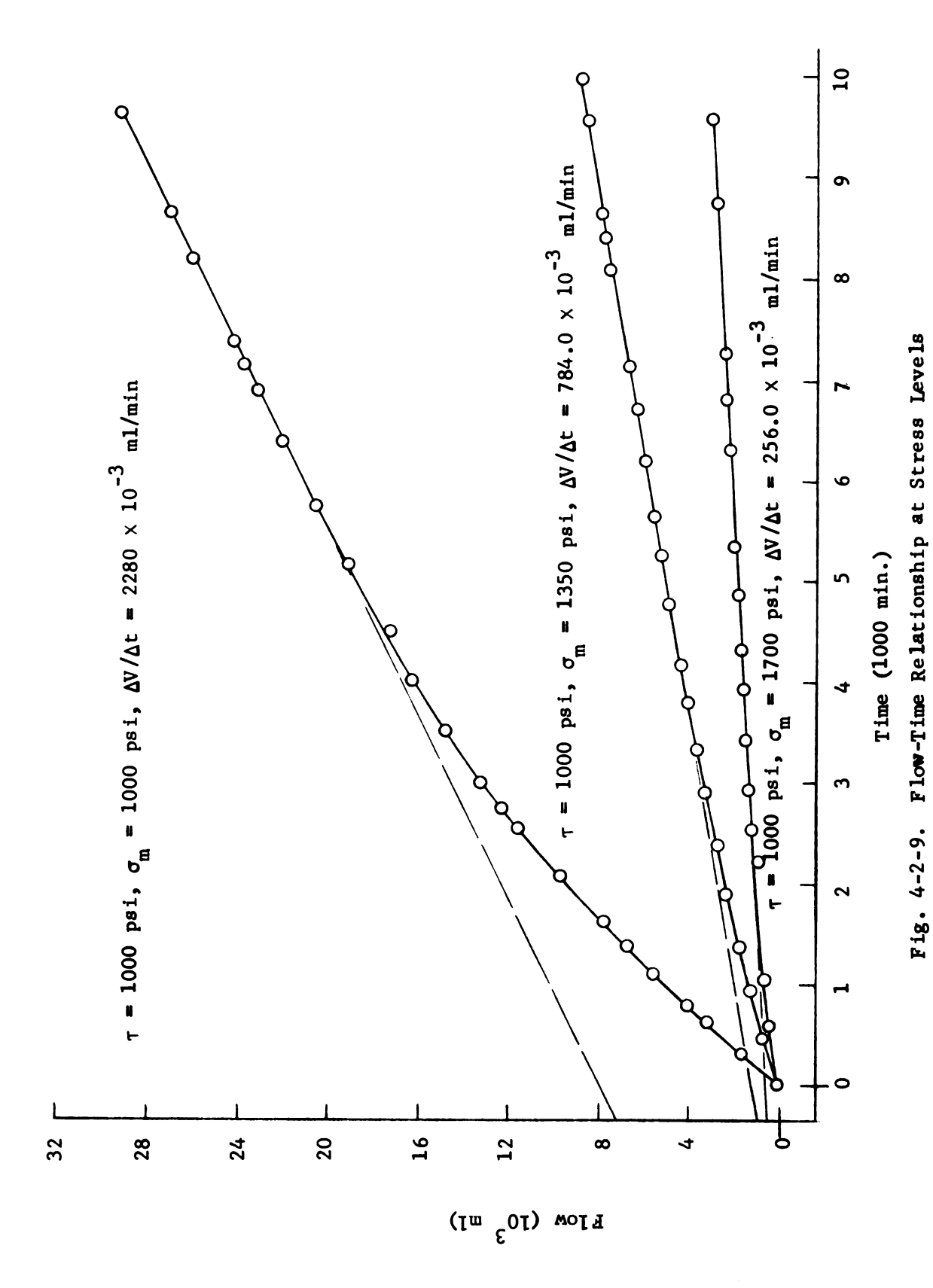
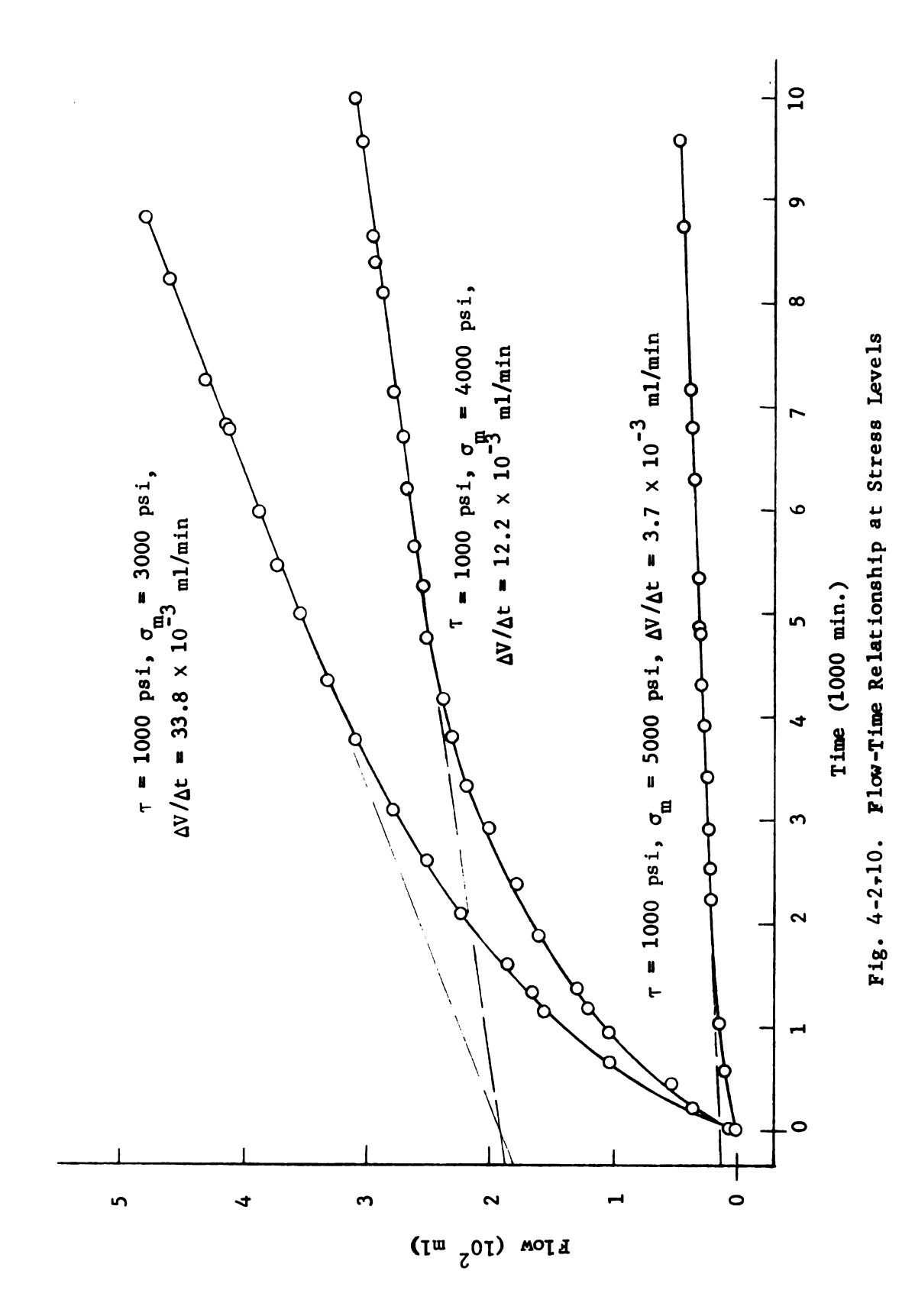


Fig. 4-2-6. Flow-Time Relationship at Stress Levels









CHAPTER V

STRESS AND STRAIN EFFECTS ON PERMEABILITY OF THE ROCK SALT

Stress Field

The flow of kerosene through rock salt decreased with time until steady state flow was reached. The rate of decrease was highest for the early stages of transient flow. As shown by Fig. 4-2-1 to Fig. 4-2-10, time periods greater than about 5,000 minutes were required to reach constant flow rates for all the stress conditions. Individual tests were run for 10,000 minutes to obtain the coefficient of permeability. The coefficient of permeability, k, was determined by observing the rate of flow equal to $\Delta V/\Delta t$. Then, according to Darcy's law, the flow rate is:

$$q = \Delta V/\Delta t = vA = k i A$$
 5.1

where $\Delta V = volume of flow$

 $\Delta t = time$

v = discharge velocity

k = permeability, ft/sec

A = cross-sectional area of sample, ft²

i = hydraulic gradient

The value of iA was constant and equal to 57 ft or all experiments with one exception for the test using the highest pressure

condition, $\sigma_{\rm m}$ = 5000 psi, where iA equals 32 ft².

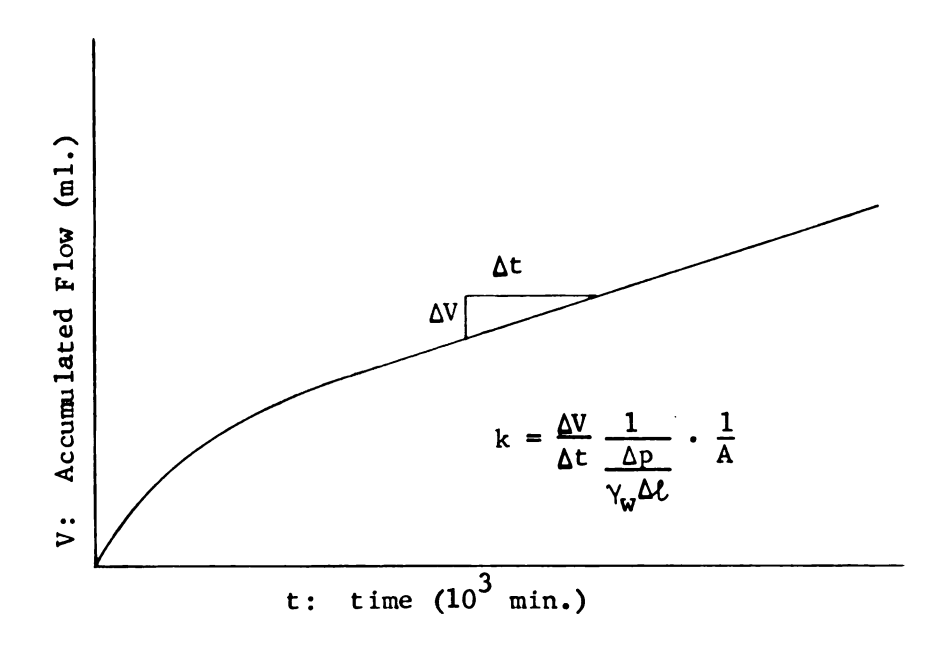


Fig. 5-1. Typical Curve Showing Time Versus Accumulated Flow.

The pore space in the rock salt contains kerosene at a pressure denoted by P. If the 'total' stress acting in a given direction at any point in the rock salt is σ , the problem is to know in what manner the 'effective' stress, denoted by σ' , is related to P and σ . The effective stress is, by definition (Skempton, 1961) the stress controlling changes in volume of soil. Change in total volume changes the volume of the pore space which is directly related to permeability.

The common opinion (Skempton, 1961) is that the effective stress is actually the intergranular stress acting between the

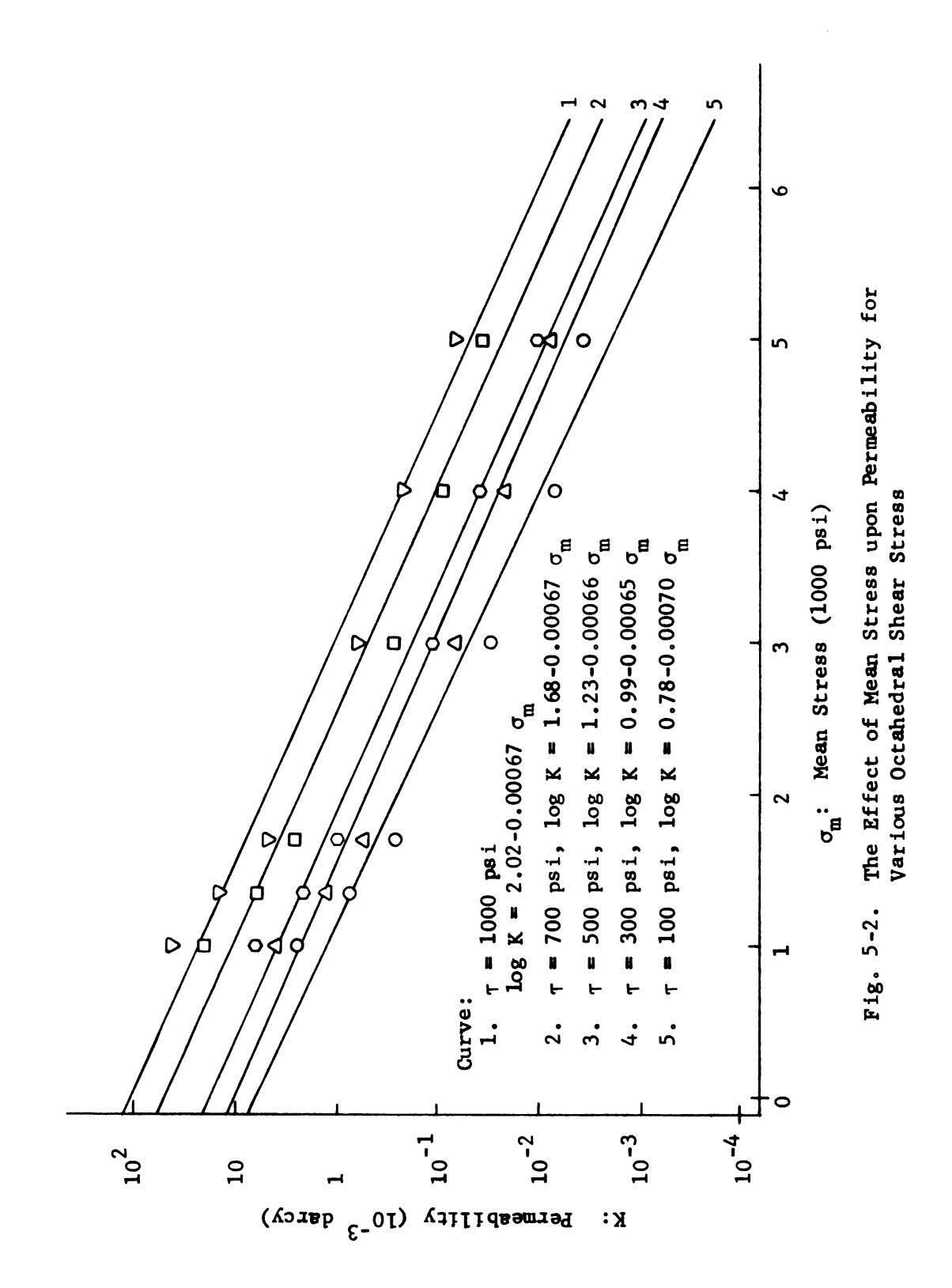
particles comprising the porous material. Skempton (1961) shows that this stress is

$$\sigma' = \sigma - (1 - a)P$$
 5.2

where a is the area of contact between the particles, per unit gross area of the material. For soils, in the stress range for practical problems, the value a is very small and can be neglected. For rock salt and the larger stresses used in this project the value of a is unknown. In the permeability tests reported, the seepage pressure decreases to almost zero at the exit end of the sample. For P = 0, the total stress will approximately equal the effective stress. For this case total stresses can be used for strain calculations. For this research, total stresses are much larger than fluid pressures and therefore will approximate the effective stresses. For field problems where P can be quite large this assumption may not be tenable and actual effective stresses will be required for stress-strain relationships.

The relationship between coefficient of permeability, mean stress, and octahedral shearing stress is summarized in Figs. 5-2, 3, 4, and 5.

The experimental data show that the coefficient of permeability of rock salt decreases with increasing mean stress and increases with increasing octahedral shearing stress. The data summarized in Fig. 5-1 can be formulated into an equation for predicting the permeability for a range of different stress conditions. Using the method of least-squares analysis and the computer the experimental points, curves 1 through 6, can be expressed by the relationship



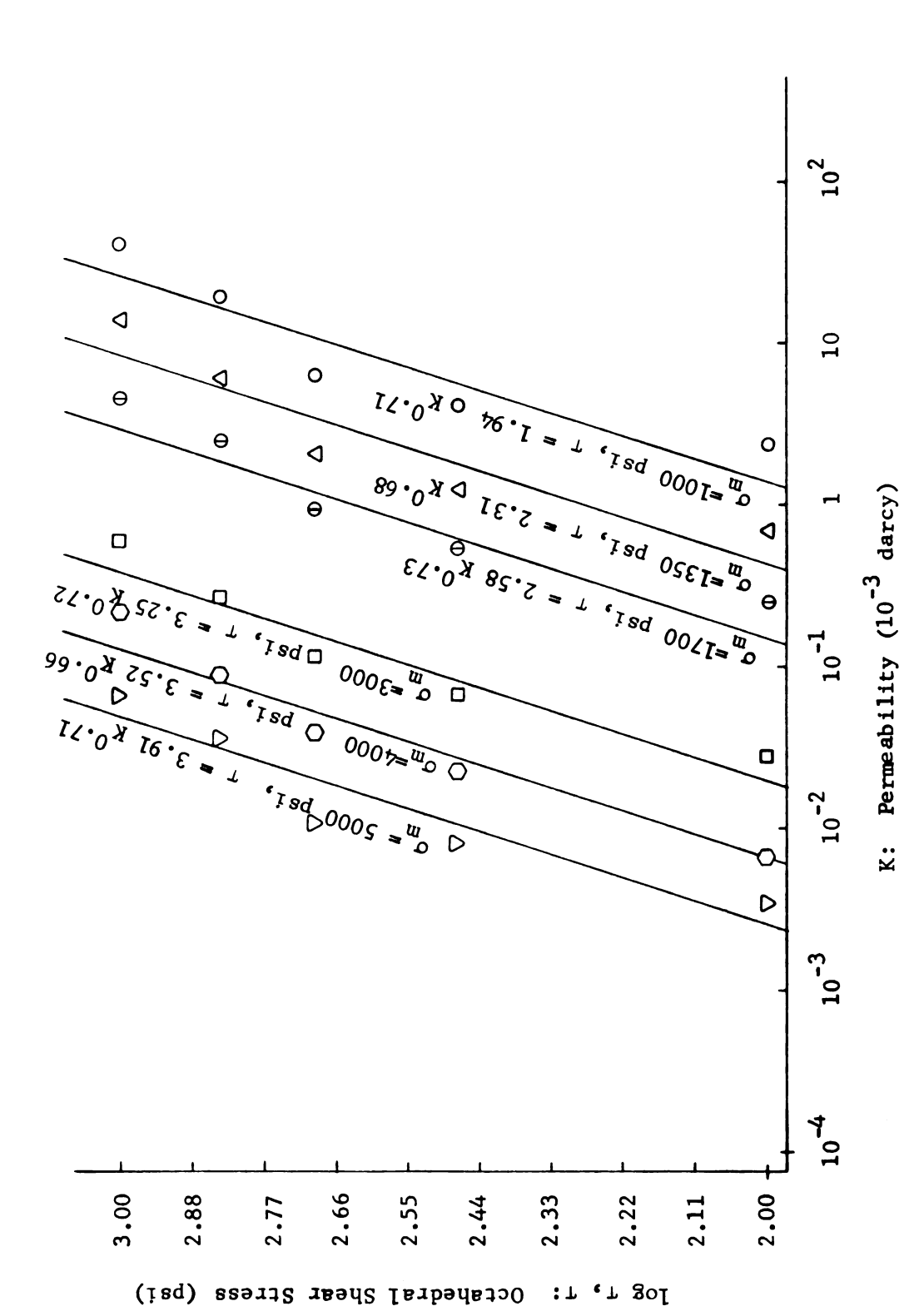


Fig. 5-3. The Effect of Octahedral Shearing Stress upon Permeability for Various Mean Stress

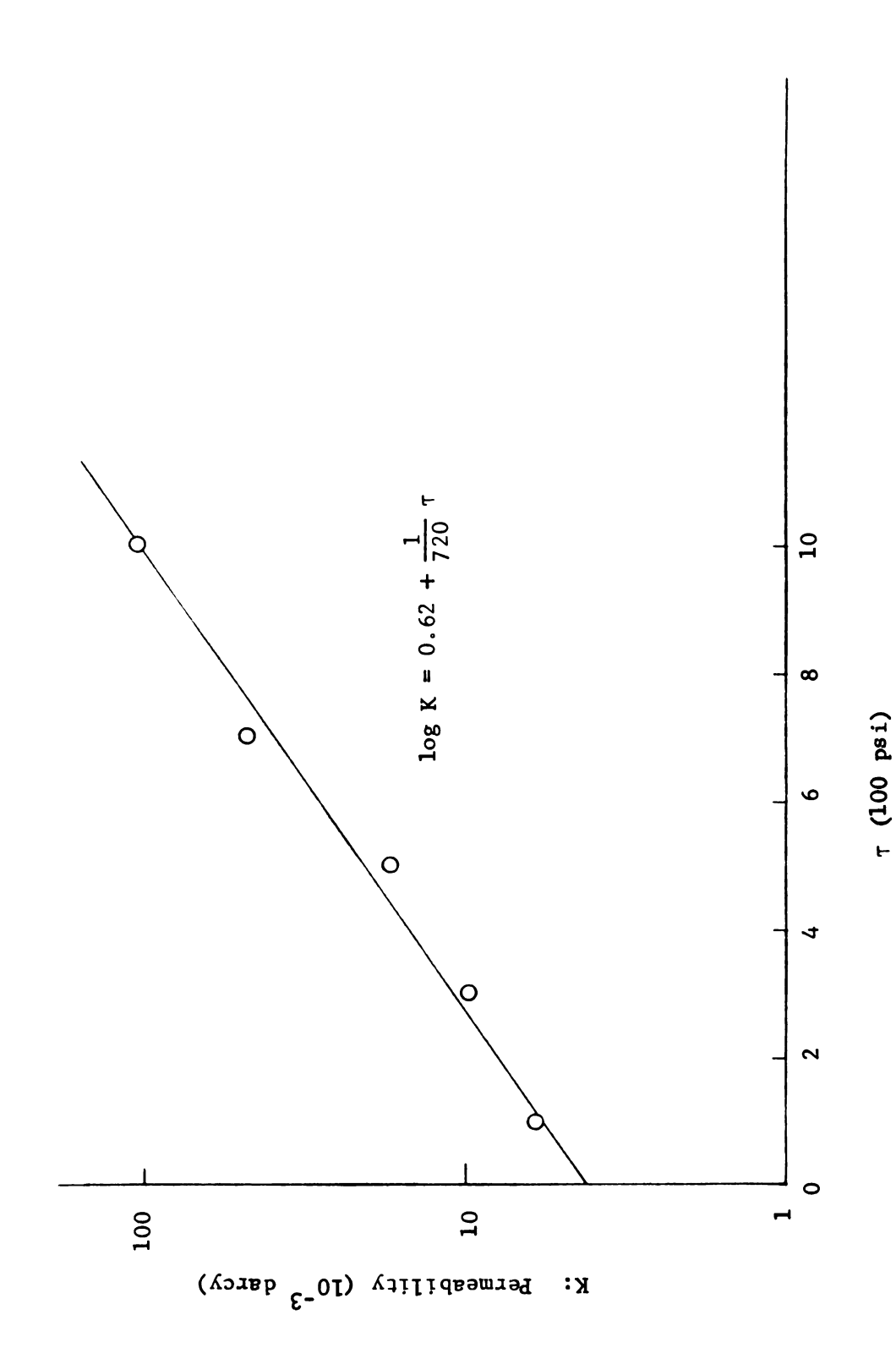


Fig. 5-4. The Effect of Octahedral Shear Stress upon Permeability When Mean Stress Equal to Zero Psi

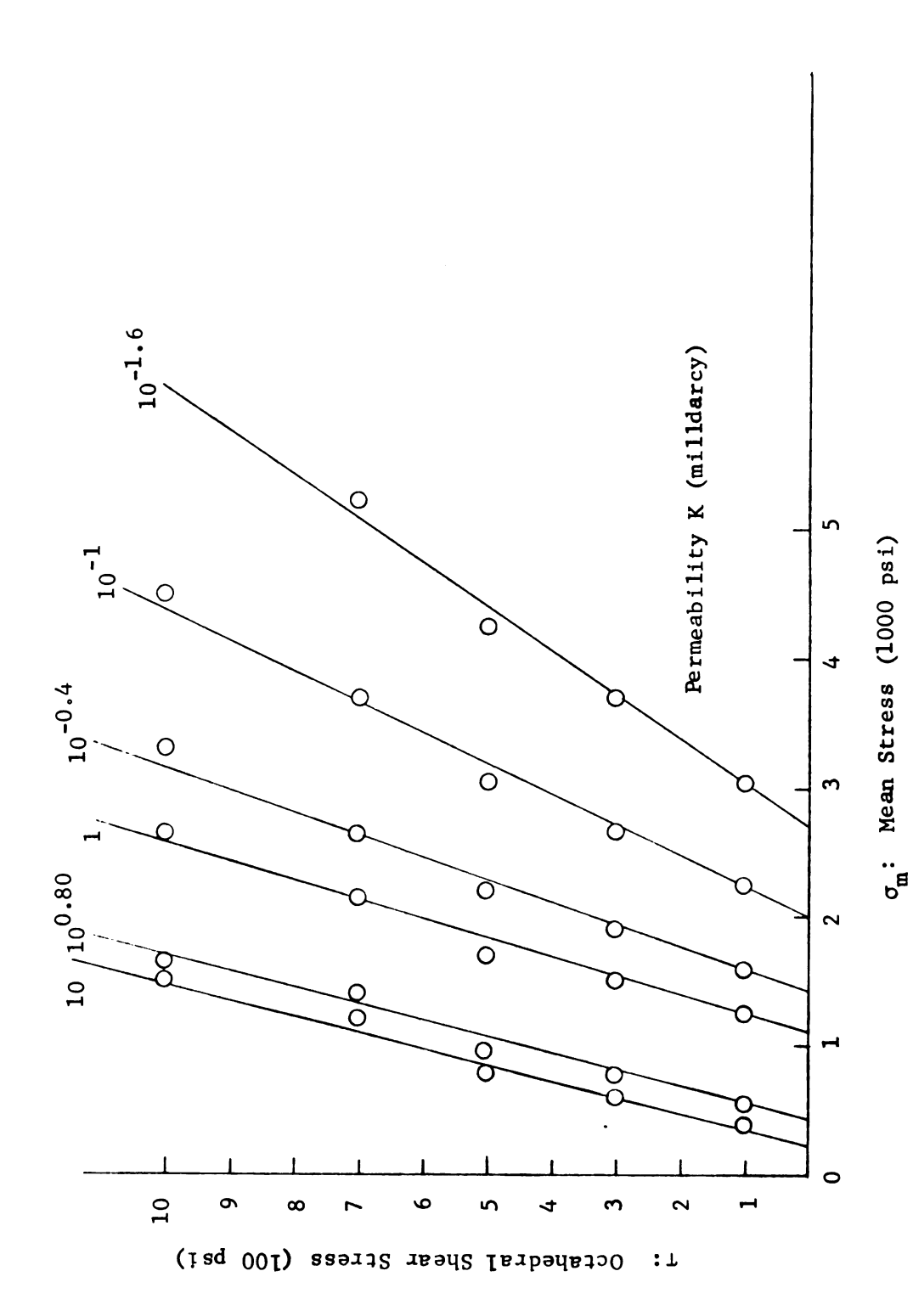


Fig. 5-5. Permeability under Various Combinations of Mean Stress and Octahedral Shear Stress

$$\log K_{\sigma_{m}} = K_{\sigma_{m}=0} + m \sigma_{m}$$
 5.3

where K = permeability in milli-darcy at $\sigma_{\rm m}$ = constant

 $K_{\sigma_{m}=0} = constant permeability in milli-darcy at <math>\sigma_{m} = 0$ psi

 τ_{o} = octahedral shearing stress in psi

m = slope of curve = $\Delta \log K/\Delta \sigma_{\rm m}$

Table 5-1 gives the equations for five different τ -value as follows:

Table 5-1. Permeability as a Function of Mean Stress at Various Octahedral Shearing Stress

τ (psi)	Equat ions	Significance of F	Simple Correlation
100	$\log K = 0.78-0.00070 \sigma_{\rm m}$	0.001	0.979
300	$\log K = 0.99-0.00065 \sigma_{\rm m}$	< 0.0005	0.985
500	$\log K = 1.23-0.00066 \sigma_{\rm m}$	< 0.0005	0.990
700	$\log K = 1.68-0.00067 \sigma_{\rm m}$	< 0.0005	0.982
1000	$\log K = 2.02-0.00067 \sigma_{\rm m}$	< 0.0005	0.984

From statistical analysis the simple correlation of K and σ_{m} fall within the range of 0.978 to 0.989. The average slope of the curve is found to be 0.00067.

An attempt was made in Fig. 5-3 to observe the correlation between octahedral shear stress and permeability when using mean stress as a parameter. Again a least square computer analysis was applied. The equations are listed in Table 5-2.

Table 5-2. Octahedral Shearing Stress as a Function of Permeability at Various Mean Stresses

σ _m (psi)	Equations	Significance of F	Simple Correlation
1000	$\tau = 1.94 \text{ K}^{0.71}$	0.19	0.913
1350	$_{T} = 2.31 \text{ K}^{0.68}$	< 0.0005	0.917
1700	$\tau = 2.58 \text{ K}^{0.73}$	0.01	0.956
3000	$_{T} = 3.25 \text{ K}^{0.72}$	0.011	0.958
4000	$\tau = 3.52 \text{ K}^{0.66}$	0.028	0.975
5000	$\tau = 3.91 \text{ K}^{0.71}$	0.030	0.936

The simple correlation of τ and K fall within the range of 0.913 to 0.974 with general equation, $\tau_{\sigma_m} = mK^{m}$. A higher correlation exists between K and σ_m than between τ and τ a

Fig. 5-4 is constructed to study the relationship between octahedral shear stress and permeability. This curve shows that permeability increases with increasing octahedral shear stress, which can be expressed with the relationship:

$$\log K = 0.62 + \frac{1}{720} \tau$$
, at $\sigma_{\rm m} = 0$ 5-4

This increase in K is probably due to dilatancy of the salt grains with the resulting small increase in pore volume.

A general equation of permeability as a function of mean stress and octahedral shear stress can be obtained as:

$$\log K = 0.62 + \frac{1}{720} \tau - 0.00067 \sigma_{\rm m}$$
 5-5

by substituting equation 5-4 in equation 5-3, assuming that the solution is linear with mean value m in Eq. 5-3.

To describe the correlation between permeability, mean stress, and octahedral shear stress, a three dimensional plot is constructed in Fig. 5-6, which proves to be more descriptive than earlier figures. Permeability can be predicted according to any one of the empirical equations given previously. However, the coefficient of permeability is not directly affected by stress itself, but is affected by porosity changes due to deformation of the rock from applied stresses. The following section presents experimental strain results and a discussion about how permeability is related to porosity and deformation.

Strain Field

Axial and tangential strain changes were measured throughout the experiments. The rate of strain change decreased with
time along with the reduction of pore space when stress was applied
to the specimen. The rate of decrease was much higher for the
early stage of the experiment before it approached a constant
value. The results show that a constant value was approached at
times greater than about 5,000 minutes.

Taylor's equation $Q = (D_s^2 \cdot \frac{\gamma_w}{\mu} \cdot \frac{e^3}{1+e} C)$ iA can be used for studying the strain effect on permeability, where:

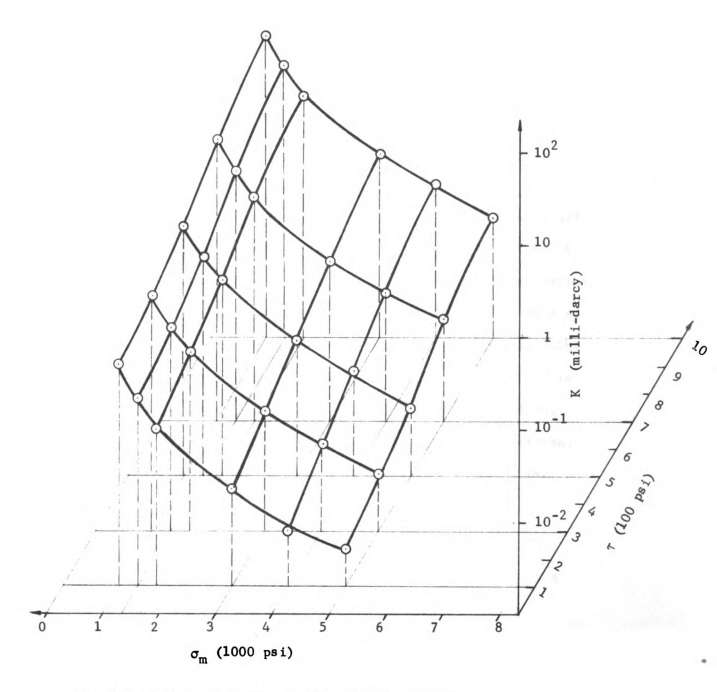


Fig. 5-6. Three Dimensional Plot of Mean Stress, Octahedral Shear Stress, and Permeability

 $Q = flow rate = \Delta V / \Delta t$

 $D_s = diameter of particle$

 $\gamma_w = fluid density$

μ = fluid viscosity

e = void ratio

C = constant

i = hydraulic gradient

A = cross-section area

Kerosene was used as the fluid with specimen size, pressure, and temperature constant. This means that D_s , γ_w , μ , C, i, and A all have constant values in this study. Laboratory determination of porosity change was computed from experimental strain data as follows: Assume that the salt crystals are incompressible. The total volume of specimen V ($V = r^2\pi \cdot 2r = 2\pi r^3$ where V is initial volume of sample) equals the Crystal or Solid Volume, V_s , plus the Void Volume, V_V . After a given axial compression, ε_1^* , of the sample a new total volume is calculated using the lateral strain ε_L^* based on dial gage readings and

$$V' = (r + \frac{2\pi r \epsilon_{L}^{\dagger}}{2\pi})^{2} \pi 2r (1 - \epsilon_{1}^{\dagger})$$

$$= 2\pi r^{3} (1 + \epsilon_{L}^{\dagger})^{2} (1 - \epsilon_{1}^{\dagger})$$
5-6

The unit volume change is represented by $\frac{V-V^{\circ}}{V} = \frac{\Delta V}{V}$

$$\frac{\Delta V}{V} = \frac{2\pi r^3 - 2\pi r^3 (1 + \epsilon_L^{\dagger})^2 (1 - \epsilon_1^{\dagger})}{2\pi r^3}$$

$$= 1 - (1 + \epsilon_L^{\dagger})^2 (1 - \epsilon_1^{\dagger}) 0$$

$$= 1 - (1 + 2\epsilon_L^{\dagger} - \epsilon_1^{\dagger} + (\epsilon_L^{\dagger})^2 - (\epsilon_1^{\dagger})^2 \epsilon_1^{\dagger} - 2\epsilon_L^{\dagger} \epsilon_1^{\dagger})$$

where higher order terms are very small and can be neglected.

$$\frac{\Delta V}{V} = 1 - (1 + 2\epsilon_{L}^{\dagger} - \epsilon_{1}^{\dagger}) = 2\epsilon_{L}^{\dagger} - \epsilon_{1}^{\dagger}$$
 5-8

Therefore, the new void ratio is:
$$e = \frac{V_v - (2\epsilon_L^{\dagger} - \epsilon_1^{\dagger})V}{V_s}$$
 5-9

To examine Taylor's (1948) equation, permeability k is plotted against $e^3/(1+e)$ in Fig. 5:-7. The results show that permeability increased with an increase in $e^3/(1+e)$. By using least square analysis, the result can be expressed by equation as follows:

$$\log \frac{e^3}{1+e} = 0.21 \log K - 8.19$$
 5-10

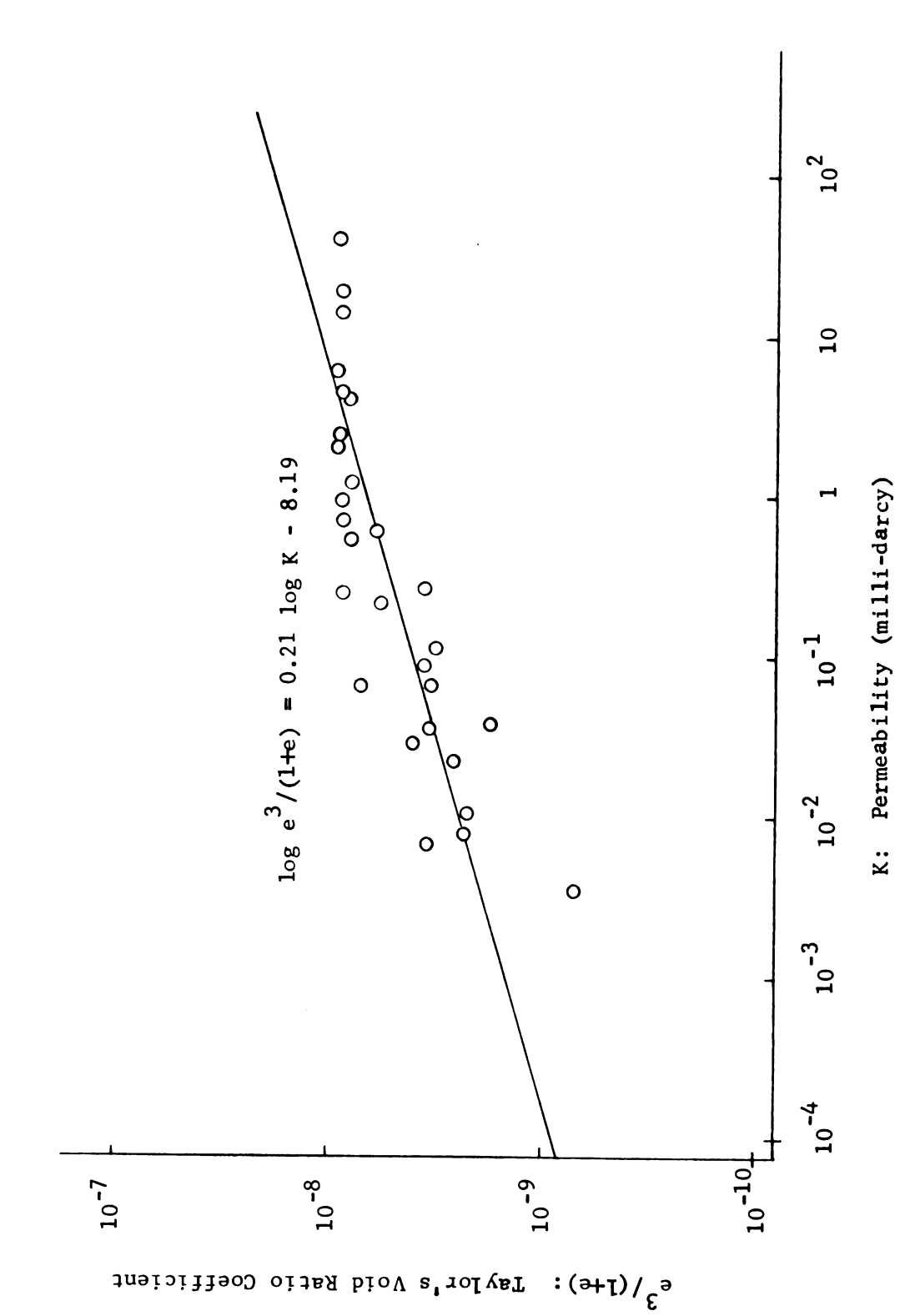
The simple correlation is 0.843 and F is significant < 0.0005.

The mean stress, $\sigma_{\rm m}$, was included with the data as shown in Fig. 5-8. Log permeability K is plotted against $\log \sigma_{\rm m}(\frac{{\rm e}^3}{1+{\rm e}})$. The plot showed that product of $\sigma_{\rm m}$ and ${\rm e}^3/(1+{\rm e})$ remained nearly constant for all K values. This indicated that a given rock salt had almost a constant value of the product of $\sigma_{\rm m}$ and ${\rm e}^3/(1+{\rm e})$ and its permeability appeared to be independent of this value. The equation obtained by using least square analysis was

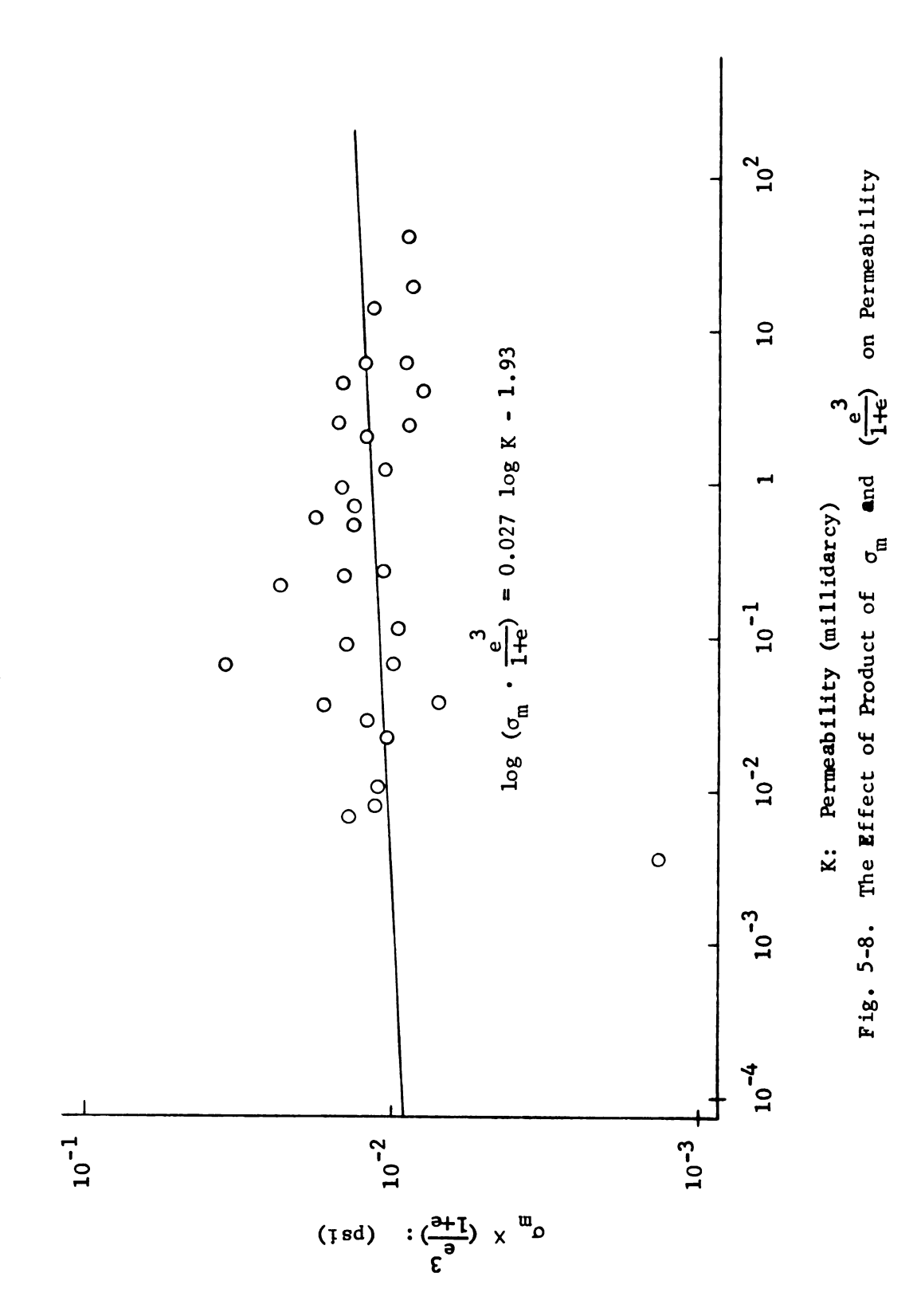
$$\log \left(\sigma_{\rm m} \frac{{\rm e}^3}{1+{\rm e}}\right) = 0.027 \log K - 1.93$$
 5-11

with a significance of F of 0.473 and a simple correlation of 0.136: this indicates a high degree of dependence between these two variables.

The effect of unit volume change on permeability was studied by plotting the unit volume change $(2e_L^{\dagger} - e_1^{\dagger})$ against permeability K in Fig. 5-9. From Fig. 5-7 it is observed that the correlation of permeability K and the unit volume change



The Relationship between Taylor's Void Ratio Coefficient and Permeability Fig. 5-7.



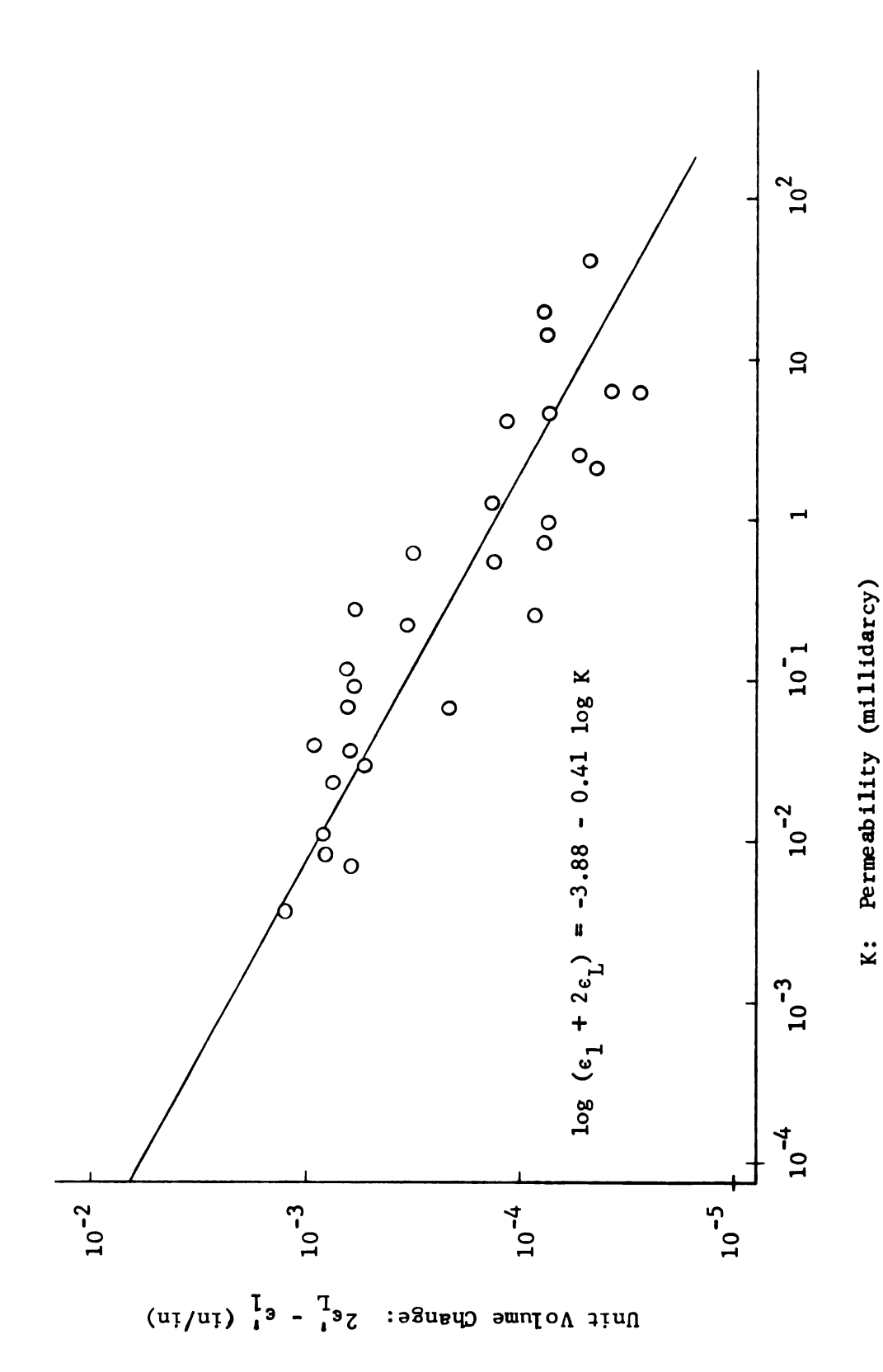


Fig. 5-9. The Relationship between Unit Volume Change and Permeability of Rock Salt

 $(2\varepsilon_L^{\dagger} - \varepsilon_1^{\dagger})$ can be expressed as:

$$\log (2\epsilon_{L}^{\dagger} - \epsilon_{1}^{\dagger}) = -3.88 - 0.41 \log K$$
 5-12

with significance of F < 0.0005 and a simple correlation of 0.885.

An attempt was made to show the correlation between mean stress $\sigma_{\rm m}$ and void ratio e. The plots in Fig. 5-10 suggest that there is a relationship,

$$\sigma_{\rm m} = 9150 - 366e$$
 5-13

with significance of F < 0.0005 and simple correlation of 0.842. The equation indicates that void ratio should approach zero when mean stress approaches 10,000 psi.

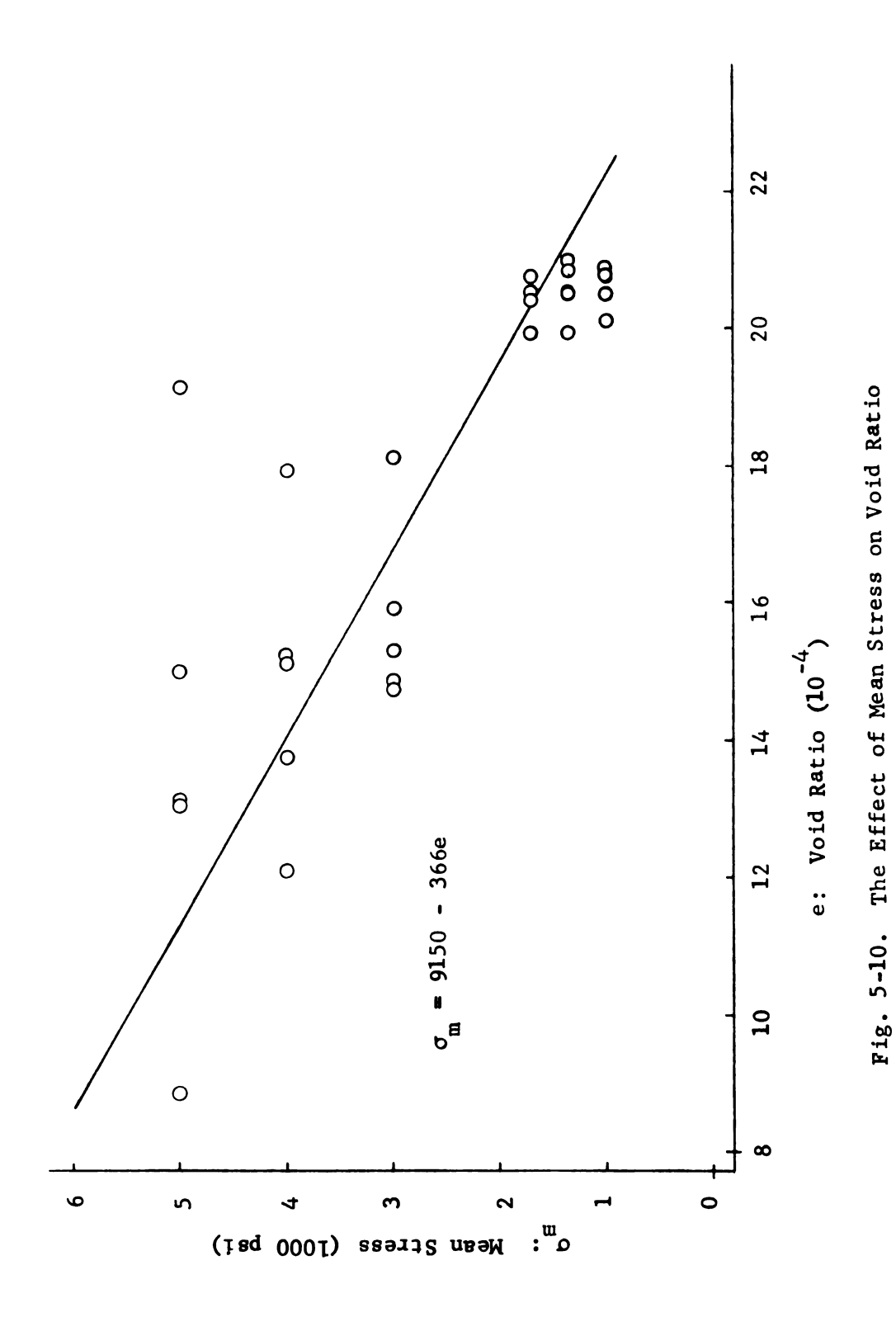
Taylor's (1948) coefficient was also examined against mean stress in Fig. 5-11. The equation obtained was

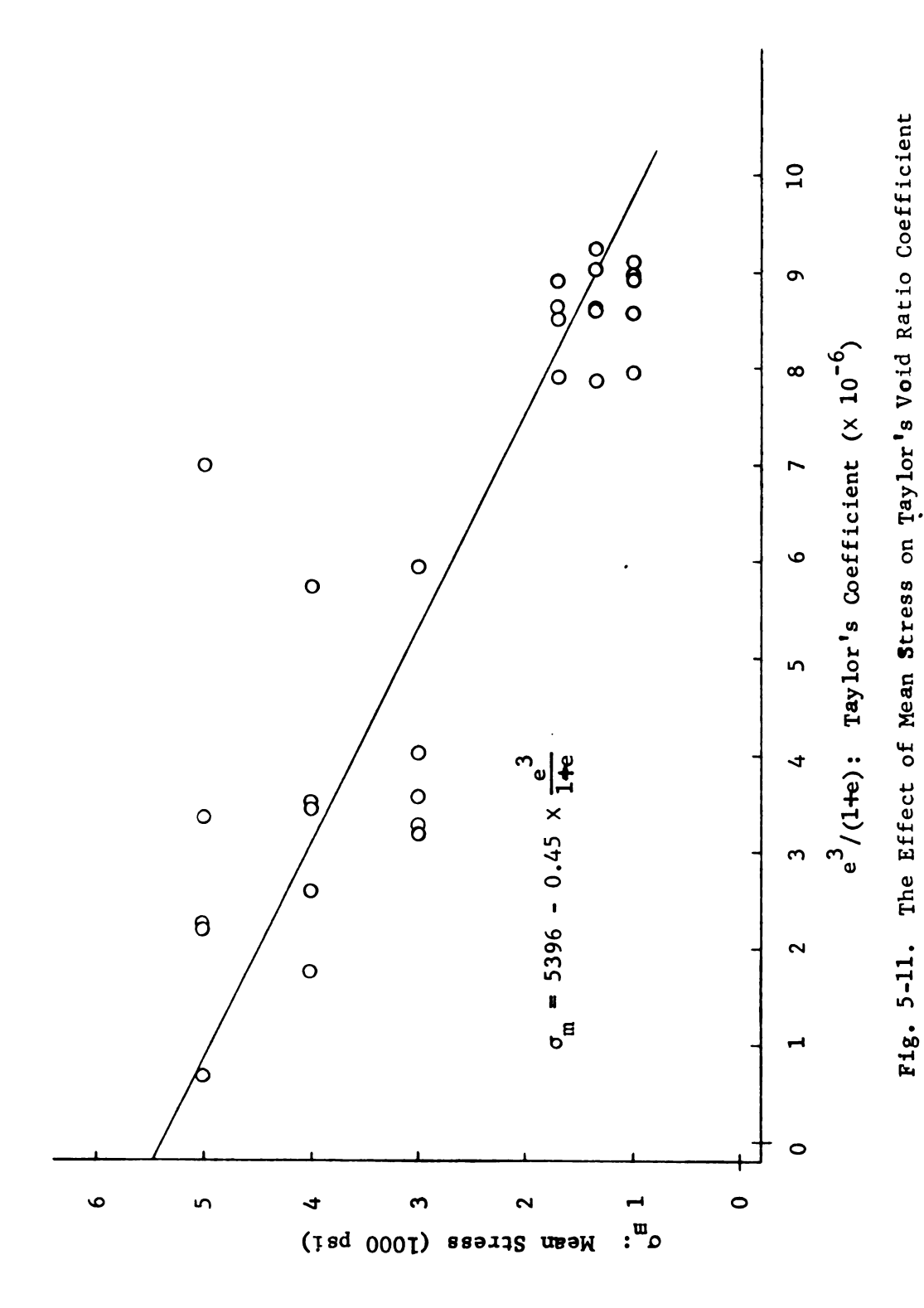
$$\sigma_{\rm m} = 5396 - 0.45 \, {\rm e}^3/(1+{\rm e})$$
 5-14

with significance of F less than 0.005 and simple correlation of 0.864.

Compressibility

Compressibility is the volume change per unit volume of the material per unit change in pressure. Compressibility of the rock salt was studied from the stress and strain observation of the tests. Three types of compressibility were considered (1) solid grains of rock salt, (2) fluid kerosene, and (3) bulk.





Rock formations surrounding a cavity are subject to external stresses from adjacent rocks and from the hydrostatic pressure of fluid in the pores. The external stress generally has the largest value in the vertical direction (overburden weight) and smaller values in the lateral directions.

When a cavity is created in a salt formation, the stress around the cavity changes with respect to distance from the cavity center. Normal stresses at the cavity walls may be reduced to zero. This section is concerned with the change of pore volume associated with this change in stress condition. The rock response to the change can be divided into the three compressibility categories.

(1) The change in solid grain volume (Knutson, C.F., B.F. Bohor, 1963) is

$$c_g = \frac{1}{V_g} \left(\frac{\partial V_s}{\partial P_i} \right)_{T_i} d_{\sigma_m} - d_{P_i} = 0$$
 5-15

where $C_g = grain compressibility (1/psi) = 0$ by assuming no volume change of salt crystal

 $v_s = volume of solid rock material, in³$

P, = internal fluid pressure, psi

 $\sigma_{\rm m}$ = active external mean stress, psi

(2) The change in fluid or liquid unit weight is expressed as

$$\gamma = \gamma_0 e^{\beta' P}$$

where γ_0 = initial unit weight at atmospheric pressure

P = pressure measured above the standard atmospheric pressure

 β' = compressibility of fluid

(for water
$$\frac{1}{\beta_w} = 300,000 \text{ psi}$$
)

(3) The change in bulk volume can be expressed as

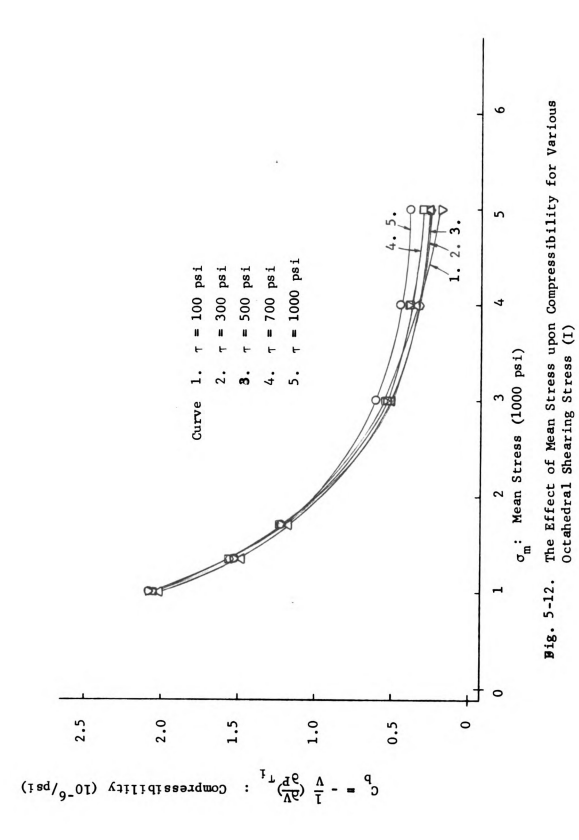
$$C_{b} = \frac{1}{V_{b}} \left(\frac{\Delta V}{\partial \sigma_{m}} \right)_{\tau_{i}}$$
 5-17

where C_b = bulk compressibility, 1/psi V_b = bulk volume, in

Since the solid volume is assumed constant and the fluid is assumed incompressible throughout this discussion, the compressibility is limited to change in pore volume only. Bulk compressibilities computed for all the experimental results are summarized in Table 5-3. Figs. 5-12, 13, and 14 show the relationship between bulk compressibility and mean stress for different values. From Fig. 5-13 the results show a reduction of compressibility with change in mean stress for each different octahedral shearing stress value. These equations are listed in Table 5-3.

Table 5-3. Compressibility as a Function of Mean Stress at Various Octahedral Shearing Stress

τ (psi)	Equations	Significance of F	Simple Correlation
100	$\log c_{b} = 1.29-1.45 \log \sigma_{m}$	< 0.0005	0.984
300	$\log c_{\rm b} = 1.75 - 1.31 \log \sigma_{\rm m}$	< 0.0005	0.998
500	$\log c_{\rm b} = 1.51-1.38 \log \sigma_{\rm m}$	< 0.0005	0.995
700	$\log c_{\rm b} = 1.91-1.25 \log \sigma_{\rm m}$	< 0.0005	0.996
1000	$\log C_{\rm b} = 2.42 - 1.09 \log \sigma_{\rm m}$	< 0.0005	0.998



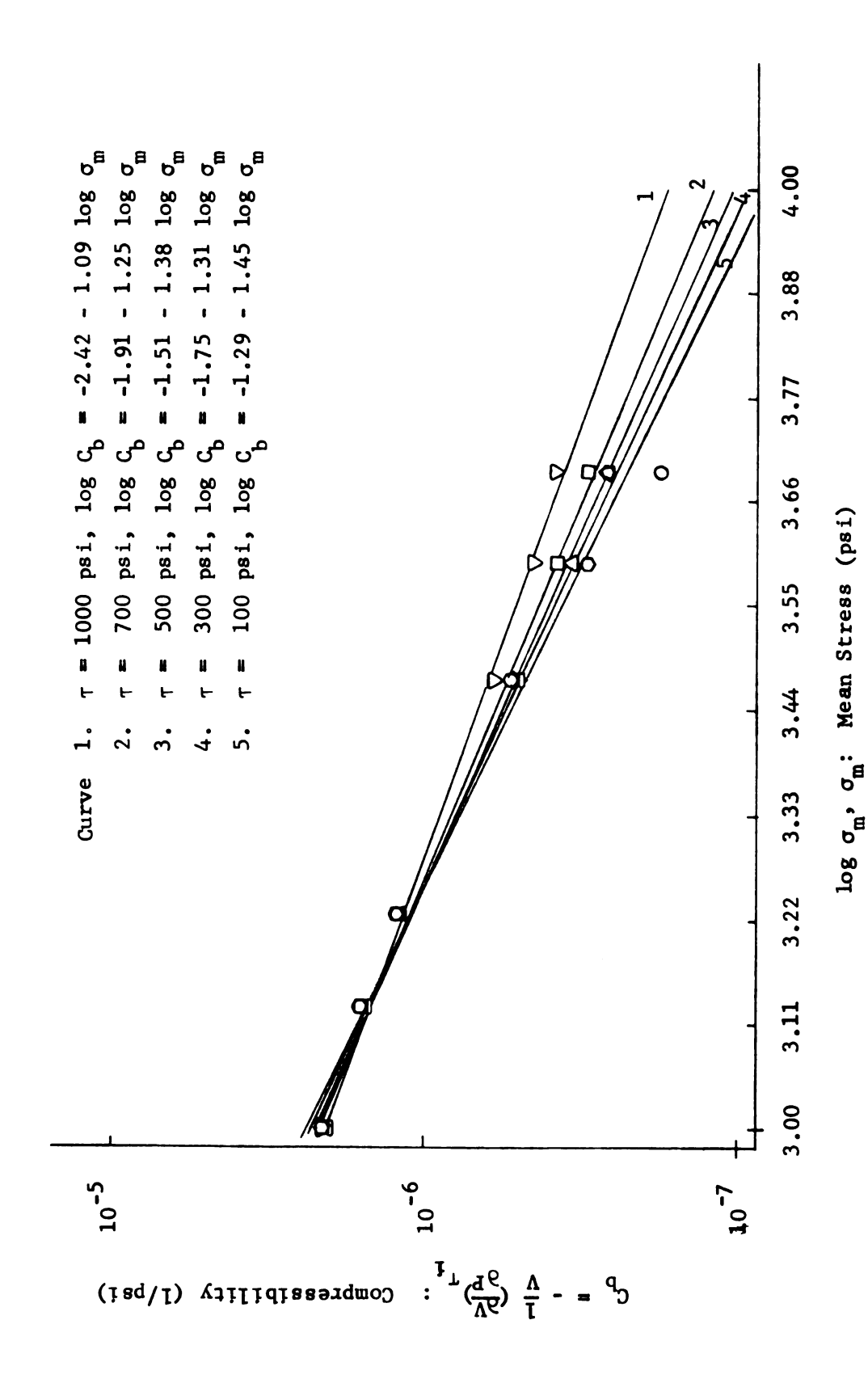
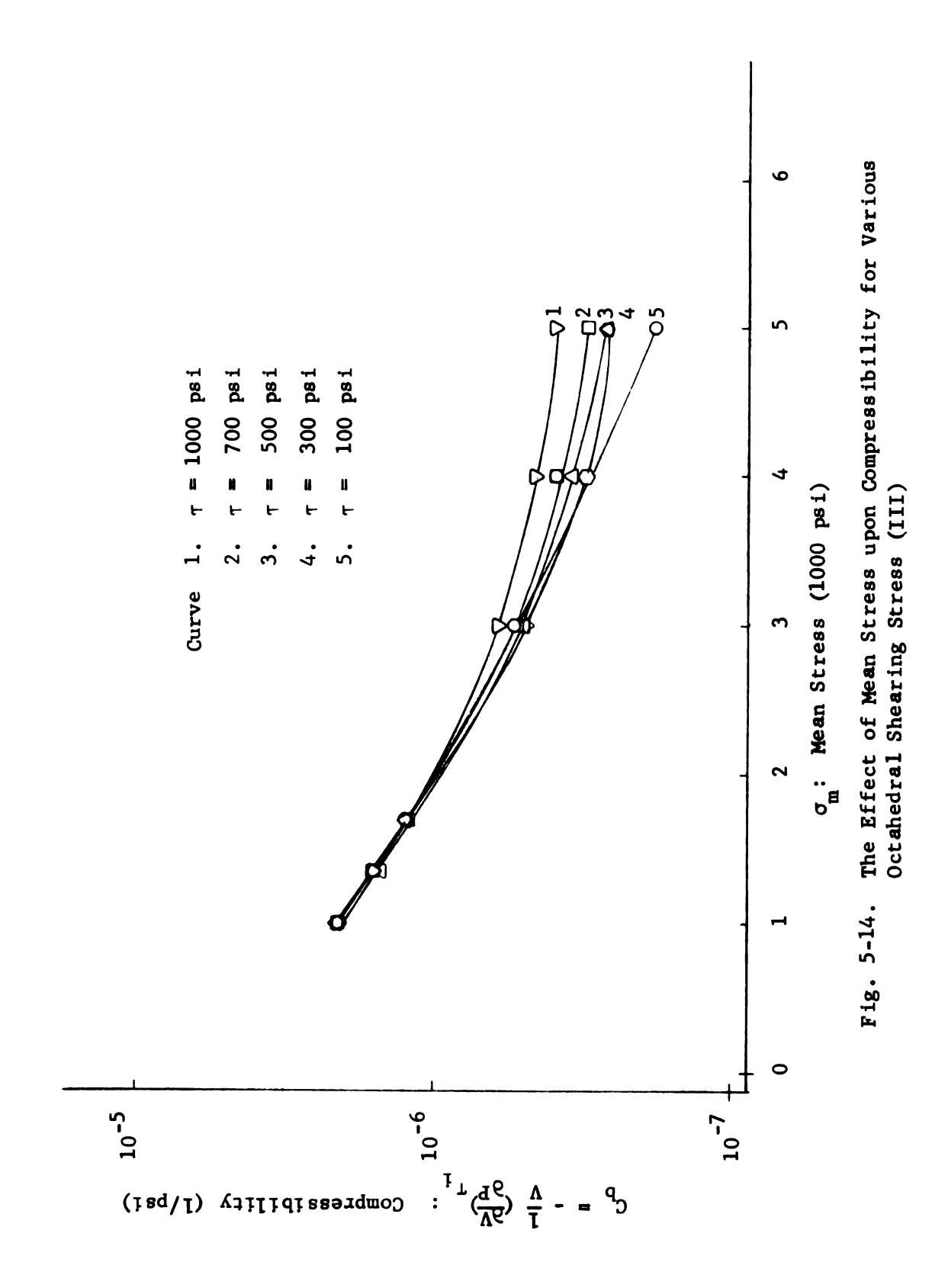


Fig. 5-13. The Effect of Mean Stress upon Compressibility for Various Octahedral Shearing Stress (II)



It is observed that the rate of compressibility is reduced approximately the same for different octahedral shearing stresses.

Skempton (1961) has presented a theory for compressibility of saturated materials where the unit volume change is

$$-\frac{\Delta V}{V} = C[\Delta p - (1-a)\Delta u], \quad a = A_s/A \qquad 5-18$$

and $\Delta p' = \Delta p - (1-a)\Delta u$

where C = compressibility

 $\Delta p = applied pressure$

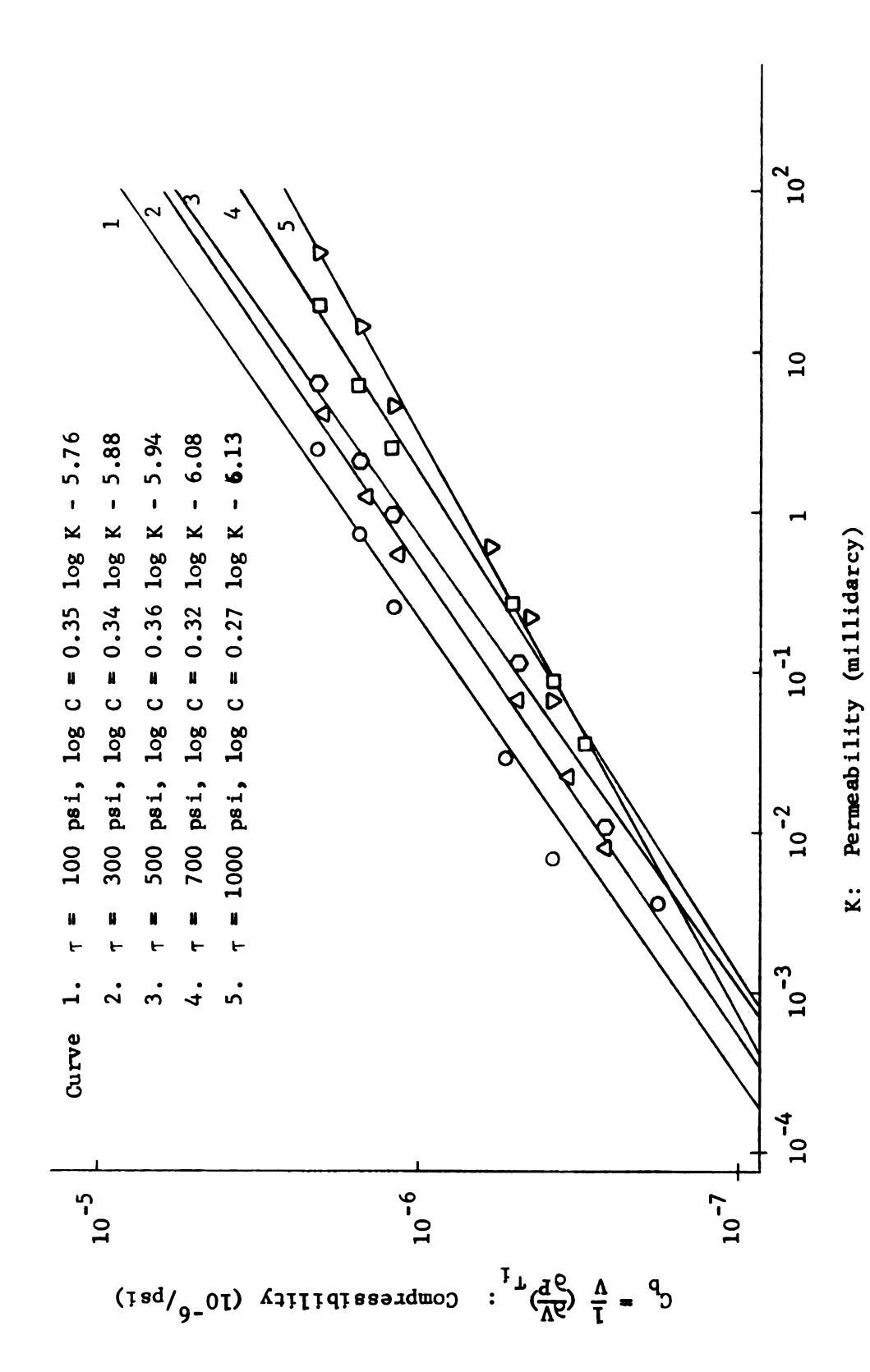
Δu = pore pressure change

A = area of contact between soil solids

A = gross area

In this study, pore pressure was held constant at 125 psi at the entrance and zero at the exit (average of 63 psi) where Δp was in the range of 1,000 psi to 5,000 psi. If the area A_8 were approximately equal to gross area A, the effect of pore pressure, $(1-a)\Delta u$, would be small in comparison to the applied pressure, Δp . In other words, the effective stress for this study is approximately equal to the applied stress. However, for the practical solution, it may be necessary to consider pore pressures and their reduction of effective stresses.

Bulk compressibility effect on permeability is shown in Fig. 5-15. Here, permeability increases with increasing compressibility and compressibility increases with increasing octahedral shearing stress. Summarizing, the experimental points, curves 1 through 5, can be expressed as shown in Table 5-4.



The Effect of Bulk Compressibility upon Permeability for Various Octahedral Shearing Stress Fig. 5-15.

Table 5-4. Compressibility as a Function of Permeability at Various Octahedral Shearing Stresses,

τ (psi)	Equations	Significance of F	Simple Correlation
100	$\log C = 0.35 \log K - 5.70$	0.001	0.979
300	$\log C = 0.34 \log K - 5.88$	0.0005	0.997
500	$\log C = 0.36 \log K - 5.94$	0.0005	0.992
700	log C = 0.32 log K - 6.08	0.0005	0.997
1000	$\log C = 0.27 \log K - 6.13$	0.0005	0.995

It is shown in Fig. 5-15 that the slope is approximately the same except for the octahedral shearing stress at 1,000 psi. In general, the flow pattern, under different octahedral shearing stress and compressibility, can be constructed.

With experimental data on the relationship between stress, strain, and compressibility to permeability one can construct a nomograph or set of general equations for different conditions. The prediction of flow through the rock salt formation can be calculated using known values of the stress or strain distribution surrounding the cavity and the experimental constants discussed.

CHAPTER VI

FLOW FROM AN UNDERGROUND SALT CAVITY

The principle of flow from a cavity can be illustrated using information from the previously described experimental study. Because of the variables involved, i.e., the geometry of salt formation, the various levels of piezometric head, and the location of a cavity in a formation, it is not within the scope of this study to present an exact solution. However, in order to illustrate a typical solution, a hypothetical salt cavity has been chosen as shown in Fig. 6-1.

Although some degree of permeability was measured in the test samples, it is recognized that these specimens were reconsolidated and may only approximate a medium which has been subjected to consolidation over a geological time period. Based on mining operations and experience (Brown and Gloyna, 1959) in the storage of liquid petroleum products in salt cavities, it is recognized that massive salt structures are almost impervious to the flow of water. Consequently, any computation using the laboratory results may include a substantial safety factor.

Assume that a salt cavity exists in an underground formation as shown in Fig. 6-1 with the following conditions given:

Lateral underground pressure = P_L psi Fluid pressure = P_i psi

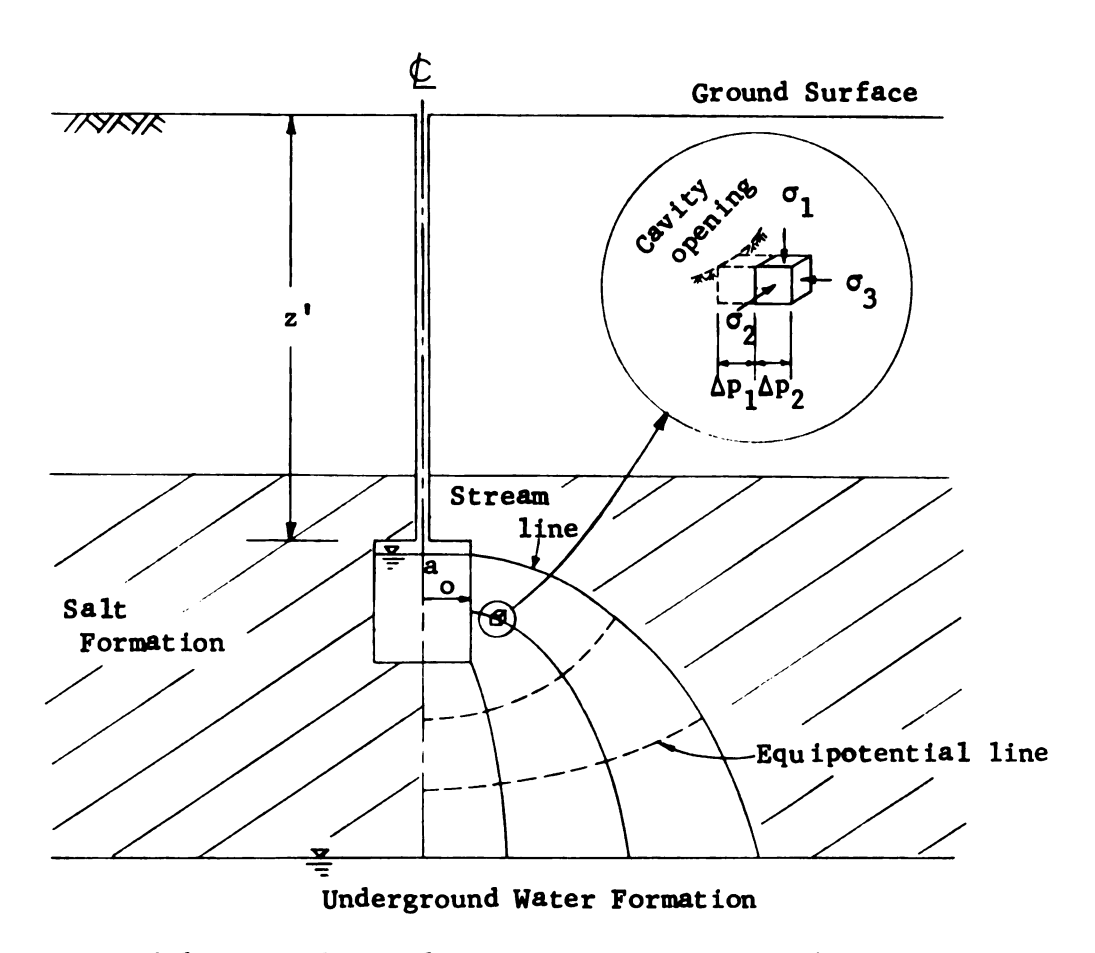


Fig. 6-1. Hypothetical Storage Cavity in a Salt Formation

Cavity radius = a ft

Octahedral shear strength = K psi

Assume that the salt formation lies above the ground water level. The problem concerns flow from the cavity through an element r feet from the cavity. The condition for plastic flow in the rock salt may be examined by computing the plastic radius, ρ_0 , by the equation (Serata and Gloyna, 1960)

$$\rho_{o} = a_{o} \exp(\frac{P_{L} - P_{i}}{\sqrt{6} K_{O}} - \frac{1}{2})$$
6-1

If this radius is less than the cavity radius, only elastic conditions need be considered. For this example assume that $\rho_0 < a_0$.

The stress distribution adjacent to natural underground cavities can be obtained by the established methods. For design and stability problems it is generally assumed that rock is an isotropic, homogeneous, linear-elastic material, and that the deformational response of a rock body to an applied force can be determined from elastic theory. In 1964, Dahir presented a solution of the general stress distribution for completely elastic thick-walled cylinders using rock salt and found that the theoretical results compared reasonably well with the experimental results. Recently, Obert and Duvall (1967) happened to encounter the identical solution on the determination of stress distribution in a thick-wall cylinder subjected to a triaxial stress field. Sakurai (1966) derived the general stress distribution in the elastic and plastic regions for a circular cylindrical cavity with infinite thickness of the formation.

The stress distribution around a cavity can be obtained from any one of the studies mentioned above. The cavity has to be carefully chosen at the location where a uniform media and a sound formation exists. The size of the cavity is also limited so that the entire formation around the cavity behaves as an elastic material.

Construction of a cavity causes a change in stresses in the vicinity of the cavity and for that region the stress distribution will not be hydrostatic. For this reason, it is

concluded that the best correlation can be obtained by using these stresses as a parameter. The expression for the permeability K is assumed to be:

$$K = f(\sigma_m, \tau, \gamma_b, e, d, C_s, A_r)$$

where $\sigma_{\rm m}$ is the mean stress, τ is the octahedral shear stress, $\gamma_{\rm b}$ is bulk density, e is void ratio, d is particle size, $C_{\rm s}$ is shape, and $A_{\rm r}$ refers to the geometry of a certain waste cavity. Since bulk density and void ratio are dependent upon stress and strain and assuming that d, $C_{\rm s}$, and $A_{\rm r}$ are constant, the equation can be reduced to

$$K = f(\sigma_m, \tau)$$

for a specific formation. Because strain is function of stress the equation can be also expressed as a function of strain. A definite correlation between permeability and effective porosity for a given medium under different strain distribution exists (Knutson and Bohor, 1963; Taylor, 1948) which is useful in determining one of the two quantities when the other is unknown.

Permeability is found by using the experimental results corresponding to each stress condition as shown in Fig. 5-6. Finally, radial flow away from the cavity may be computed using the equation (Muskat, 1946) for flow given as

$$Q = \frac{2\pi k_{N-1} [p_e - p_w]/\mu}{\log r_o / r_w + \frac{k_{N-1}}{k_N} \log r_e / r_o}$$
6-2

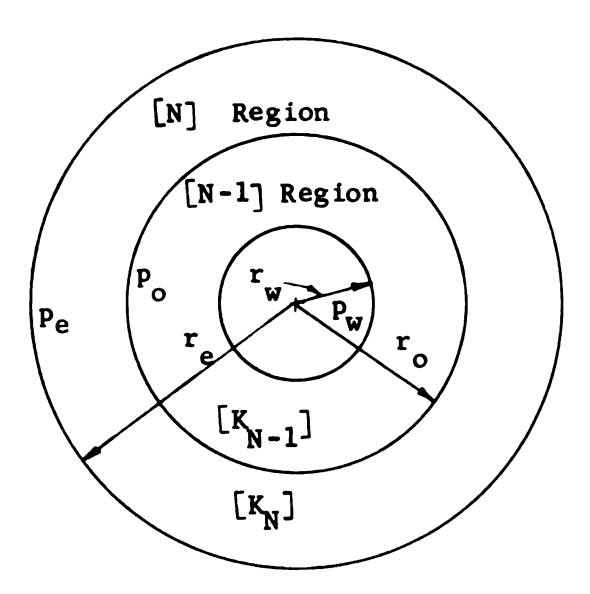


Fig. 6-2. Two Dimensional Configuration of an Underground Formation

where Q is the rate of fluid flow, μ is the viscosity of fluid, k_N and k_{N-1} are coefficients of permeability at two adjacent concentric annular regions (N) and (N-1), p_W is fluid pressure inside the cavity, p_e is fluid pressure at radius r_e , and r_W , r_O , r_e are radii as shown in Fig. 6-2.

When the wastes are placed in the cavity, a frontal zone of the liquid waste will penetrate through the formation outward with a flow rate of Q. For practical engineering purposes, the distance between the cavity floor and the underground water formation, and the cavity radius should be selected so that it is within the safety range. To obtain the entire flow pattern and pressure difference such as Δp_1 , and Δp_2 , as shown in Fig. 6-1, the stream lines away from the cavity must be constructed. Due to the non-homogeneous permeability, numerical methods would be most applicable

for a solution to the flow net. Since Q is the function of r_{w} in equation 6-2, the safety dimension of r_{w} can be selected as a cavity radius within a range of permissible leakage.

It is noted from the experimental results that permeability decreases when mean stress increases. If the cavity is constructed in a deeper formation (i.e. increase the overburden pressure) then the possibility of leakage will be considerably reduced.

Based upon the experimental investigations in this thesis, the permeability, under mean stress in the range of 1000 to 5000 psi and octahedral shear stress of 100 to 1000 psi, was in the range of 0.0036 to 40.6752 milli-darcy. This low permeability indicates that leakage of radioactive waste materials from underground salt cavities will vary from small to almost negligible. As a result the waste liquid in the cavities can be confined in salt beds for a long period of time. Furthermore, due to plastic behavior (Sakurai, 1966), rock salt acts as a self sealer for the storage cavity and the high density of an underground formation provides permanent shielding and ion-exchange media for any release of radioactivity.

CHAPTER VII

SUMMARY AND CONCLUSIONS

The conclusions are summarized under three headings:

(1) high pressure triaxial cell, (2) the effect of stress, strain,
and compressibility upon permeability, and (3) feasibility of
radioactive waste disposal in an underground formation.

High Pressure Triaxial Cell

A high pressure triaxial cell was constructed to permit the application of uniform confining pressures and axial loads to simulate the complex stress conditions existing in an underground formation adjacent to the disposal cavity. Pressure control was maintained reasonably constant for the various stress conditions by the automatic control system. The measurement of fluid flow and strain of the specimen were recorded properly. Cylindrical specimens of rock salt were prepared so that the flow and strain properties could be obtained accurately.

The experiment showed that the high pressure triaxial cell can be used to study the deformation and/or flow property of rock salt without modifying the parts of cell. The results revealed that the accuracy of the equipment would be adequate for research projects on similar materials.

The Effect of Stress, Strain, and Compressibility upon Permeability

Data showing the effect of mean stress and octahedral shearing stress upon permeability of the rock salt was obtained. By statistical analysis, empirical equations were derived, which predict the permeability in terms of mean stress and octahedral shearing stress. A high degree of correlation with the experimental data was obtained.

Observations of strain changes were converted into void changes within the specimen to study the relationship to permeability. The effect of change in void ratio upon permeability was expressed by empirical equations with high correlations resulting. The effect of mean stress on void ratio was studied in the same manner.

A high correlation was found between permeability and compressibility (with τ as a parameter). Empirical equations were also derived for permeability in terms of compressibility and octahedral shearing stress.

From the results of the data analysis, it was concluded that pore volume reduction is the main factor in decreasing permeability. Pore volume reduction again depends upon the combination of mean stress and octahedral shearing stress.

Feasibility of Radioactive Waste Disposal

Based upon the experimental investigation of permeability in this study it is concluded that leakage of radioactive waste from salt cavities will be almost negligible. Laboratory permeabilities for the rock salt varied from 0.0036 to 40.6752 milli-

darcy for various stress states. A procedure for predicting the degree of leakage was proposed for a given cavity and assumed boundary conditions. This research also suggests that underground storage cavities may also be utilized to store other substances such as fuel.

CHAPTER VIII

FUTURE RESEARCH

Further research is needed in certain areas to find solutions for related problems. In particular, future research would be useful:

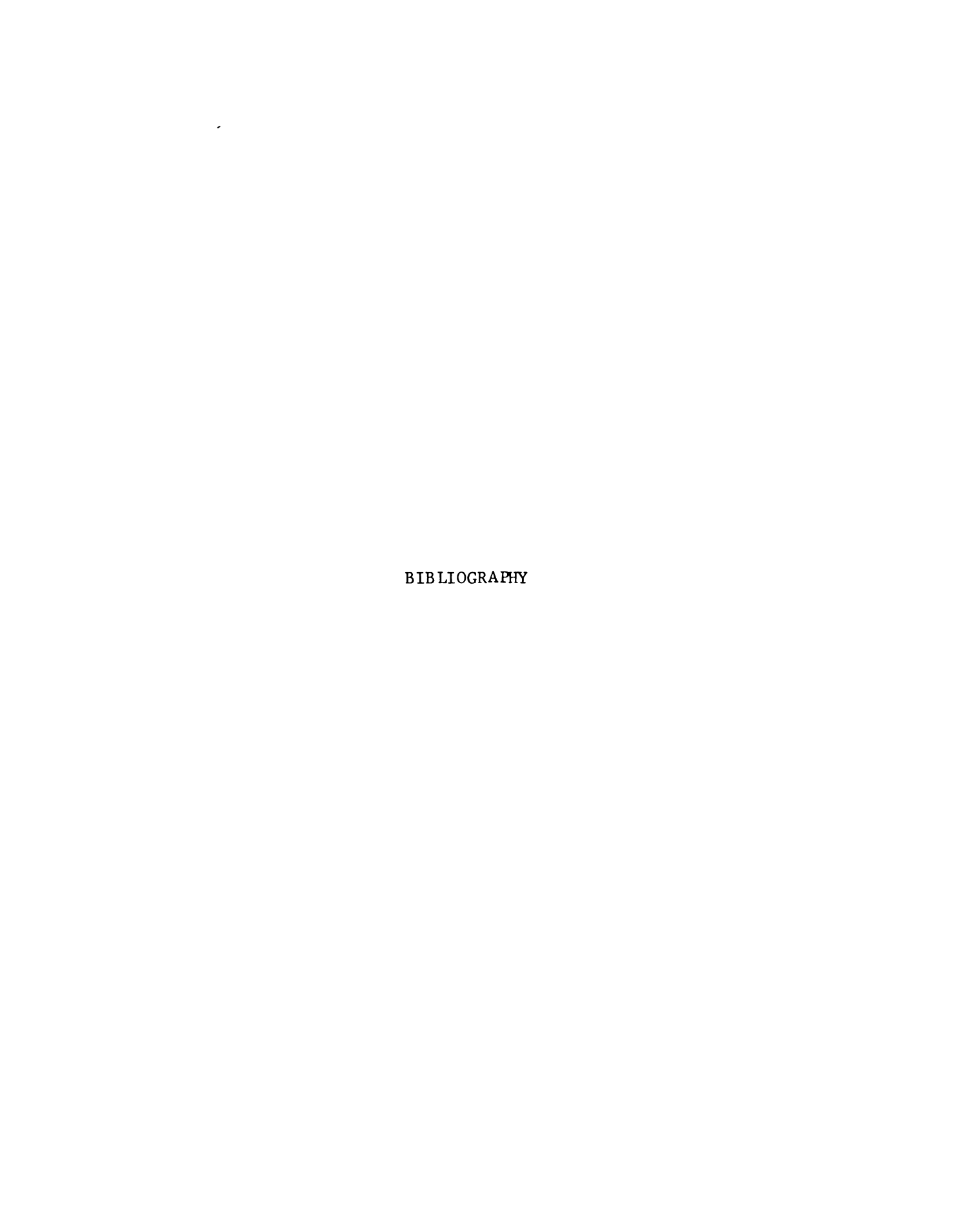
(1) To study the effect of temperature on sample compressibility and related effect on flow.

The storage cavity temperature may rise above the temperature of the surrounding formation as a result of radioactive decay of the fission products in the stored wastes. Structural stability and permeability should be studied for various temperatures.

- (2) In order to extend the theory and techniques presented in this study, other rocks should be investigated to determine the possibility of applying this technique to different materials.
- (3) To modify the experimental approach.

For the purpose of substantiating the flow equations derived in this study the experimental set-up could be modified.

Various sizes of cavities can be drilled at the center of cylindrical sample. Flow through the media toward the center can then be measured using the external fluid pressure as the confining pressure and flow pressure.



This set-up is advantageous because the flow effect can be studied, and the stress-strain effect due to the cavity existence can also be checked.

BIBLIOGRAPHY

- Athy, L.F. "Density Porosity, and Compaction of Sedimentary Rocks",

 <u>American Association of Petroleum Geologist</u> (Bulletin),

 Vol. 14, No. 1, Jan. 1930, pp. 1-24.
- Bergelin, O.P. "Flow of Gas-Liquid Mixtures", Chemical Engineering, Vol. 56, No. 5, May 1949, pp. 104-7.
- Birch, F. and H. Clark. "Thermal Conductivity of Rock and Its Dependence Upon Temperature and Composition", American Journal of Science, Vol. 238, Aug. 1940, p. 552.
- Brown, K., and E.F. Gloyna. "Pressure Temperature Effect on Salt Cavities and Survey of Liquified Petroleum Gas Storage",

 The University of Texas Sanitary Engineer Research Laboratory

 Technical Report to U.S. Atomic Energy Commission, Austin:
 Univ. of Texas Press, Jan. 15, 1959.
- Burdine, N.T. "Relative Permeability Calculations from Pore Size Distribution Data", AIME: Transactions, Vol. 198, Mar. 1953, pp. 71-8.
- Burns, R.H. "The Treatment of Radioactive Liquid Effluent",

 Radioactive Wastes: Their Treatment and Disposal, 1960,
 pp. 114-5.
- Carman, P.C. "Fluid Flow through Granular Beds", Transactions of the Institute of Chemistry, Vol. 15, May 1937, pp. 150-66.
- . "Foundamental Principles of Industrail Filtration", Transactions of the Institute of Chemistry, Vol. 16, Oct. 1938, pp. 168-88.
- . Journal of Agricultural Science, Vol. 29, 1939, p. 262.
- Dahir, A.G. "Continuous Medium Analysis of Elastic, Plastic and Viscoelastic Behavior of a Model Salt Cavity", Unpublished Ph.D. dissertation, Michigan State University, E. Lansing, 1964.
- Douglas, J., Jr., P.M. Blair, and R.J. Wagner. "Calculation of Linear Waterflood Behavior Including the Effect of Capillary Pressure", AIME: Transactions, Vol. 213, June 1953, pp. 96-102.

- Fatt, I. and D.H. Davis. "Reduction in Permeability with Over-burden Pressure", AIME: Transactions, Vol. 195, Dec. 1952, p. 329.
- Fatt, I. and H. Dykstra. "Relative Permeability Studies", AIME: Transactions, Vol. 192, Sept. 1951, pp. 249-56.
- Fatt, I. "Effect of Overburden Pressure on Relative Permeability", AIME: Transactions, Vol. 198, Oct. 1953, pp. 325-6.
- Pack Models", American Association of Petroleum Geologists:
 Bulletin, Vol. 42, July 1958, pp. 1914-23.
- Fenimore, J.W. "Land Burial of Solid Radioactive Waste During a 10-Year Period", <u>Health Physics</u>, Vol. 10, April 1964, pp. 229-36.
- Gates, J.I. and W.T. Lietz. American Petroleum Industry Drilling Procedures and Practices, 1950.
- Gray, Donald and I. Fatt. "The Effect of Stress on Permeability of Sandstone Cores", AIME: Transactions, Vol. 228, 1962-1963, pp. 95-100.
- Happel, J. and B.J. Byrne. "Motion of a Sphere and Fluid in a Cylindrical Tube", <u>Industrial and Engineering Chemistry</u>, Vol. 46, June 1954, pp. 1181-6.
- Hassan, M.E. and R.F. Nielsen. "How to Calculate Relative Permeability of Bradford Sand from Capillary Pressure Data", Petroleum Engineering, Vol. 25, No. 3, Mar. 1953, pp. B61-2.
- Hawkins, R.H. and J.H. Horton. "Bentonite as a Protective Cover for Buried Radioactive Wastes", <u>Health Physics</u>, Vol. 13, Marc. 1967, pp. 287-92.
- Inman, A.E. "Salt, An Industrial Potential for Kansas", Univ. of Kansas Research Foundation, 1951.
- Irmay, S. Transactions of American Geophysics, Vol. 35, 1954, p. 463.
- Kaufmann, W.J., et. al. "Disposal of Radioactive Waste into Deep Geological Formation", <u>Journal: Water Pollution Control</u> Federation, Vol. 33, 1961, p. 73.
- Knutson, C.F. and B.F. Bohor. "Reservoir Rock Behavior Under Moderate Confining Pressure", Rock Mechanics Proceedings of 5th Symposium, 1963.
- Lang, W.B. "Annoted Bibliography and Index Map of Salt Deposits in the United States", <u>Bulletin of Geological Survey</u>, No. 1019-j, Washington, D.C.: Government Printing Office, 1957.

- McLatchie, A.S., R.A. Hemstock and J.W. Young. "The Effective Compressibility of Reservoir Rock and Its Effects on Permeability", AIME: Transactions, Vol. 213, June 1958, pp. 386-88.
- Mann, R.L. and I. Fatt. "Effect of Pore Fluids on the Elastic Properties of Sandstone", Geophysics, Vol. 25, No. 2, April 1960, pp. 433-44.
- Merritt, W.F. and P.J. Parsons. "Safe Burial of High-Level Fission Product Solution Incorporated into Glass", <u>Health Physics</u>, Vol. 10, Sept. 1964, pp. 655-64.
- Mineral Resources of the United States, Washington: Public Affairs Press, 1958.
- Muskat, M. The Flow of Homogeneous Fluids Through Porous Media, Ann Arbor: J.W. Edwards, Inc., 1946.
- National Petroleum Council. 'Feasibility of Underground Storage', World Petroleum Report, Vol. 23, No. 7, 1952, p. 40.
- National Research Council of National Academy of Science, The Disposal of Radioactive Waste on Land, The Committee on Waste Disposal of the Division of Earth Science, National Academy of Science, 1957.
- Obert, L. and W.I. Duvall. Rock Mechanics and the Design of Structures in Rock, New York: John Wiley & Sons, Inc., 1967.
- Osoba, J.S., J.G. Richardson and J.K.Kerver. "Laboratory Measurements of Relative Permeability", AIME: Transactions, Vol. 192, Feb. 1951, pp. 47-56.
- Parsons, P.J. 'Migration From a Disposal of Radioactive Liquid in Sands", Health Physics, Vol. 9, Mar. 1963, pp. 333-42.
- Porkhaev, A.P. Kolloid Zhur, Vol. 11, 1949, pp. 346-52.
- Reidel, J.C. "LPG Goes Underground", The Oil and Gas Journal, Vol. 51, No. 10, July 14, 1952, pp. 70-o.
- Reynolds, T.D. "Reactor Fuel Waste Disposal Project: Permeability of Rock Salt and Creep of Underground Salt Cavities", Atomic Energy Commission Report (Unpublished), Dec. 30, 1960.
- Ruth, B.F. "Correlation Filtration Theory with Industrial Practice", Industrial and Engineering Chemistry, Vol. 38, No. 6, June 1946, pp. 564-71.

- Sakurai, S. "Time-Dependent Behavior of Circular Cylindrical Cavity in Continuous Medium of Brittle Aggregate", (Ph.D. Thesis) E. Lansing: Michigan State University, 1966.
- Scheidegger, A.E. The Physics of Flow Through Porous Media, New York: The MacMillan Co., 1960.
- Secchi, I.M. Chimica e Industria, Vol. 18, 1936, pp. 514-63.
- Serata, S. "Development of Design Principle for Disposal of Reactor Fuel Waste into Underground Salt Cavities", Unpublished Ph.D Dissertation, Univ. of Texas, Austin, 1959.
- Serata, S. and E.G. Gloyna. "Principles of Structural Stability of Underground Salt Cavities", <u>Journal of Geophysics Research</u>, Vol. 65, No. 9, Sept. 1960, pp. 2979-87.
- Skempton, A.W. 'Effective Stress in Soils, Concrete and Rocks",

 Pore Pressure and Suction in Soil, Butterworth, London, 1961,

 pp. 4-16.
- Taylor, D.W. Fundamentals of Soil Mechanics, New York: John Wiley & Sons, 1948.
- Templeton, C.C. "A Study of Displacements in Microscopic Capillaries", AIME: Transactions, Vol. 201, July 1953, pp. 162-8.
- Bulletin of American Physics Society, Vol. 29, No. 2, 1954, p. 16.
- Tiller, F.M. "Role of Porosity in Filtration", Chemical Engineering Progress, Vol. 49, No. 9, Sept. 1953, pp. 467-79.
- U.S. Department of Health, Education, and Welfare. Radiological Handbook, Washington, D.C.: Government Printing Office, 1960.
- Van Fossan, N.E. "Underground Storage", The Oil and Gas Journal, Vol. 54, April 1955, pp. 80-93.
- Wilson, J.W. "Determination of Relative Permeability Under Simulated Reservoir Conditions", American Institute of Chemical Engineers Journal, Vol. 2, No. 1, Mar. 1956, pp. 94-100.

APPENDIX

DATA

Table A-1. Strain-rate, Deformation, and Flow-Test Data

Test 1.

 $\tau = 100 \text{ psi}$

 $\sigma = 1000 \text{ psi}$

at time = 0

Initial $\epsilon_1 = 0$

Initial $\epsilon_{\tau} = 0$

Initial $\epsilon_1' = 0$

Total $\epsilon_1 = 615 \times 10^{-6}$ in/in

Total $\epsilon_{L} = 145 \times 10^{-6}$ in/in

Total $\epsilon_{L}^{1} = 36 \times 10^{-4} \text{ in/in}$

Computed $\epsilon_{L}^{1} = 8.7 \times 10^{-4}$ in/in

Time (min.)	⁶ 1 (10 ⁻⁶ in/in)	ε _L (10 ⁻⁶ in/in)	¢1 (10 ⁻⁴ in/in)	Time (min.)	ΣV (m1.)
0000	000	000	000	0000	0000
0058	324	020	006	411	96
0411	454	052	016	458	107
0458	4 64	060	016	954	220
0945	509	085	019	1369	306
1369	534	095	022	1903	410
1903	546	105	024	2383	498
2383	552	112	024	2672	546
2672	554	115	024	3339	656
3339	574	120	027	3825	730
3825	569	122	030	4154	782
4154	575	129	129	4773	874
4773	584	132	030	5270	948
5270	574	131	027	5766	1019
5766	582	142	028	6218	1086
6218	584	140	029	6708	1153
6708	586	138	031	7250	1229
1250	604	132	034	9258	1497
9258	614	147	036	9435	1522
9435	615	145	036		

^{*} Data listed as ϵ_1 = Axial strain gage observation, ϵ_L = Lateral Strain gage observation, ϵ_1^{\dagger} = Axial dial gage reading, Σ^{V} = Accumulated flow reading, ϵ_L^{\dagger} = ϵ_1^{\dagger} × $\epsilon_L^{\dagger}/\epsilon_1$, and constant flow rate was obtained from plotting.

Test 2.

$$\tau$$
 = 100 psi
 σ = 1350 psi
at time = 0
Initial ϵ_1 = 315 × 10⁻⁶ in/in
Initial ϵ_L = 0
Initial ϵ_L^{\dagger} = 0
Total ϵ_1 = 1200 × 10⁻⁶ in/in
Total ϵ_L = 100 × 10⁻⁶ in/in
Total ϵ_L^{\dagger} = 67 × 10⁻⁴ in/in
Computed ϵ_L^{\dagger} = 5.7 × 10⁻⁴ in/in

Time (min.)	⁶ 1 (10 ⁻⁶ in/in)	$\epsilon_{ m L}$ (10 ⁻⁶ in/in)	61 (10 ⁻⁴ in/in)	Time (min.)	ΣV (m1.)
0000	000	000	000	0000	0000
0005	000	005	036	0210	0021
0210	225	030	048	0585	0055
0585	400	050	053	1074	0094
1074	7 50	059	053	1560	0136
1 560	778	061	055	2052	0174
2052	785	062	056	2510	0208
2510	787	066	056	3001	0230
3001	7 95	068	057	3404	0266
3404	7 97	070	058	39 5 6	0286
3956	805	070	059	4430	0314
4430	808	075	058	4755	0312
4755	815	077	059	5399	0342
5399	820	078	060	5879	0359
5879	827	080	061	6392	0376
6392	840	083	063	6832	0392
6832	845	086	063	7320	0415
7 3 20	846	088	063	7706	0433
7706	855	089	064	9034	0482
9034	870	0 98	066	9999	0523
9999	885	100	067		

Test 3.

$$\tau = 100 \text{ psi}$$

$$\sigma = 1700 \text{ psi}$$

at time
$$= 0$$

Initial
$$\epsilon_1 = 1195 \times 10^{-6}$$
 in/in

Initial
$$\epsilon_L = 0$$

Initial
$$\epsilon_1' = 0$$

Total
$$\epsilon_1 = 1448 \times 10^{-6}$$
 in/in

Total
$$\epsilon_{L} = 28 \times 10^{-6}$$
 in/in

Total
$$\epsilon_1^{\bullet} = 82 \times 10^{-4}$$
 in/in

Computed
$$\epsilon_{L}^{\bullet} = 1.7 \times 10^{-4} \text{ in/in}$$

Time (min.)	⁶ 1 (10 ⁻⁶ in/in)	⁶ L (10 ⁻⁶ in/in)	ε <mark>1</mark> (10 ⁻⁴ in/in)	Time (min.)	ΣV (m1.)
	(20 111, 111)	(20 111, 111)	(20 111/111)		
0000	000	000	000	0000	0000
0005	005	003	024	0254	0011
0254	073	009	048	1059	0041
1059	1 42	017	067	1544	0056
1544	144	019	070	1942	0068
1942	146	020	069	2502	0086
2502	149	021	069	2991	0102
2991	147	021	070	3298	0109
3298	165	022	071	3 948	0130
3 948	173	023	076	4432	0143
4432	178	023	074	4842	0153
4848	184	023	075	5386	0168
5386	193	024	076	5872	0170
5872	200	024	075	6182	0175
6182	202	024	076	6827	0182
6827	213	025	07 9	7315	0194
7315	220	025	07 9	7 6 7 8	0199
7 678	225	026	081	87 67	0208
87 67	235	027	082	9785	0222
9785	253	028	082	9785	0222

Test 4.

$$\tau = 100 \text{ psi}$$

$$\sigma$$
 = 3000 psi

Initial
$$\epsilon_1 = 5273 \times 10^{-6}$$
 in/in

Initial
$$\epsilon_{L} = 1835 \times 10^{-6}$$
 in/in

Initial
$$\epsilon_1^{\dagger} = 0$$

Total
$$\epsilon_1 = 5977 \times 10^{-6}$$
 in/in

Total
$$\epsilon_L = 2280 \times 10^{-6}$$
 in/in

Total
$$\epsilon_1' = 303 \times 10^{-4} \text{ in/in}$$

Computed
$$\epsilon_L^{\dagger} = 116 \times 10^{-4}$$
 in/in

0000 000 000 0000 0000 0396 261 230 216 0040 0026 0440 259 237 229 0440 0178 0941 456 323 280 0941 0528 1370 549 361 292 1370 0813 1885 626 401 295 1885 1118 2377 669 417 297 2377 1325 2656 686 429 299 2656 1501 3321 696 432 300 3321 1722 3809 697 440 301 3809 2997 4133 698 439 301 4133 2010 4767 699 445 301 4767 2302	Time (min.)	⁶ 1 (10 ⁻⁶ in/in)	ε _L (10 ⁻⁶ in/in)	ε'1 (10 ⁻⁴ in/in)	Time (min.)	ΣV (m1.)
0440 259 237 229 0440 0178 0941 456 323 280 0941 0528 1370 549 361 292 1370 0813 1885 626 401 295 1885 1118 2377 669 417 297 2377 1325 2656 686 429 299 2656 1501 3321 696 432 300 3321 1722 3809 697 440 301 3809 2997 4133 698 439 301 4133 2010	0000	000	000	000	0000	0000
0941 456 323 280 0941 0528 1370 549 361 292 1370 0813 1885 626 401 295 1885 1118 2377 669 417 297 2377 1325 2656 686 429 299 2656 1501 3321 696 432 300 3321 1722 3809 697 440 301 3809 2997 4133 698 439 301 4133 2010	0396	261	230	216	0040	0026
1370 549 361 292 1370 0813 1885 626 401 295 1885 1118 2377 669 417 297 2377 1325 2656 686 429 299 2656 1501 3321 696 432 300 3321 1722 3809 697 440 301 3809 2997 4133 698 439 301 4133 2010	0440	259	237	229	0440	0178
1885 626 401 295 1885 1118 2377 669 417 297 2377 1325 2656 686 429 299 2656 1501 3321 696 432 300 3321 1722 3809 697 440 301 3809 2997 4133 698 439 301 4133 2010	0941	456	323	280	0941	0528
2377 669 417 297 2377 1325 2656 686 429 299 2656 1501 3321 696 432 300 3321 1722 3809 697 440 301 3809 2997 4133 698 439 301 4133 2010	1370	549	361	292	1370	0813
2656 686 429 299 2656 1501 3321 696 432 300 3321 1722 3809 697 440 301 3809 2997 4133 698 439 301 4133 2010	1885	626	401	2 95	1885	1118
3321 696 432 300 3321 1722 3809 697 440 301 3809 2997 4133 698 439 301 4133 2010	2377	669	417	2 97	2377	1325
3809 697 440 301 3809 2997 4133 698 439 301 4133 2010	2656	686	429	299	2656	1501
4133 698 439 301 4133 2010	3321	696	432	300	3321	1722
	3809	697	440	301	3809	2997
4767 600 445 301 4767 2302	4133	698	439	301	4133	2010
4707 099 449 301 4707 2302	4767	699	445	301	47 67	2302
5248 700 446 3 02 5456 2505	5248	700	446	3 02	5456	2505
5753 701 442 303 5602 2550	5753	701	442	303	5602	2550
6202 702 440 302 5795 2655	6202	702	440	302	5795	2655
6692 702 443 303 6202 2675	6692	702	443	303	6 202	2675
7236 703 447 303 6692 2780	7236	703	447	303	6692	2780
9243 704 445 303 7236 2855	9243	704	445	303	7236	2855
9243 704 445 303 9243 3160	9243	704	445	303	9243	3160
9243 704 445 303 9424 3185	9243	704	445	303	9424	3185

Test 5.

$$\tau = 100 \text{ psi}$$

$$\sigma$$
 = 4000 psi

at time
$$= 0$$

Initial
$$\epsilon_3 = 5722 \times 10^{-6}$$
 in/in

Initial
$$\varepsilon_{T} = 2057 \times 10^{-6}$$
 in/in

Initial
$$\epsilon_1^{\prime} = 302 \times 10^{-4} \text{ in/in}$$

Total
$$\epsilon_1 = 6015 \times 10^{-6} \text{ in/in}$$

Total
$$\epsilon_L = 2182 \times 10^{-6}$$
 in/in

Total
$$\epsilon_1' = 355 \times 10^{-4}$$
 in/in

Computed
$$\epsilon_L^{\dagger} = 129 \times 10^{-4} \text{ in/in}$$

Time (min.)	⁶ 1 (10 ⁻⁶ in/in)	$\epsilon_{ m L}$ (10 ⁻⁶ in/in)	ε <mark>1</mark> (10 ⁻⁴ in/in)	Time (min.)	ΣV (m1.)
0000	000	000	000	0000	0000
0205	090	060	027	0205	0149
0572	131	096	039	0572	0264
1058	163	113	043	1058	0468
1546	180	115	044	1546	0637
2045	195	113	044	2045	0786
2495	210	115	046	2495	0945
2987	220	117	046	2987	1004
33 95	233	115	046	3395	1123
3941	237	115	048	3941	1206
4416	245	113	050	4416	1245
4746	245	115	050	4746	1251
5380	253	116	050	5380	1276
5864	256	116	050	5864	1301
6379	262	116	050	6379	1319
6817	261	123	050	6817	1340
7306	266	124	050	7306	1376
7 602	268	124	051	7692	1381
9035	284	135	053	9035	1400
9999	293	125	053	9999	1451

Test 6.

$$\tau = 100 \text{ psi}$$

$$\sigma$$
 = 5000 psi

at time = 0

Initial
$$\epsilon_1 = 5940 \times 10^{-6}$$
 in/in

Initial
$$\epsilon_{L} = 1834 \times 10^{-6}$$
 in/in

Initial
$$\epsilon_1^{\bullet} = 672 \times 10^{-4}$$
 in/in

Total
$$\epsilon_1 = 6129 \times 10^{-6}$$
 in/in

Total
$$\epsilon_L = 2123 \times 10^{-6}$$
 in/in

Total
$$\epsilon_1' = 733 \times 10^{-4}$$
 in/in

Computed
$$\epsilon_L^{\dagger} = 254 \times 10^{-4}$$
 in/in

Time (min.)	$^{\epsilon}$ 1	$\epsilon_{ m L}$	ϵ_1^{\prime}	Time (min.)	ΣV (m1.)
(=,	(10 ⁻⁶ in/in)	(10 ⁻⁶ in/in)	$(10^{-4}in/in)$	(====,	(/
0000	000	000	000	0000	0000
0005	001	003	000	0233	0031
0233	052	067	018	1040	0106
1040	135	186	018	1523	0146
1523	158	221	057	1930	0154
1930	170	233	057	2481	0204
2481	179	246	058	2972	0229
2972	182	256	056	3280	0246
3280	183	251	057	3926	0251
3926	179	258	057	4411	0254
4411	178	258	058	4829	0275
4829	182	259	058	5363	0284
5363	184	270	058	5850	0300
5850	184	268	058	6805	0316
6166	186	266	059	7291	0325
6805	187	267	059	7660	0345
7291	1 85	273	060	8751	0350
7660	187	269	060	97 67	0375
8751	189	286	061	97 67	0375
				97 67	0375

Test 7.

$$\tau = 300 \text{ psi}$$

$$\sigma = 1000 \text{ psi}$$

Initial
$$\epsilon_1 = 2321 \times 10^{-6}$$
 in/in

Initial
$$\epsilon_{L} = 999 \times 10^{-6}$$
 in/in

Initial
$$\epsilon_1^{\bullet} = 11 \times 10^{-4}$$
 in/in

Total
$$\epsilon_1 = 2790 \times 10^{-6} \text{ in/in}$$

Total
$$\epsilon_L = 1210 \times 10^{-6}$$
 in/in

Total
$$\epsilon_1^{\prime} = 68 \times 10^{-4} \text{ in/in}$$

Computed
$$\epsilon_L^{\dagger} = 29.3 \times 10^{-4}$$
 in/in

Time (min.)	$^{\epsilon}_{1}$	$\epsilon_{ m L}$	ϵ_1^{\prime}	Time (min.)	ΣV (m1.)
()	(10 ⁻⁶ in/in)	(10 ⁻⁶ in/in)	(10 ⁻⁴ in/in)	(,	(,
0000	000	000	000	0000	0000
0536	086	069	010	0187	0144
1052	170	111	016	0536	0350
1541	219	13 4	054	1052	0620
1925	246	150	058	1541	0850
2492	271	160	060	1925	1010
2992	289	171	061	2492	1248
3304	299	173	061	2992	1443
3933	314	181	061	3304	1550
4418	321	190	062	3933	1776
4824	339	189	064	4418	1921
5372	349	199	052	4824	2027
5856	369	201	052	5372	2175
6333	379	206	053	5856	2292
6811	396	211	053	6333	2402
7332	401	216	053	6811	2515
7863	409	217	053	7332	2632
8451	431	221	055	7863	2746
9999	469	231	057	8451	2876
				9999	3211

Test 8.

$$\tau = 300 \text{ psi}$$

$$\sigma$$
 = 1350 psi

at time
$$= 0$$

Initial
$$\epsilon_1 = 2790 \times 10^{-6} \text{ in/in}$$

Initial
$$\epsilon_{L} = 856 \times 10^{-6}$$
 in/in

Initial
$$\epsilon_1^{\dagger} = 168 \times 10^{-4}$$
 in/in

Total
$$\epsilon_1 = 3047 \times 10^{-6}$$
 in/in

Total
$$\epsilon_{L} = 1018 \times 10^{-6}$$
 in/in

Total
$$\epsilon_1' = 82 \times 10^{-4} \text{ in/in}$$

Computed
$$\epsilon_L^{\bullet} = 27.7 \times 10^{-4} \text{ in/in}$$

Time (min.)	[€] 1	ε _L	ε <mark>1</mark> 1	Time (min.)	ΣV (m1.)
	(10 ⁻⁰ in/in)	(10 in/in)	(10 in/in)		
0000	000	000	000	0000	0000
0005	001	002	056	0417	0050
0417	082	072	070	0905	00 9 7
0905	101	086	079	1398	0154
1398	165	087	082	1708	0186
1708	174	099	082	2350	0244
2350	186	102	082	2835	0290
2835	190	104	082	3105	0312
3205	190	099	082	3724	0374
3724	201	104	082	4280	0410
4280	202	108	082	4697	0441
4697	205	117	082	523 3	0483
5233	215	127	082	5708	0518
5708	216	129	082	6050	0547
6050	220	129	082	6669	0592
6669	229	143	082	7 1 54	0626
7154	228	135	082	8487	0692
8487	240	1 54	082	9999	0798
9999	257	162	082		

Test 9.

$$\tau = 300 \text{ psi}$$

$$\sigma$$
 = 1700 psi

at time
$$= 0$$

Initial
$$\epsilon_1 = 4020 \times 10^{-6}$$
 in/in

Initial
$$\epsilon_{L} = 658 \times 10^{-6}$$
 in/in

Initial
$$\epsilon_1' = 64 \times 10^{-4}$$
 in/in

Total
$$\epsilon_1 = 4417 \times 10^{-6}$$
 in/in

Total
$$\epsilon_{L} = 887 \times 10^{-6} \text{ in/in}$$

Total
$$\epsilon_1' = 95 \times 10^{-4}$$
 in/in

Computed
$$\epsilon_{L}^{\dagger} = 19 \times 10^{-4}$$
 in/in

Time (min.)	⁶ 1 (10 ⁻⁶ in/in)	ε _L (10 ⁻⁶ in/in)	ε'1 (10 ⁻⁴ in/in)	Time (min.)	ΣV (m1.)
0000	000	000	000	0000	0000
0914	160	144	024	0914	0043
1403	218	17 5	026	1403	0063
1719	239	188	027	1719	0073
2355	280	204	030	2355	0098
2844	2 95	208	030	2844	0116
3179	310	210	031	3179	0125
3793	315	211	031	3793	0147
4284	329	213	031	4284	0162
4661	331	209	031	4461	0172
5238	341	217	031	5283	0194
57 2 4	348	217	031	5724	0208
6109	348	217	031	6109	0217
6679	360	227	031	6679	0235
7168	360	227	031	7168	0249
8979	385	227	031	8 97 9	0297
98 97	3 97	229	031	9897	0322

Test 10.

$$\tau = 300 \text{ psi}$$

$$\sigma$$
 = 3000 psi

at time
$$= 0$$

Initial
$$\epsilon_1 = 3908 \times 10^{-6}$$
 in/in

Initial
$$\epsilon_{L} = 1810 \times 10^{-6}$$
 in/in

Initial
$$\epsilon_1' = 0$$

Total
$$\epsilon_1 = 4293 \times 10^{-6}$$
 in/in

Total
$$\epsilon_L = 2210 \times 10^{-6}$$
 in/in

Total
$$\epsilon_1^{\bullet} = 314 \times 10^{-4}$$
 in/in

Computed
$$\epsilon_L^{\dagger} = 161.7 \times 10^{-4} \text{ in/in}$$

Time (min.)	⁶ 1 (10 ⁻⁶ in/in)	ε _L (10 ⁻⁶ in/in)	ε <mark>'</mark> 1 (10 ⁻⁴ in/in)	Time (min.)	ΣV (m1.)
0000	000	000	000	0000	0000
0176	060	050	279	0176	0295
0533	115	098	288	0260	0826
1040	165	142	297	0533	1380
1531	190	176	303	1040	2186
1922	210	185	306	1531	2767
2478	230	210	308	1922	3122
2980	242	225	309	2478	3690
3300	244	231	309	2980	3993
3922	260	248	310	3300	4154
4406	269	25 8	311	3922	4589
4818	280	270	312	4406	4804
5360	291	287	312	4 81 8	4975
5845	298	298	311	5360	5185
6329	310	309	311	5845	5316
6799	322	322	312	6 3 29	5515
7319	331	330	313	6 7 99	5725
7857	340	347	313	7319	5801
8441	350	360	314	78 57	6076
9999	385	400	314	8441	6211

<u>Test 11</u>.

$$\tau = 300 \text{ psi}$$

$$\sigma$$
 = 4000 psi

at time
$$= 0$$

Initial
$$\epsilon_1 = 4305 \times 10^{-6}$$
 in/in

Initial
$$\epsilon_L = 2002 \times 10^{-6}$$
 in/in

Initial
$$\epsilon_1' = 0$$

Total
$$\epsilon_1 = 4665 \times 10^{-6}$$
 in/in

Total
$$\epsilon_L = 2152 \times 10^{-6}$$
 in/in

Total
$$\epsilon_1' = 390 \times 10^{-4}$$
 in/in

Computed
$$\epsilon_L^{\bullet} = 180 \times 10^{-4}$$
 in/in

Time (min.)	$^{\epsilon}1$	$\epsilon_{ m L}$	ϵ_1^{\bullet}	Time (min.)	ΣV (m1.)
(1111.0)	(10 ⁻⁶ in/in)	(10 ⁻⁶ in/in)	(10 ⁻⁴ in/in)	(,	(,
0000	000	000	000	0000	0000
0005	145	002	359	0401	0251
0401	190	020	354	8880	0484
0888	220	038	377	1382	0715
1382	238	050	381	1697	0806
1697	248	053	383	2331	1004
2331	256	060	385	2818	1143
2818	265	068	385	3120	1203
3120	270	070	385	3133	1205
3766	280	076	386	3766	1306
4262	285	080	385	4262	1394
4685	290	088	386	4685	1485
5216	300	099	387	4750	1488
5692	305	106	387	5216	1557
6037	310	105	387	5692	1655
6650	318	116	388	6037	1711
7137	320	118	388	6650	1784
8467	342	133	389	7137	1851
9946	360	150	390	8467	1994
				9946	2185

<u>Test 12</u>.

$$\tau = 300 \text{ psi}$$

$$\sigma$$
 = 5000 psi

Initial
$$\epsilon_1 = 3771 \times 10^{-6}$$
 in/in

Initial
$$\epsilon_L = 1900 \times 10^{-6}$$
 in/in

Initial
$$\epsilon_1' = 355 \times 10^{-4}$$
 in/in

Total
$$\epsilon_1 = 4155 \times 10^{-6}$$
 in/in

Total
$$\epsilon_L = 2088 \times 10^{-6}$$
 in/in

Total
$$\epsilon_1^{1} = 406 \times 10^{-4} \text{ in/in}$$

Computed
$$\epsilon_{L}^{\bullet} = 204.3 \times 10^{-4}$$
 in/in

Time (min.)	⁶ 1 (10 ⁻⁶ in/in)	$\epsilon_{ m L}$ (10 ⁻⁶ in/in)	ε <mark>΄</mark> 1 (10 ⁻⁴ in/in)	Time (min.)	ΣV (m1.)
0000	000	000	000	0000	0000
0005	055	005	002	0005	0007
08 94	270	098	036	08 9 4	0107
1385	2 95	112	041	13 85	0153
1402	243	115	041	1702	0184
2335	325	128	045	2335	0235
2826	340	139	046	2826	0275
3166	345	138	046	3166	0291
3774	359	145	047	3774	0331
4265	370	152	047	4265	0342
4650	378	150	048	4650	0363
5218	388	162	049	5218	0379
5704	400	162	049	5704	0405
6098	410	162	049	6098	0419
6659	420	170	049	665 9	0441
71 50	428	172	050	7150	0465
8966	368	181	051	8966	0429
9884	384	188	051	9884	0580

<u>Test 13</u>.

$$\tau = 500 \text{ psi}$$

$$\ddot{\sigma}$$
 = 1000 psi

at time
$$= 0$$

Initial
$$\epsilon_1 = 3350 \times 10^{-6}$$
 in/in

Initial
$$\epsilon_L = 634 \times 10^{-6}$$
 in/in

Initial
$$\epsilon_1^{\dagger} = 0$$

Total
$$\epsilon_1 = 3854 \times 10^{-6}$$
 in/in

Total
$$\epsilon_{L} = 800 \times 10^{-6} \text{ in/in}$$

Total
$$\epsilon_1' = 27 \times 10^{-4}$$
 in/in

Computed
$$\epsilon_{L}^{\bullet} = 5.7 \times 10^{-4}$$
 in/in

Time (min.)	⁶ 1 (10 ⁻⁶ in/in)	^e L (10 ⁻⁶ in/in)	ε <mark>1</mark> (10 ⁻⁴ in/in)	Time (min.)	ΣV (m1.)
0000	000	000	000	0000	0000
0169	135	033	001	0169	0275
0396	205	059	005	0189	0300
0872	280	089	012	0396	0545
1366	340	101	016	0872	1015
1521	355	106	016	1366	1415
1768	375	111	018	1521	1535
2312	405	126	019	1 756	1690
2807	419	132	019	1784	2035
31 93	435	139	019	2312	2380
3753	444	140	020	2807	2645
4246	448	144	021	3193	2840
4859	453	151	022	3753	3105
5193	455	1 50	023	4246	3330
5683	462	150	023	4859	3605
6639	463	1 52	024	5193	3742
7114	475	154	024	5683	3937
8395	487	161	024	5967	4047
8987	489	162	025	5972	4052
9999	504	166	027	5 98 2	4062
				6639	4312
				7114	4477
				8395	4902
				8987	5102
				9999	5422

Test 14.

$$\tau = 500 \text{ psi}$$

$$\sigma = 1350 \text{ psi}$$

Initial
$$\epsilon_1 = 4025 \times 10^{-6}$$
 in/in

Initial
$$\epsilon_L = 80 \times 10^{-6}$$
 in/in

Initial
$$\epsilon_1' = 0$$

Total
$$\epsilon_1 = 4310 \times 10^{-6}$$
 in/in

Total
$$\epsilon_{L} = 224 \times 10^{-6}$$
 in/in

Total
$$\epsilon_1^{\bullet} = 40 \times 10^{-4}$$
 in/in

Computed
$$\epsilon_L^{\bullet} = 2 \times 10^{-4}$$
 in/in

Time				Time	ΣV
(min.)	-6	-6	-4	(min.)	(m1.)
	(10 ⁻⁶ in/in)	(10 ⁻⁶ in/in)	(10 ⁻⁴ in/in)		
0000	000	000	000	0000	0000
0005	025	005	000	0389	0100
0389	130	065	000	0924	0210
0924	116	094	011	1415	0300
1415	209	112	021	2363	0465
2363	244	126	031	2859	0545
2895	250	127	034	3389	0628
3389	257	128	036	3304	0698
3804	257	129	036	4623	0817
3300	255	133	036	5244	0903
4623	263	136	039	57 38	0973
5244	265	138	036	6217	1036
5738	266	136	036	6680	1093
6217	271	130	036	7180	1153
6680	275	134	037	7363	1208
718 0	275	132	038	9010	1369
7630	275	130	038	9999	1421
9010	281	135	039		
9999	285	144	040		

Test 15.

$$\tau = 500 \text{ psi}$$

$$\sigma = 1700 \text{ psi}$$

at time
$$= 0$$

Initial
$$\epsilon_1 = 4916 \times 10^{-6}$$
 in/in

Initial
$$\epsilon_L = 513 \times 10^{-6}$$
 in/in

Initial
$$\epsilon_1^{\dagger} = 0$$

Total
$$\epsilon_1 = 5230 \times 10^{-6}$$
 in/in

Total
$$\epsilon_{T} = 615 \times 10^{-6}$$
 in/in

Total
$$\epsilon_1^{\prime} = 60 \times 10^{-4} \text{ in/in}$$

Computed
$$\epsilon_L^{\bullet} = 7.0 \times 10^{-4} \text{ in/in}$$

Time (min.)	⁶ 1 (10 ⁻⁶ in/in)	⁶ L (10 ⁻⁶ in/in)	ε' ₁ (10 ⁻⁴ in/in)	Time (min.)	ΣV (m1.)
0000	000	000	000	0000	0000
0450	093	035	027	0450	0040
0945	130	055	036	0945	0075
1394	155	067	041	1394	0105
1890	174	071	044	1890	0138
2385	185	076	046	2385	0168
2839	196	079	046	2839	0197
3 330	204	081	046	3330	0225
382 5	213	082	047	3825	0255
4223	217	084	049	4223	0276
4770	230	087	051	4770	0305
5260	241	088	051	5260	0330
5676	246	089	053	5676	0349
6210	256	089	054	6210	0370
6705	265	092	056	6705	0390
7061	273	094	056	7061	0400
8 638	297	101	057	8 6 3 8	0505
9418	314	102	060	9418	0530
9418	314	102	060		

Test 16.

$$\tau = 500 \text{ psi}$$

$$\sigma = 3000 \text{ psi}$$

at time
$$= 0$$

Initial
$$\epsilon_1 = 2360 \times 10^{-6}$$
 in/in

Initial
$$\epsilon_L = 1880 \times 10^{-6}$$
 in/in

Initial
$$\epsilon_1' = 0$$

Total
$$\epsilon_1 = 2709 \times 10^{-6}$$
 in/in

Total
$$\epsilon_L = 1980 \times 10^{-6}$$
 in/in

Total
$$\epsilon_1' = 265 \times 10^{-4}$$
 in/in

Computed
$$\epsilon_1^{\dagger} = 194 \times 10^{-4} \text{ in/in}$$

Time (min.)	⁶ 1 (10 ⁻⁶ in/in)	⁶ L (10 ⁻⁶ in/in)	ε <mark>1</mark> (10 ⁻⁴ in/in)	Time (min.)	ΣV (m1.)
0000	000	000	000	0000	0000
0379	079	031	229	0159	0095
0852	126	059	246	0379	1800
1345	153	072	253	0852	0325
1503	160	073	254	1345	0435
1752	169	075	255	1503	0475
2290	195	083	259	1752	0520
2785	211	087	259	2290	0610
3178	214	081	261	2785	0670
3790	221	082	262	3178	0730
4225	224	086	262	3710	0775
4840	228	089	262	4225	0825
5173	225	090	262	4840	0865
5664	230	092	262	5173	0885
5950	231	093	262	5664	0915
6618	232	093	263	5 9 50	0930
7094	235	091	266	6628	0975
8384	241	096	263	7094	0995
8 9 7 3	245	099	264	8384	1075
9989	249	100	265	8973	1115
				9989	1180

<u>Test 17</u>.

$$\tau = 500 \text{ psi}$$

$$\sigma$$
 = 4000 psi

Initial
$$\epsilon_1 = 2439 \times 10^{-6}$$
 in/in

Initial
$$\epsilon_L = 1727 \times 10^{-6}$$
 in/in

Initial
$$\epsilon_1^{\bullet} = 314 \times 10^{-6}$$
 in/in

Total
$$\epsilon_1 = 2717 \times 10^{-6}$$
 in/in

Total
$$\epsilon_L = 1855 \times 10^{-6}$$
 in/in

Total
$$\epsilon_1' = 348 \times 10^{-4}$$
 in/in

Computed
$$\epsilon_L^{\dagger} = 238 \times 10^{-4} \text{ in/in}$$

Time (min.)	⁶ 1 (10 ⁻⁶ in/in)	ε _L (10 ⁻⁶ in/in)	61 (10 ⁻⁴ in/in)	Time (min.)	ΣV (m1.)
0000	000	000	000	0000	0000
0374	052	000	010	0374	0405
0907	100	067	019	0907	0785
1397	133	078	008	1397	1005
2347	178	095	028	2347	1500
2841	182	098	030	2841	1652
3376	202	100	030	3376	1806
3788	208	101	030	3 788	1923
4282	212	108	030	4282	2089
4609	213	098	031	4609	2157
522 7	220	107	031	4722	2206
5722	227	108	032	5227	2294
6203	238	110	033	5722	2304
6667	240	114	032	6203	24 91
71 52	241	115	032	6667	2549
7 608	25 1	116	033	7152	2641
8996	268	122	033	7608	2754
9999	278	128	034	8996	3002

<u>Test 18</u>.

$$\tau = 500 \text{ psi}$$

 $\sigma = 5000 \text{ psi}$

at time = 0

Initial
$$\epsilon_1 = 2878 \times 10^{-6}$$
 in/in

Initial
$$\epsilon_L = 1574 \times 10^{-6}$$
 in/in

Initial
$$\epsilon_1^{\dagger} = 369 \times 10^{-4}$$
 in/in

Total
$$\epsilon_1 = 3097 \times 10^{-6}$$
 in/in

Total
$$\epsilon_{L} = 1655 \times 10^{-6}$$
 in/in

Total
$$\epsilon_1^{\dagger} = 397 \times 10^{-4} \text{ in/in}$$

Computed
$$\epsilon_1^* = 212 \times 10^{-4} \text{ in/in}$$

Time (min.)	⁶ 1 (10 ⁻⁶ in/in)	ε _L (10 ⁻⁶ in/in)	6 ¹ 1 (10 ⁻⁴ in/in)	Time (min.)	ΣV (m1.)
0000	000	000	000	0000	0000
0435	054	032	013	0435	0205
0930	093	054	019	0930	0378
1385	129	062	021	1385	0464
1 875	151	072	022	1875	0569
2371	169	072	023	2371	0636
2830	177	072	023	2830	0700
3316	179	073	024	3316	0701
3810	184	074	024	3810	0702
4212	184	075	024	4212	0745
4756	188	075	025	4 756	0791
5248	192	076	024	5248	0802
5667	194	076	024	5667	0803
61 95	199	077	025	61 95	0870
6690	200	078	026	6690	0899
7054	204	079	026	7054	0902
8631	216	080	027	8631	1003
9408	219	081	028	9408	1005

Test 19.

$$\tau = 700 \text{ psi}$$

$$\sigma$$
 = 1000 psi

at time
$$= 0$$

Initial
$$\epsilon_1 = 6536 \times 10^{-6}$$
 in/in

Initial
$$\epsilon_{L} = 3950 \times 10^{-6}$$
 in/in

Initial
$$\epsilon_1' = 319 \times 10^{-4}$$
 in/in

Total
$$\epsilon_1 = 6710 \times 10^{-6} \text{ in/in}$$

Total
$$\epsilon_L = 4140 \times 10^{-6}$$
 in/in

Total
$$\epsilon_1' = 339 \times 10^{-4}$$
 in/in

Computed
$$\epsilon_{L}^{\bullet} = 209 \times 10^{-4} \text{ in/in}$$

	ь				
Time (min.)	⁶ 1 (10 ⁻⁶ in/in)	⁶ L (10 ⁻⁶ in/in)	ε <mark>1</mark> (10 ⁻⁴ in/in)	Time (min.)	ΣV (m1.)
0000 0029 0337 0706 1202 1500 1695 2273 2942 3587 4081 4556 5026 5527 5845 6471 6967 7389 8282	000 002 040 070 096 111 120 138 143 148 152 152 154 161 162 164 166 168 172	000 002 045 075 102 118 125 138 152 158 159 162 163 170 170 171 178 179 183	000 002 007 010 013 014 014 014 017 017 017 018 019 019 019 019 020 020 020	0000 0029 0037 0039 0102 0106 0337 0706 1202 1365 1417 1500 1520 1695 2273 2942 2955 3587 4081 4556 5026 5527 5845 5895 6471 7389	00000 00100 00135 00141 00341 00350 00982 01884 02938 03588 03687 03839 03877 04214 04876 05919 05938 06840 07477 08088 08692 09285 09278 09738 10417 10914
				7523	11075

<u>Test 20</u>.

$$\tau = 700 \text{ psi}$$

$$\sigma$$
 = 1350 psi

at time
$$= 0$$

Initial
$$\epsilon_1 = 6672 \times 10^{-6}$$
 in/in

Initial
$$\epsilon_L = 3122 \times 10^{-6}$$
 in/in

Initial
$$\epsilon_1^{\prime} = 333 \times 10^{-4}$$
 in/in

Total
$$\epsilon_1 = 7035 \times 10^{-6}$$
 in/in

Total
$$\epsilon_L = 3240 \times 10^{-6}$$
 in/in

Total
$$\epsilon_1' = 350 \times 10^{-4}$$
 in/in

Computed
$$\epsilon_L^{\dagger} = 161 \times 10^{-4}$$
 in/in

Time (min.)	⁶ 1 (10 ⁻⁶ in/in)	⁶ L (10 ⁻⁶ in/in)	61 (10 ⁻⁴ in/in)	Time (min.)	ΣV (m1.)
0000	000	000	000	0000	0000
0005	008	001	000	0860	1725
0860	223	065	012	1345	2468
1345	250	081	015	1791	3050
1791	278	093	015	1808	3059
2295	303	097	015	2295	3827
2785	318	100	015	2785	4316
3184	326	103	015	3184	4567
3734	337	105	016	3734	4989
4224	338	104	016	4224	5206
4692	339	105	017	4692	5478
5167	343	113	016	5167	5625
5 6 6 8	348	104	016	5668	5801
6011	348	107	016	6081	5891
6542	347	111	017	6612	6013
7007	350	113	017	7077	6202
7309	351	112	017	7379	6365
8476	357	115	017	8546	6687
8918	358	116	017	8988	68 97
9874	363	118	017	9944	7164

Test 21.

$$\tau = 700 \text{ psi}$$

$$\sigma$$
 = 1700 psi

at time
$$= 0$$

Initial
$$\epsilon_1 = 6255 \times 10^{-6}$$
 in/in

Initial
$$\epsilon_{I} = 3416 \times 10^{-6}$$
 in/in

Initial
$$\epsilon_1' = 0$$

Total
$$\epsilon_1 = 8360 \times 10^{-6}$$
 in/in

Total
$$\epsilon_L = 4797 \times 10^{-6}$$
 in/in

Total
$$\epsilon_1^{\bullet} = 375 \times 10^{-4}$$
 in/in

Computed
$$\epsilon_L^{\dagger} = 215 \times 10^{-4}$$
 in/in

Time (min.)	⁶ 1 (10 ⁻⁶ in/in)	ε _L (10 ⁻⁶ in/in)	ε <mark>1</mark> (10 ⁻⁴ in/in)	Time (min.)	ΣV (m1.)
0000	0000	0000	0000	0000	0000
0085	0183	0079	0270	0085	0036
0974	1184	0660	0341	0974	07 9 0
1469	1452	0803	0357	1469	1354
1943	1600	0933	0369	1943	1402
2410	1690	1034	0369	2410	1864
2905	17 57	1084	0370	2905	200 3
3307	1804	1120	0370	3307	2215
37 90	1 845	1137	0369	37 90	2247
4280	1857	1164	0371	4280	2379
4692	1885	1184	0376	4692	2386
5236	1900	1197	0374	5236	2404
5 721	1934	1215	0375	5721	2518
6085	1944	1235	0377	6085	2525
6670	1955	1244	0374	6670	2630
71 50	1985	1264	0375	7150	2737
7488	1990	1280	0374	7488	2783
8361	6036	1300	0374	8361	2799
9191	2082	1335	0375	9191	2932
9957	2105	1381	0375	9957	3084

<u>Test 22</u>.

$$\tau = 700 \text{ ps i}$$

$$\sigma = 3000 \text{ psi}$$

at time
$$= 0$$

Initial
$$\epsilon_1 = 6590 \times 10^{-6}$$
 in/in

Initial
$$\epsilon_L = 361 \times 10^{-6}$$
 in/in

Initial
$$\epsilon_1^{\prime} = 496 \times 10^{-4}$$
 in/in

Total
$$\epsilon_1 = 6788 \times 10^{-6}$$
 in/in

Total
$$\epsilon_L = 509 \times 10^{-6}$$
 in/in

Total
$$\epsilon_1^{\prime} = 518 \times 10^{-4}$$
 in/in

Computed
$$\epsilon_L^{\bullet} = 39 \times 10^{-4}$$
 in/in

Time (min.)	⁶ 1 (10 ⁻⁶ in/in)	$\epsilon_{ m L}$ (10 ⁻⁶ in/in)	¢'1 (10 ⁻⁴ in/in)	Time (min.)	ΣV (m1.)
0000	000	000	000	0000	0000
0326	043	056	007	0017	0005
0689	067	080	010	0029	0010
1185	094	102	013	0098	0018
1364	100	110	013	0326	0065
1487	102	111	014	0689	0105
1683	105	115	015	1185	0167
2260	122	126	015	1364	0190
2926	133	128	016	1420	0195
3570	137	130	016	1487	0200
4065	141	132	017	1506	0202
4541	145	132	017	1683	0235
5010	151	1 3 4	017	2260	0251
5509	155	136	017	2926	0275
5832	158	137	018	3077	0281
6455	165	138	019	3570	0296
6948	165	142	020	4065	0308
73 55	167	142	020	4541	0320
8266	179	143	020	5010	0325
9817	198	148	022	5509	0331
				6455	0346
				6948	0350
				7355	0357
				7511	0361
				8266	0373
				8868	0386
				9817	03 95

Test 23.

$$\tau = 700 \text{ psi}$$

 σ = 4000 psi

at time = 0

Initial
$$\epsilon_1 = 6700 \times 10^{-6}$$
 in/in

Initial
$$\epsilon_{T} = 8 \times 10^{-6}$$
 in/in

Initial
$$\epsilon_1^{\prime} = 486 \times 10^{-4}$$
 in/in

Total
$$\epsilon_1 = 6943 \times 10^{-6}$$
 in/in

Total
$$\epsilon_{I} = 314 \times 10^{-6}$$
 in/in

Total
$$\epsilon_1' = 531 \times 10^{-4}$$
 in/in

Computed $\epsilon_L^{\bullet} = 25 \times 10^{-4} \text{ in/in}$

Time (min.)	⁶ 1 (10 ⁻⁶ in/in)	ε _L (10 ⁻⁶ in/in)	ε' ₁ (10 ⁻⁴ in/in)	Time (min.)	ΣV (m1.)
	(20 2, 2)	(== 111, 111)	(======================================		
0000	000	000	000	0000	0000
0081	040	020	004	0081	0040
0958	194	095	023	0958	0380
1457	240	112	028	1457	0515
1947	272	130	031	1947	0600
2398	296	133	033	2398	0650
2894	312	140	034	2894	0720
3298	321	138	036	32 9 8	0740
3779	326	150	036	4269	0815
4269	339	144	037	4682	0830
4682	347	147	037	5224	0865
5224	356	148	038	5709	08 90
5709	367	150	038	6077	0905
6077	374	151	038	6658	0925
6658	383	152	039	7138	0955
7138	392	154	039	7480	0970
7480	401	156	039	8350	1005
8350	422	157	042	9186	1045
9186	4 36	162	044	9959	1080
9959	451	164	045		

Test 24.

 $\tau = 700 \text{ psi}$

 $\sigma = 5000 \text{ psi}$

at time = 0

Initial
$$\epsilon_1 = 7017 \times 10^{-6}$$
 in/in

Initial
$$\epsilon_L = 42 \times 10^{-6}$$
 in/in

Initial
$$\epsilon_1^{\bullet} = 534 \times 10^{-4}$$
 in/in

Total
$$\epsilon_1 = 7468 \times 10^{-6}$$
 in/in

Total
$$\epsilon_L = 206 \times 10^{-6} \text{ in/in}$$

Total
$$\epsilon_1^{\bullet} = 594 \times 10^{-4}$$
 in/in

Computed
$$\epsilon_L^{\dagger} = 16.3 \times 10^{-4}$$
 in/in

Time (min.)	⁶ 1 (10 ⁻⁶ in/in)	[€] L (10 ⁻⁶ in/in)	ε'1 (10 ⁻⁴ in/in)	Time (min.)	ΣV (m1.)
0000	000	000	000	0000	0000
0002	001	119	035	0850	0050
0850	110	149	043	1336	1052
1336	143	169	047	1783	1250
1783	159	188	050	2285	1449
2285	166	195	051	2775	1647
2775	172	200	054	3175	1751
31 95	173	210	055	3725	1900
37 25	181	218	055	4215	1951
4215	18 6	230	055	4688	2002
4688	190	232	054	5160	2053
5760	193	239	057	5660	2149
5660	199	250	057	6071	2301
6071	206	259	057	6605	2350
6605	211	268	058	7070	2400
7070	216	267	058	7378	2450
7378	221	270	057	8545	2601
8545	231	290	058	8950	2699
8950	233	300	050	9941	2901
9941	243	314	060		

<u>Test 25</u>.

$$\tau = 1000 \text{ psi}$$

 σ = 1000 psi

at time = 0

Initial
$$\epsilon_1 = 5806 \times 10^{-6}$$
 in/in

Initial
$$\epsilon_L = 140 \times 10^{-6}$$
 in/in

Initial $\epsilon_1' = 0$

Total
$$\epsilon_1 = 8315 \times 10^{-6}$$
 in/in

Total
$$\epsilon_{L} = 4835 \times 10^{-6}$$
 in/in

Total
$$\epsilon_1' = 294 \times 10^{-4}$$
 in/in

Computed
$$\epsilon_L^{\bullet} = 171 \times 10^{-4} \text{ in/in}$$

Time (min.)	⁶ 1 (10 ⁻⁶ in/in)	[€] L (10 ⁻⁶ in/in)	¢1 (10 ⁻⁴ in/in)	Time (min.)	ΣV (m1.)
0000	0000	0000	0000	0000	00000
0301	0520	185 0	0052	0301	01568
0629	0759	2242	0099	0629	03193
1118	0986	2648	0145	0806	
1390	1120	2840	0169	1118	05496
1625	1221	2085	0186	1390	06715
2076	1373	3201	0210	1625	07749
2556	1532	3415	0223	2076	09695
2750	1586	3 511	0238	2556	11559
3517	1770	3747	0240	2750	12296
4012	1856	3865	0240	3 005	13242
4503	1906	3 98 5	0241	3517	14763
5178	1986	408 5	0257	4012	16263
5753	2049	41 6 5	0260	4503	17227
6391 6880	2119 2166	4238 4305	0260 0262 0260	5178 5753	19084 20513
7376	2221	4378	0273	6391	22004
8186	2300	4485	0277	6880	23084
8649 9999	2371 2509	4525 4695	0285 0294	7146 7376 8186 8649	23673 24184 25984 26966
				9631	29139

Test 26.

$$\tau = 1000 \text{ psi}$$

$$\sigma = 1350 \text{ psi}$$

at time
$$= 0$$

Initial
$$\epsilon_1 = 7754 \times 10^{-6}$$
 in/in

Initial
$$\epsilon_{L} = 4830 \times 10^{-6}$$
 in/in

Initial
$$\epsilon_1' = 0$$

Total
$$\epsilon_1 = 8125 \times 10^{-6}$$
 in/in

Total
$$\epsilon_L = +5085 \times 10^{-6}$$
 in/in

Total
$$\epsilon_1' = 310 \times 10^{-4}$$
 in/in

Computed
$$\epsilon_L^{\bullet} = 194 \times 10^{-4}$$
 in/in

Time (min.)	⁶ 1 (10 ⁻⁶ in/in)	[€] L (10 ⁻⁶ in/in)	ε' ₁ (10 ⁻⁴ in/in)	Time (min.)	ΣV (m1.)
0000	000	000	000	0000	0000
0000	000	000	000	0000	0000
0454	067	048	288	0454	0643
0949	120	070	295	0949	1229
1376	154	088	298	1376	1720
1894	181	102	301	1894	2288
23 8 9	210	108	303	2389	2774
2910	230	126	305	2910	3265
3334	233	138	305	3334	3627
3804	244	140	305	3804	4020
4177	252	1 46	306	4177	4341
4773	263	155	306	4773	4823
5269	271	165	306	5269	5212
5656	280	175	306	5656	5519
6214	294	185	306	6214	5944
6709	307	192	307	6709	6315
7140	314	201	308	7140	6636
8089	330	219	308	8089	7493
8401	337	223	308	8401	7718
9555	362	242	309	8640	7893
9971	371	255	310	9555	8511
				9971	8770

Test 27.

$$\tau = 1000 \text{ psi}$$

$$\sigma = 1700 \text{ psi}$$

at time
$$= 0$$

Initial
$$\epsilon_1 = 8060 \times 10^{-6} \text{ in/in}$$

Initial
$$\epsilon_L = 4964 \times 10^{-6}$$
 in/in

Initial
$$\epsilon_1' = 249 \times 10^{-4}$$
 in/in

Total
$$\epsilon_1 = 8325 \times 10^{-6}$$
 in/in

Total
$$\epsilon_{L} = .5135 \times 10^{-6}$$
 in/in

Total
$$\epsilon_1' = 322 \times 10^{-4}$$
 in/in

Computed
$$\epsilon_{L}^{\bullet} = 198.7 \times 10^{-4} \text{ in/in}$$

Time (min.)	€1	$\epsilon_{ m L}$	ϵ_1^{\prime}	Time (min.)	ΣV (m1.)
(,	(10 ⁻⁶ in/in)	$(10^{-6}in/in)$	(10 ⁻⁴ in/in)	((/
0000	000	000	00	0000	0000
0005	001	800	36	0580	0371
0580	060	058	51	1044	0625
1044	087	080	57	2232	0886
2232	118	108	66	2540	1204
2540	127	112	66	2925	1333
2925	135	114	66	3420	1479
3429	145	119	67	3924	1618
3924	154	122	68	4309	1707
4309	163	128	69	4869	1859
4869	173	132	69	5354	1986
5354	185	139	69	6309	2222
6309	202	145	71	6799	2333
6799	213	150	72	7258	2440
7258	218	1 54	73	8739	27 95
8739	247	165	74	9578	2995
9578	265	171	73		

<u>Test 28</u>.

$$\tau$$
 = 1000 psi

$$\sigma$$
 = 3000 psi

Initial
$$\epsilon_1 = 6220 \times 10^{-6}$$
 in/in

Initial
$$\epsilon_L = 1370 \times 10^{-6}$$
 in/in

Initial
$$\epsilon_1^{\dagger} = 0$$

Total
$$\epsilon_1 = 7590 \times 10^{-6} \text{ in/in}$$

Total
$$\epsilon_L = +890 \times 10^{-6}$$
 in/in

Total
$$\epsilon_1' = 411 \times 10^{-4}$$
 in/in

Computed
$$\epsilon_L^{\dagger} = 48.3 \times 10^{-4} \text{ in/in}$$

Time (min.)	ϵ_1	$\epsilon_{ m L}$	ε ' 1	Time (min.)	ΣV (ml.)
	(10 ⁻⁶ in/in)	(10 ⁻⁶ in/in)	(10 ⁻⁴ in/in)	•	
0000	0000	0000	0000	0000	0000
0001	0030	1200	0065	8000	0005
8000	0050	1350	0093	0216	0035
0216	0498	1600	0240	0659	0101
0659	0790	1801	0332	1140	0155
1140	0948	1915	0362	1331	0165
1331	0994	1 945	0373	1598	0185
1 5 98	1050	1981	0383	2099	0223
2099	1120	2025	0396	25 94	0251
2594	1200	2042	0399	30 91	0278
3091	1230	2100	0401	3770	0309
3770	1272	2145	0403	4339	0333
4339	1280	2160	0403	4974	0354
4974	1300	2160	0405	5464	0373
5464	1310	2170	0405	5972	0388
5 97 2	1230	2170	0405	6769	0412
6769	1335	2215	0407	6804	0414
7236	1342	2225	0408	7236	0431
8218	13 50	2248	0411	8218	0460
8829	1370	2260	0411	8829	0480

<u>Test 29</u>.

$$\tau = 1000 \text{ psi}$$

$$\sigma$$
 = 4000 psi

at time
$$= 0$$

Initial
$$\epsilon_1 = 5198 \times 10^{-6}$$
 in/in

Initial
$$\epsilon_L = 784 \times 10^{-6}$$
 in/in

Initial
$$\epsilon_1^{\bullet} = 420 \times 10^{-6}$$
 in/in

Total
$$\epsilon_1 = 7930 \times 10^{-6}$$
 in/in

Total
$$\epsilon_{L} = 1020 \times 10^{-6}$$
 in/in

Total
$$\epsilon_1' = 451 \times 10^{-4}$$
 in/in

Computed
$$\epsilon_L^{\dagger} = 58 \times 10^{-4} \text{ in/in}$$

Time (min.)	⁶ 1 (10 ⁻⁶ in/in)	ε _L (10 ⁻⁶ in/in)	ε <mark>1</mark> (10 ⁻⁴ in/in)	Time (min.)	ΣV (m1.)
0000	000	000	000	0000	0000
0443	073	075	800	0443	0051
0939	107	108	013	0939	0102
1370	123	125	017	1175	0119
1883	137	141	018	1370	0129
2379	145	1 52	018	1883	0159
2920	155	161	018	2379	0178
3324	160	168	019	2920	0201
3794	170	170	020	3324	0218
4168	1 75	172	020	37 94	0230
4764	185	180	021	4168	0238
5259	192	185	022	4764	0252
5659	197	190	023	5259	0254
6205	205	195	025	5649	0262
6699	205	201	027	6205	0268
7128	226	206	031	6699	0271
8081	240	213	029	7128	0279
8392	245	215	029	8081	0289
9552	267	231	030	8392	0293
9965	273	236	031	8635	0296
				9552	0304
				9965	0311

<u>Test 30</u>.

$$\tau = 1000 \text{ psi}$$

$$\sigma = 5000 \text{ psi}$$

at time
$$= 0$$

Initial
$$\epsilon_1 = 7912 \times 10^{-6}$$
 in/in

Initial
$$\epsilon_L = 2013 \times 10^{-6}$$
 in/in

Initial
$$\epsilon_1' = 0$$

Total
$$\epsilon_1 = 9560 \times 10^{-6}$$
 in/in

Total
$$\epsilon_{L} = 2745 \times 10^{-6}$$
 in/in

Total
$$\epsilon_1^{\prime} = 501 \times 10^{-4}$$
 in/in

Computed
$$\epsilon_L^{\bullet} = 144 \times 10^{-4}$$
 in/in

Time (min.)	⁶ 1 (10 ⁻⁶ in/in)	⁶ L (10 ⁻⁶ in/in)	ε <mark>΄</mark> 1 (10 ⁻⁴ in/in)	Time (min.)	ΣV (m1.)
0000	0000	0000	0000	0000	000
0005	0055	0020	0401	0570	085
0570	0514	0235	0457	1034	126
1034	0780	0345	0480	2223	205
2223	1224	0530	0501	2535	212
2535	1300	0531	0497	2915	227
2915	1380	0600	0498	3419	251
3419	1430	0601	0499	3914	266
3914	1453	0621	0499	4303	283
43 03	1472	0625	0499	4803	295
4860	1485	0631	0499	4860	297
5344	1503	0642	0499	5344	3 13
6299	1530	0665	0499	6299	348
67 90	1551	0671	0499	6790	366
7251	1 555	0685	0500	7152	382
8735	1609	0714	0501	8735	435
9572	1648	0732	0501	9572	480

Table A-2. Flow-rate, Permeability, Strain, and Deformation

т (psi)	σ (psi)	Q 10 ³ (m1/min)	K (milli-darcy)	e1 × 10 ⁻⁶ (in/in)	e _L × 10 ⁻⁶ (in/in)	61-4 × 10-4 (in)	6 _L -4 × 10 (in)	2e' - e' x 10-4 x 10'4 (in /in 3
100	1000 1350 1700 3000 4000 5000	135.50 40.00 14.00 1.62 .38	2.4173 0.7136 0.2498 0.0289 0.0068	615 1200 1448 5977 6015	145 100 28 2280 2182 2123	109 201 247 909 1066 2198	26 17 5 347 287 761	53 78 85 535 613 1240
300	1000 1350 1700 3000 4000 5000	227.50 68.75 30.00 3.75 1.25	4.0586 1.2265 0.5352 0.0669 0.0223	2790 3047 4417 4293 4665	1210 1018 887 2210 2152 2088	204 248 285 942 1170	88 83 57 485 540 613	117 136 133 638 750 811
500	1000 1350 1700 3000 4000 5000	350.00 114.00 53.00 6.40 2.15	6.2440 2.0338 0.9455 0.1142 0.0384	3854 4310 5230 2709 2717 3097	800 224 615 1980 1855	81 120 182 796 1045	17 6 21 582 713 637	38 44 75 653 917 821
700	1000 1350 1700 3000 4000 5000	1080.00 340.00 140.00 15.05 5.00	19.2672 6.0656 2.4976 0.2685 0.0892	6710 7035 8360 6788 6943 7468	+4140 +3240 +4797 + 509 + 314 + 206	1017 1051 1126 1554 1653 1783	627 484 646 117 75	79 28 53 596 601 627
1000	1000 1350 1700 3000 4000 5000	2280.00 784.00 256.00 33.80 12.20 3.70	40.6752 13.9866 4.5670 0.6030 0.2176 0.0660	8315 8125 8325 7590 7930 9560	+4835 +5085 +5135 + 890 +1020 +2745	882 930 967 1233 1352 1504	513 582 596 145 174 432	48 76 74 315 335 213

Table A-3. Stress, Taylor's Coefficient, Void Ratio, Void, and Bulk Compressibility

т (psi)	σ m (psi)	K (milli-darcy)	e ³ /1+e (x 10 ⁻⁶)	$\sigma_{\rm m}^{\rm a} {\rm e}^{3/1 + {\rm e}}$ (x 10 ⁻⁶ psi)	$^{2}_{L}^{'}_{L}^{-}_{-4}^{'}_{in}^{'}_{1n}^{3}$	e (× 10 ⁻³)	c (× 10 ⁻⁶ /psi)
100	1000 1350 1700 3000 4000 5000	2.4173 0.7136 0.2498 0.0289 0.0068	8.915 8.597 8.509 4.027 3.457	08915 13425 14450 12100 13800 01346	0053 0078 0085 0535 0613	2.075 2.050 2.043 1.592 1.513	2.075 1.519 1.202 0.531 0.378
300	1000 1350 1700 3000 4000 5000	4.0586 1.2265 0.5352 0.0669 0.0223	7.960 7.875 7.921 3.289 2.601	07 960 10600 13450 09860 10400	0117 0136 0133 0638 0750 0811	2.010 1.991 1.994 1.488 1.376	2.010 1.475 1.173 0.496 0.263
500	1000 1350 1700 3000 4000 5000	6.2440 2.0338 0.9455 0.1142 0.0384	9.109 9.031 8.653 3.191 1.764 2.219	09109 12200 14700 09570 07050	0038 0044 0075 0653 0917	2.090 2.084 2.053 1.473 1.209	2.090 1.544 1.208 0.491 0.302
700	1000 1350 1700 3000 4000 5000	19.2672 6.0656 2.4976 0.2685 0.0892	8.584 9.241 8.915 3.575 3.540	08584 12480 15150 10720 14150 16820	0079 0028 0053 0596 0601	2.049 2.100 2.075 1.530 1.525	2.049 1.556 1.221 0.510 0.381
1000	1000 1350 1700 3000 4000 5000	40.6752 13.9866 4.5670 0.6030 0.2176 0.0660	8.979 8.622 8.647 5.938 5.743 6.997	08979 11610 14680 17800 23350 34950	0048 0076 0074 0315 0335	2.080 2.052 2.054 1.812 1.792	2.080 1.520 1.207 0.604 0.448

